

DISSERTATION

**Recovering Spatially and Temporally Dynamic
Regional Scale Carbon Flux Estimates**

Submitted by:

Andrew Schuh

Graduate Degree Program in Ecology

In partial fulfillment of the requirements

For the Degree of Doctor of Philosophy

Colorado State University

Fort Collins, Colorado

Spring 2009

UMI Number: 3374618

INFORMATION TO USERS

The quality of this reproduction is dependent upon the quality of the copy submitted. Broken or indistinct print, colored or poor quality illustrations and photographs, print bleed-through, substandard margins, and improper alignment can adversely affect reproduction.

In the unlikely event that the author did not send a complete manuscript and there are missing pages, these will be noted. Also, if unauthorized copyright material had to be removed, a note will indicate the deletion.

UMI[®]

UMI Microform 3374618
Copyright 2009 by ProQuest LLC
All rights reserved. This microform edition is protected against
unauthorized copying under Title 17, United States Code.

ProQuest LLC
789 East Eisenhower Parkway
P.O. Box 1346
Ann Arbor, MI 48106-1346

COLORADO STATE UNIVERSITY

December 29, 2008

WE HEREBY RECOMMEND THAT THE DISSERTATION PREPARED
UNDER OUR SUPERVISION BY ANDREW E. SCHUH BE ACCEPTED AS
FULFILLING IN PART REQUIREMENTS FOR THE DEGREE OF DOCTOR OF
PHILOSOPHY.

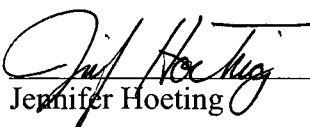
Committee on Graduate Work



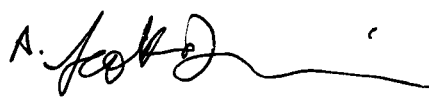
Niall Hanan



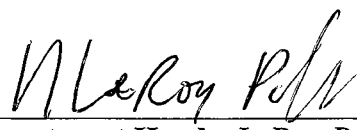
Stephen Ogle



Jennifer Hoeting



Adviser – Scott Denning



Department Head – LeRoy Poff

ABSTRACT OF DISSERTATION

Recovering Spatially and Temporally Dynamic

Regional Scale Carbon Flux Estimates

This dissertation presents two review type chapters and three new research chapters that contribute to our theoretical and practical knowledge about terrestrial carbon fluxes on the regional scale. This research expands on previous carbon dioxide inversion work by providing estimates of ecosystem respiration and gross primary productivity, as opposed to only net ecosystem exchange, and provides estimates on scales in time and space not previously available.

The first two chapters provide an introduction and review material. This is necessary to provide the reader with an understanding of the relatively complex geostatistical atmospheric inversion process which uses carbon dioxide concentration data to provide terrestrial carbon flux estimates. Issues of scale are discussed as well previous work which was fundamental to the research presented here.

The third and fourth chapters use simulated data to present an analysis of the methodology to a case study of North America in 2004. In particular, simulated data is used to investigate the sensitivity of the inversion to theoretical components of the inversion process and it is concluded that reasonably robust estimates of ecosystem respiration and gross primary productivity can be achieved by using a limited network of eight carbon dioxide observing towers. Chapter 4 specifically looks at the issue of small

scale variability in carbon fluxes and the impact it has on obtaining larger scale regional estimates.

Chapter five contains an analysis of real collected CO₂ observation data from 2004 at the aforementioned eight observing sites. Results show significant seasonal and annual corrections to the a priori carbon flux estimates, in particular to the individual components of net ecosystem exchange, ecosystem respiration and gross primary productivity. Furthermore, the annual net ecosystem exchange, when presented spatially, provides clues to annual sources and sinks in 2004. Sensitivity is investigated with respect to numerous components of the inversion. Although large confidence bounds on estimates indicate statistical uncertainty in the mean estimate of net ecosystem exchange, estimates match reasonably well with previously conducted research as well as observational data. The research provides the estimates within a spatial context (and resolution) that was not previously available, allowing for the construction, and support, of much more descriptive hypotheses about carbon fluxes than was previously possible. Chapter six contains a summary of the results of the dissertation.

Andrew E. Schuh
Graduate Degree Program in Ecology
Colorado State University
Fort Collins, CO 80523
Spring 2009

ACKNOWLEDGEMENTS

I would like to thank several individuals at Colorado State University for their support on this dissertation. First and foremost, my advisor Scott Denning, whose support both academically and personally were of great importance to the finishing of this manuscript. I would also like to thank my committee, Jennifer Hoeting for her knowledge of Bayesian statistical theory and continuous reminders that I need to improve my writing 'skeels'. Niall Hanan and Stephen Ogle provided perspectives as professional ecologists that were very insightful and provided me with a much more professional dissertation. I would also like to thank Dennis Ojima who comments early on in my dissertation process were helpful to honing my research plan.

Absolutely critical to my work was the assistance of many fellow graduate students and research scientists in Scott Denning's Biocycle group. In particular, Nick Parazoo, Kathy Corbin, Erica McGrath-Spangler, Ian Baker, and Marek Uliasz provided essential advice, models, results and general personal support for the completion of this dissertation.

This research was funded by NOAA Contract No. NA17RJ1228 and by Department of Energy Grant No. DE-FG02-02ER63474. We wish to thank the North American Carbon Program and the Office of Science as well as the Numerical Terradynamics Simulation Group (NTSG) at University of Montana for providing the FPAR/LAI data that was used in this paper. We thank the following tower PIs who provided data that was used for this paper, WLEF: Arlyn Andrews, NOAA GMD, ARM (Great Plains): Sebastien Biraud LBNL, Harvard Forest: William Munger, Harvard University, Argyle, ME: Arlyn Andrews, NOAA GMD, WKWT (Moody, TX): Arlyn

Andrews, NOAA GMD, Fraserdale: Douglas Worthy, MSC, Western Peatland: Larry Flanagan, University of Lethbridge, BERMS (Candle Lake): Douglas Worthy, MSC.

Lastly, and definitely most important, I would like to thank the support of my wife Valerie and our two children, Evan and Zane, who endured my absence on many nights, so that this dissertation could be completed. I love you guys tremendously, thanks.

TABLE OF CONTENTS

List of Tables.....	vi
List of Figures.....	vii
I. Introduction.....	1
Dissertation Organization and Purpose.....	4
Literature Cited.....	8
II. Introduction to the carbon cycle and atmospheric inversions.....	10
The Carbon Cycle.....	10
Modeling Carbon Dioxide Dynamics.....	19
Inversion Methods.....	26
Literature Cited.....	40
III. Investigation of the sensitivity of Bayesian carbon dioxide inversions.....	46
Introduction.....	46
Methods.....	49
Results.....	68
Discussion.....	76
Literature Cited.....	79
IV. Seeing the forest through the Trees.....	83
Abstract.....	83
Introduction.....	84
Methods.....	88
Results.....	98
Conclusions.....	101
Literature Cited.....	103
V. A Regional High-Resolution Carbon Flux Inversion of North America for 2004.....	106
Abstract.....	106
Introduction.....	106
Methods.....	109
Results.....	123
Conclusions.....	160
Literature Cited.....	164
VI. Summary.....	169

LIST OF TABLES

Table 4.1	Summary statistics for example inversion shown in Fig. 1.....	97
-----------	---	----

LIST OF FIGURES

Figure 2.1	The Carbon Cycle.....	11
Figure 2.2	Carbon dioxide record from Mauna Loa Observatory	12
Figure 2.3	Transcom Basis Regions.....	31
Figure 2.4	Temperate North America Basis Function	32
Figure 2.5	Carbon dioxide observing network used in Transcom 3	33
Figure 3.1	Inversion Region	61
Figure 3.2	Net Photosynthesis and Ground Respiration Biases	68
Figure 3.3	Aggregation Error.....	70
Figure 3.4	Evolution of Error with Aggregation	71
Figure 3.5	Error as function of sample size	71
Figure 3.6	Effect of observation error variance on prediction.....	72
Figure 3.7	Effect of spatial correlation on inversion	76
Figure 4.1	Example Bias Patterns.....	97
Figure 4.2	Inversion sensitivity to 100 km noise.....	100
Figure 4.3	Cumulative NEE, a priori and a posterior	101
Figure 5.1	Soil Classes Map.....	112
Figure 5.2	Biome Map.....	113
Figure 5.3	Time Series of carbon dioxide observations and predictions.....	125
Figure 5.4	Carbon Dynamics for North America, annual time series.....	126
Figure 5.5	Mapped Uncertainty Measures.....	127
Figure 5.6	Boundary Inflow Difference between PCTM/Carbon Tracker.....	128

Figure 5.7	Inversion Estimates for three inflow scenarios	131
Figure 5.8	Difference in annual sink inference as function of fossil fuel inv.....	133
Figure 5.9	Sensitivity of sink estimate to varying inversion parameters.....	135
Figure 5.10	Inversion estimates using long decorrelation length scale (1000 km) .	138
Figure 5.11	MODIS 17 NPP anomaly plots (2000-2005).....	139
Figure 5.12	Comparison to CarbonTracker (JFM).....	141
Figure 5.13	Comparison to CarbonTracker (AMJ).....	142
Figure 5.14	Comparison to CarbonTracker (JAS).....	143
Figure 5.15	Comparison to CarbonTracker (OND).....	144
Figure 5.16	Comparison to Ameriflux ARM Site Observations.....	145
Figure 5.17	INTEX Comparison Time Series	153
Figure 5.18	Vertical Profiles Comparisons for WLEF in July 2004	155
Figure 5.19	July 2004 NEE Average.....	156
Figure 5.20	Biological Tracer Morning Buildup Plot.....	157
Figure 5.21	Average 30 meter wind speeds for 18 UMT for July 2004.....	158
Figure 5.22	Vertical profiles over location in WV for July 21 – July 30, 2004	159
Figure 5.23	Influence function for location in WV for July 29 th	159

I. Introduction

A thorough understanding of the dynamics of the carbon cycle is critical to predicting future climate change. The current pool of carbon in the atmosphere is approaching 800 petagrams (PgC) and growing exponentially. At no point in the past 20,000 years has there been this much carbon in the atmosphere (IPCC, 2007). There are numerous lines of evidence that link this rise to increasing anthropogenic carbon dioxide emissions and changing agricultural practices. Fossil fuel combustion, land-use change, and cement production contribute about 8.5 PgC per year into this atmospheric pool. There are no current indications that this rate of carbon dioxide production will slow in the future. Estimates of carbon dioxide concentrations for the year 2100 range between 500 ppm and 1000 ppm over a variety of emissions scenarios (IPCC, 2007). This would imply a 50% - 200% increase in carbon dioxide in the atmosphere over the next century. These estimates are highly uncertain due to variability in the estimation of future fossil fuel emissions and the lack of mechanistic knowledge regarding the fate of anthropogenic carbon. However, due to its radiative properties as a greenhouse gas, any sustained period of exponentially increasing atmospheric carbon dioxide concentrations could potentially have a large impact upon the future climate.

The current input of anthropogenic carbon is about 8.5 PgC per year, but the actual realized carbon dioxide increases in the atmosphere are only about half of that amount. This implies that approximately 4 PgC per year, on average, is absorbed by other near surface carbon pools, namely the terrestrial biosphere and the surface ocean layers. This carbon sink varies annually from 1 to 6 PgC per year (Conway et al, 1994) and appears to be evenly distributed between the oceans and terrestrial biosphere (IPCC,

2007). There is growing consensus that the northern hemisphere is responsible for a large portion of the terrestrial biosphere carbon uptake over the last two decades. The supporting research generally involves either the upscaling/extrapolation of ground based measurements of annual change in biomass or atmospheric inversion based inferences using atmospheric carbon dioxide concentrations. Results based upon either method (atmospheric inversion or land-based measurements) are quite variable, both between each method as well as within each of the methods. Land-based analyses of the carbon flux for the coterminous United States are in the range of 0.08 to 0.35 PgC per year (Houghton et al., 1999; Birdsey and Heath, 1995, SOCCR 2007) while atmospheric inversion estimates are substantially larger and more variable, in the range of 0.5 to 1.7 PgC per year (Fan et al., 1998; Gurney et al., 2002, Peters et al., 2007). Surprisingly, the high end estimates of the sink for the United States would mitigate its entire current anthropogenic carbon contribution.

Despite the acknowledged existence of a northern hemispheric carbon sink, the lack of understanding regarding the mechanisms responsible for it preclude the ability to accurately predict its strength into the future. Several hypotheses for this sink have been proposed, and investigated, including fertilization effects from carbon and/or nitrogen (Oren et al., 2001; Caspersen et al., 2000; Joos et al., 2002), anthropogenic land use changes (Houghton et al., 1999), and forest fire suppression (Mouillot and Field, 2005). Many hypothesized sink mechanisms are limited in capacity, such as forest fire suppression (Tilman et al., 2000), implying that at some time in the future anthropogenic carbon emissions may begin to be fully realized in the atmosphere (Hurtt et al., 2002). The carbon fertilization hypothesis has been studied extensively and under appropriate

situations might constitute a much longer time scale sink mechanism than fire suppression, for instance. Nevertheless, this sink is dependent upon factors other than carbon dioxide concentration and thus is also likely to be limited in capacity (Oren et al., 2001). There is also little evidence that these sinks could not turn into sources in the near future, providing a further increase in carbon dioxide in the atmosphere. For example, it is possible that continued global warming could cause a large release of carbon from boreal soils, which constitute 40% of world's reactive carbon (McGuire et al., 1995, Zimov et al., 2006) but are currently locked away in permafrost. In order to better understand these sink processes, tools are needed with which to test regional and ecosystem-level hypotheses.

One of these tools is the atmospheric CO₂ inversion. The concept behind the atmospheric inversion technique is as follows. Carbon dioxide is chemically inert once it enters the atmosphere. However, biologically, it is not. For example, carbon dioxide concentrations fluctuate daily through the light-dependent process of photosynthesis. If mechanistic information can be obtained about how atmospheric carbon interacts with the ocean and terrestrial biosphere, inferences can be made about this carbon sink from atmospheric carbon dioxide concentrations.

In particular, assume that one "guesses" the carbon dioxide fluxes of the biosphere and their associated local changes on the surrounding carbon dioxide concentrations. If one can accurately predict the tracer transport of carbon dioxide through the atmosphere, for example through the use of a coupled meteorological model, then predictions can be made regarding what carbon dioxide concentrations should be in the atmosphere, at any point in space and time. If the initially guessed flux pattern

induced by the biosphere is wrong than one is likely to incorrectly predict carbon dioxide concentrations in the atmosphere. Conversely, if the carbon dioxide flux pattern is correctly specified, then one should be able to correctly predict carbon dioxide concentrations. Atmospheric inversion techniques attempt to correct for these initial carbon flux guesses in such a way as to reduce the differences between “expected” modeled carbon dioxide concentrations and actual carbon dioxide measurements. By proceeding in a fashion similar to this, one is able to derive spatially smooth regional estimates that are representative of large scale patterns of carbon exchange between the biosphere and atmosphere. It is this technique and its associated results applied over North America that will be investigated in this dissertation.

Outline and Purpose of Dissertation

Ch. 2 of the dissertation provides background material necessary for understanding the carbon cycle, the implications of potential changes in the carbon cycle on the earth’s climate, and techniques and methods which can be used to investigate carbon cycle dynamics from the standpoint of the atmosphere.

Ch. 3 and Ch. 4 provide an investigation into the regional atmospheric inversions. In particular, we investigate the effect of local scale variability in ecosystem respiration (ER) and gross primary production (GPP) and the effect upon prediction of larger scale regional patterns of net ecosystem exchange (NEE). Flux tower data has shown that incredible variability in NEE can exist at very fine scales in nature. These towers generally represent flux footprint areas of a few square kilometers and are often located hundreds or thousands of kilometers apart. It is often difficult to extrapolate these NEE

measurements due to their variability in space but they do provide important mechanistic and conceptual information at very specific locations. We investigate the ability to use atmospheric CO₂ to “see” through this fine scale NEE variability and discover larger scale trends in NEE.

While no real data is used in this chapter, we do use locations of actual towers, atmospheric transport patterns, and estimated biosphere fluxes. CO₂ mixing ratio data is simulated from a mixed pattern of flux errors, representing larger scale patterns of NEE errors as well as smaller scale local variability. We then compare results at different spatial scales using both pre-aggregated flux regions and post-aggregated flux regions and report the robustness of the estimates. While the main point of this chapter is to explore the sensitivity of the inversion, it also provides a *check* on the ability of the inversion to do what it is supposed to, namely recover ER and GPP biases with a very small network of observation towers.

In Ch. 5 we perform an inversion using carbon dioxide concentration data from eight flux towers in North America. Our goal in performing this inversion is to recover meaningful high resolution optimized NEE estimates. Since our underlying biosphere model is annually balanced with respect to NEE and it is widely believed that North America is still providing a sink for carbon, we expect to estimate a sink for the year on the order of 0.5 to 1.5 PgC per year. We use a global atmospheric transport and biosphere model to provide boundary conditions to the inversion. This is of particular interest given that this is often a very difficult quantity to estimate. Ideally, one would like to optimize global fluxes that contribute to the boundary inflow but this is currently beyond the capability of our system, however we do include boundary conditions

generated from an independent optimized global model as a comparison. Most of the inversions performed over the last decade share the same basic underpinnings (Fan et al. 1998, Gurney et al. 2002, Rodenbeck et al. 2003, Gerbig et al. 2003, Michalak et al. 2004, Peters et al. 2007) but each has enough distinction such that when each is convoluted with the great lack of data constraining the problem, the results show significant variance. As one of these inversions, our inversion shares many similarities with previous inversions while also differing in a few ways. It is a high-resolution inversion, with the forward model being run at 40 km resolution over North America for both the atmospheric transport and the biosphere making it of a much higher resolution than available global inversions (Fan et al. 1998, Gurney et al. 2002, Rodenbeck et al. 2003, Michalak et al. 2004). It incorporates spatial smoothing to regularize the solution similar to [Michalak et al. 2004] and [Rodenbeck et al. 2003]. It is also biome independent, with corrections being made in space with little pre-aggregation of grid cells in contrast to [Peters et al. 2007]. We use a weekly time-step to assimilate observations and recalculate optimized NEE similar to [Peters et al. 2007]. Furthermore, in contrast to many other inversions, we provide optimized ER and GPP estimates which are then aggregated a posteriori to an optimized NEE estimate.

When this dissertation was begun in 2004, there were virtually no NEE estimates available at scales less than that of continents. Even with the advent of the latest global nested flux estimates, such as CarbonTracker (Peters et al., 2007), this work establishes higher spatial resolution estimates of NEE as well as ecosystem respiration and gross primary productivity for North America. This body of work promises to bring robust atmospheric based NEE estimates to scales closer to that of biogeochemical model

estimates and field-based observations by using the increasing availability of calibrated CO₂ measurements from eddy covariance towers. This will allow the synthesis of estimates from different communities of researchers and help to illuminate the differences in estimates between these research communities.

LITERATURE CITED

- Birdsey, R. A. & Heath, L. S. (1995), 'Productivity of America's Forest Ecosystems', *Forest Service General Technical Report RM-GTR-271*, U.S. Forest Service, Fort Collins, CO, 56-70.
- Caspersen, J. P.; Pacala, S. W.; Jenkins, J. C.; Hurtt, G. C.; Moorcroft, P. R. & Birdsey, R. A. (2000), 'Contributions of Land-Use History to Carbon Accumulation in U.S. Forests', *Science* **290**, 1148-1150.
- Fan, S.; Gloor, M.; Mahlman, J.; Pacala, S.; Sarmiento, J.; Takahashi, T. & Tans, P. (1998), 'A large terrestrial carbon sink in North America implied by atmospheric and oceanic carbon dioxide data and models', *Science* **282**, 442-446.
- Gerbig, C.; Lin, J. C.; Wofsy, S. C.; Andrews, A. E.; Daube, B. C.; Davis, K. J. & Grainger, C. A. (2003), 'Toward constraining regional-scale fluxes of CO₂ with atmospheric observations over a continent: 2. Analysis of COBRA data using a receptor-oriented framework', *Journal of Geophysical Research* **108**, ACH 6 1-19.
- Gerbig, C.; Lin, J. C.; Wofsy, S. C.; Daube, B. C.; Andrews, A. E.; Stephens, B. B.; Bakwin, P. S. & Grainger, C. A. (2003), 'Toward constraining regional-scale fluxes of CO₂ with atmospheric observations over a continent: 1. Observed spatial variability from airborne platforms', *Journal of Geophysical Research* **108**.
- Gurney, K. R.; Law, R. M.; Denning, A. S.; Rayner, P. J.; Baker, D.; Bousquet, P.; Bruhwiler, L.; Chen, Y.; Clais, P.; Fan, S.; Fung, I. Y.; Gloor, M.; Helmann, M.; Higuchi, K.; John, J.; Maki, T.; Maksyutov, S.; Masarie, K.; Peylin, P.; Prather, M.; Pak, B. C.; Randerson, J.; Sarmiento, J.; Tagucki, S.; Takahashi, T. & Yuen, C. (2002), 'Towards robust regional estimates of CO₂ sources and sinks using atmospheric transport models', *Nature* **415**, 626-630.
- Houghton, R. A. (1999), 'The annual net flux of carbon to the atmosphere from changes in land use 1850-1990', *Tellus* **51B**, 298-313.
- Hurtt, G. C.; Pacala, S. W.; Moorcroft, P. R.; Caspersen, J.; Shevliakova, E.; Houghton, R. A. & III, B. M. (2002), 'Projecting the future of the U.S. carbon sink', *Ecology* **99(3)**, 1389-1394.
- IPCC (2007), *Climate Change 2007: The Fourth IPCC Assessment Report*, Cambridge, Cambridge University Press.
- Joos, F.; Prentice, I. C. & House, J. I. (2002), 'Growth enhancement due to global atmospheric change as predicted by terrestrial ecosystem models: consistent with US forest inventory data', *Global Change Biology* **8**, 299-303.
- McGuire, A. D.; Melillo, J. M. & Joyce, L. A. (1995), 'The role of nitrogen in the

response of forest net primary production to elevated atmospheric carbon dioxide.', *Annual Review of Ecology and Systematics* **26**, 472-503.

Michalak, A. M.; Bruhwiler, L. & Tans, P. P. (2004), 'A geostatistical approach to surface flux estimation of atmospheric trace gases', *Journal of Geophysical Research* **109**, 1-19.

Mouillot, F. & Field, C. B. (2005), 'Fire history and the global carbon budget: A 1 deg by 1 deg fire history reconstruction for the 20th century', *Global Change Biology* **11**, 398-420.

Oren, R.; Ellsworth, D. S.; Johnsen, K. H.; Phillips, N.; Ewers, B. E.; Maler, C.; Schafer, K. V.; McCarthy, H.; Hendrey, G.; McNulty, S. G. & Katul, G. G. (2001), 'Soil fertility limits carbon sequestration by forest ecosystems in a CO₂-enriched atmosphere', *Nature* **411**, 469-471.

Peters, W.; Jacobson, A. R.; Sweeney, C.; Andrews, A. E.; Conway, T. J.; Masarie, K.; Miller, J. B.; Bruhwiler, L. M. P.; Pétron, G.; Hirsch, A. I.; Worthy, D. E. J.; van der Werf, G. R.; Randerson, J. T.; Wennberg, P. O.; Krol††, M. C. & Tans, P. P. (2007), 'An atmospheric perspective on North American carbon dioxide exchange: CarbonTracker', *Proceedings of the National Academy of Sciences of the United States of America* **104**, 18925-18930.

Rodenbeck, C.; Houweling, S.; Gloor, M. & Heimann, M. (2003), 'CO₂ flux history 1982-2001 inferred from atmospheric data using a global inversion of atmospheric transport', *Atmospheric Chemistry and Physics* **3**, 1919-1964.

SOCCR (2007), 'The first state of the carbon cycle report (SOCCR)', Technical report, U.S. Climate Change Science Program and the Subcommittee on Global Change Research.

Tilman, D.; Reich, P.; Phillips, H.; Menton, M.; Patel, A.; Vos, E.; Peterson, D. & Knops, J. (2000), 'Fire Suppression and Ecosystem Carbon Storage', *Ecology* **81(10)**, 2680-2685.

Zimov, S. A., E. A. G. Schuur, F. S. Chapin III (2006), Permafrost and the Global Carbon Budget. *Science* **312**, 1612-1613

II. Introduction to the carbon cycle and atmospheric inversions

The Carbon Cycle

Carbon is of particular interest to those studying biogeochemical processes. It is the building block upon which all organisms are built. Photosynthetic organisms, such as plants, capture sunlight and use the energy to reduce carbon dioxide. These organisms release oxygen during the metabolic process. Heterotrophic organisms use the oxygen and subsequently oxidize and extract energy from the organic compounds created by these photosynthetic organisms, returning carbon dioxide to the overall cycle. The location of carbon in the environment as well as the dynamics that govern its movements are critical to scientists in many fields.

Carbon storage and general carbon dynamics

Over 99.99% of the earth's carbon is essentially non-active, buried away in sedimentary rocks and carbonate. The remaining amount consists of about 40,000 PgC in labile pools. The ocean pool is the largest of the labile pools, containing over 95% of this labile carbon mainly in the form of dissolved carbonate and DIC (dissolved inorganic carbon). The remaining non-oceanic labile carbon is distributed between soils, vegetation and the atmosphere in a ratio of approximately 2:1:1 respectively. There are also 4000 PgC in extractable fossil fuel sources. This source of carbon is currently being exploited for energy and enters into the active pool cycle (Fig. 2.1) with no apparent short term mitigating output back into a subsurface pool. There are pathways back to non-labile pools, such as sedimentation processes in the oceans (Tans, 1998), but the time

scales at which they occur are orders of magnitude larger than those associated with fossil fuel extraction for energy.

There are many available pathways by which carbon can be exchanged between different storage

pools. For example, photosynthesis

provides a pathway by which carbon in the atmosphere, in the form of carbon dioxide, is reduced and fixed into vegetative organic matter.

Assuming

steady state dynamics, e.g. constant rates of exchange between pools and constant pool sizes, one can characterize pools in terms of their turnover times, e.g. the pool size divided by the net rate of balanced loss/gain. For instance, the atmosphere exchanges an amount equal to its pool size in the course of about 3 to 4 years. From a modeling standpoint, it is important to note that *turnover time* is just a simple measure of average exchange and does not necessarily imply that every atom of carbon, or even the majority, is exchanged within the turnover time. For example, carbon exchange is much more vigorous within the boundary layer of the atmosphere than in the upper atmosphere, while the carbon that is used to create wood in a Redwood tree, or humus in deep soil,

while the carbon that is used to create wood in a Redwood tree, or humus in deep soil,

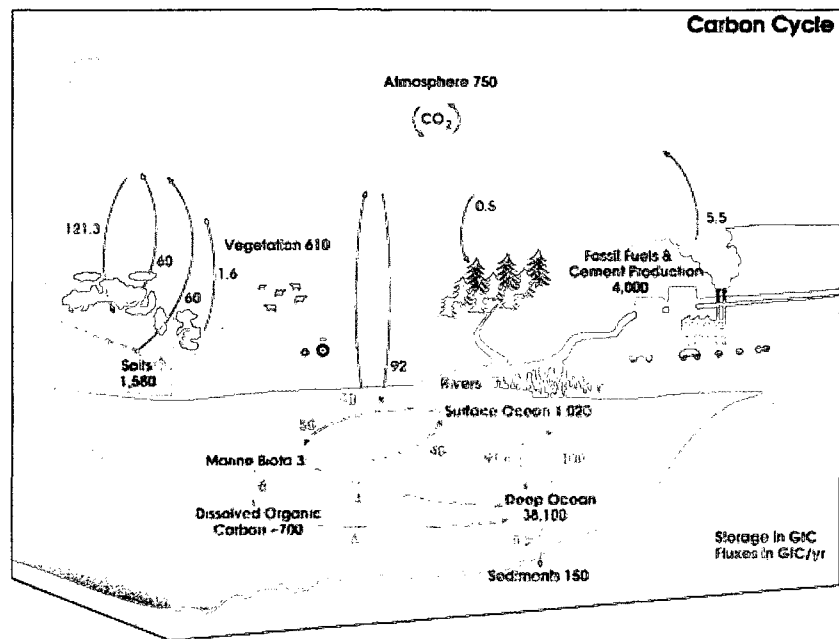


Figure 2.1. The Carbon Cycle (courtesy: NASA)

will likely be there much longer than 10 years. This implies the need for further partitioning of carbon pools, such as those in soils, into subpools homogeneous in content and dynamics in order to provide accurate turnover times. To further illustrate this point, the turnover rates for soil may range anywhere from a decade to several millenia depending upon the location in the soil profile (Schlesinger et al., 1977).

Anthropogenic carbon emissions represent a significant contribution to near surface carbon pools. With the exception of the deep ocean, there is more carbon stored in extractable fossil fuel

pools than in the atmosphere, the upper ocean, soils, and vegetation combined. However, the rate at which it enters the atmosphere is small relative to the rate of exchange of carbon between the atmosphere

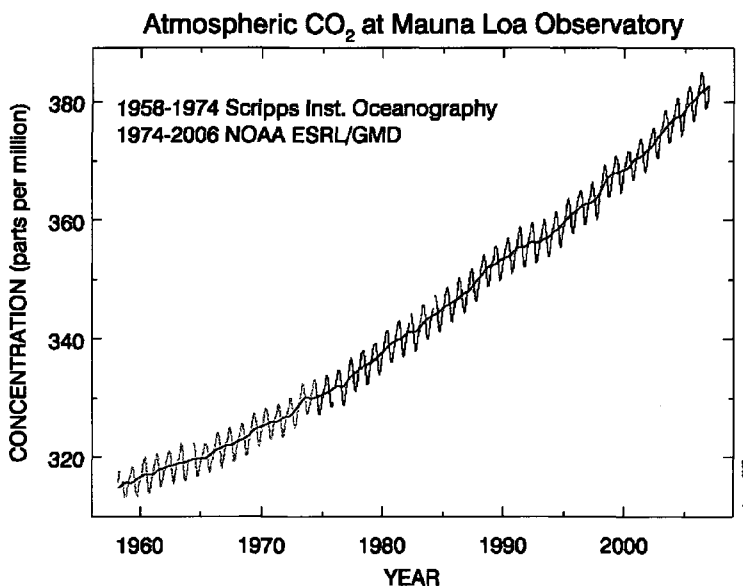


Figure 2.2. Carbon dioxide record from Mauna Loa Observatory (NOAA)

and other near surface pools, namely the shallow ocean and terrestrial biosphere. Anthropogenic carbon dioxide emissions are estimated around 8 PgC/yr while the atmosphere annually exchanges around 200 PgC/yr with terrestrial and oceanic carbon pools. This becomes important in a signal-to-noise context because the annual terrestrial and surface ocean exchanges are so much larger than the annual anthropogenic carbon

signal. It is also uncertain what effect incorporating the fossil fuel reserves into the near surface carbon cycle will have on the vegetative, soil, and atmospheric pools and their associated dynamics.

The issue of scale in carbon dynamics

Carbon dynamics must be understood better in order to predict future carbon cycle dynamics under increased carbon scenarios. Knowledge of the carbon cycle can be obtained at many different spatial and temporal resolutions, each of which might be of interest to different researchers. For plant physiologists, this knowledge might consist of a better understanding of temporally fine plant carbon assimilation rates at the leaf level and how these measurements scale to canopy estimates under differing light conditions and nitrogen levels. Foresters and farmers might be interested in the effect that increased carbon dioxide concentrations has on biomass production (Long et al., 2006). Ecologists might wonder if increasing the carbon dioxide concentrations in the atmosphere, considered along with increased nitrogen deposition, would provide a certain species with a competitive advantage over another (Zhu et al., 2007). Increasing carbon dioxide in the atmosphere could affect mesoscale weather through global warming and this might interest atmospheric scientists (Elsner et al., 2008). A different kind of data is required to answer each of these questions, often at different scales in both time and space.

At the finest spatial and temporal scales, carbon dynamics are driven by the physiological responses of plants and microbes to varying environmental conditions (Farquhar et al., 1980). Given the difficulty of obtaining isolated fine scale measurements of carbon flux in the field, most leaf level flux measurements must be

performed in a laboratory setting. These laboratory results of leaf level physiology are then used extensively in process-based models of photosynthesis (Sellers et al., 1996). This is often performed by making broad assumptions about photosynthesis in the canopy, as a function of height, in order to simplify modeling equations. These results are then extrapolated in space to reach canopy level flux estimates. Although uncertain and variable due to the upscaling, these microscale measurements have been critical to resolving sub-diurnal net ecosystem exchange (NEE) rates and associated effects in the surface energy balance in coupled atmosphere-biosphere models (Baker et al.2003, Denning et al., 2003).

Inferences may be made about NEE at very coarse levels, such as continental-scale to global scale, by using atmospheric carbon dioxide data and satellite-based estimates of NPP. The ocean is a relatively homogeneous pool of carbon governed by equilibrium chemistry relationship in contrast to the very dynamic heterogeneous land pool. Being governed by relatively simple chemistry and covering over 70% of the earth's surface, the oceans provide a strong constraint for inferences to be made about carbon transfer at continental scales (Tans 1998). Due largely to the ability to accurately estimate ocean fluxes, researchers have been able to use inversions on a variety of trace gases to partition carbon fluxes between the ocean and land (Tans et al., 1990; Battle et al., 2000). Carbon fluxes over land may be further partitioned via empirical relationships between satellite-based measures such as normalized difference vegetation indices (NDVI) and ground based measurements. The annual cycle of carbon flux is well understood relative to interannual and subannual scales and large scale circulation patterns of the atmosphere are also well understood. By using crude estimates of land

and ocean fluxes, coarse relationships between many pools can be established. Atmospheric carbon dioxide inversion studies performed at the global scale have provided strong evidence for the widely accepted hypothesis of a northern hemispheric land carbon sink over the last two decades (Tans et al., 1990; Fan et al., 1998; Rayner et al., 1999; Gurney et al. 2002). The spatial details of this sink are still relatively unknown but the results have allowed researchers to focus their efforts at finer scales in the area of the sink in order to better understand the mechanistic foundation for these continental-scale sources/sinks (Goodale et al., 2002).

With the increasing realization of the importance of land use change and agricultural practices to the carbon cycle, questions have become more focused on spatial and temporal resolutions that are tangible either in a management sense, (e.g. a large expanse of agricultural land, a national forest, or a watershed managed over the course of a few years to several decades), or in a mechanistic and biologically informative way, (e.g. a young pine forest, a mature old growth forest, or a forest downwind of pollution sources). Research has shown that eddy covariance methods can be used to estimate carbon fluxes between the atmosphere and an area of land at these scales (Baldocchi et al., 2003; Barford et al., 2001). It is important to note that the eddy covariance method measures the combined effect of the land on atmospheric carbon dioxide, including the effect of microbial respiration in the soil, and thus is a measure of the net ecosystem exchange (NEE) of carbon and not the net primary productivity (NPP). The footprint, or the area of influencing fluxes, of these eddy covariance measurements is usually on the order of less than a square kilometer. These measurements provide information from which hypotheses about mechanistic details of carbon transfer can be tested. For

example, important local-scale experiments have been run using this technique, such as the effect of stand-age on NEE (Amiro et al., 2001).

Ground-based field studies are another important tool in increasing the understanding of the carbon cycle at the scales just mentioned. Recent field research has shown that soil organic matter pools are sensitive to varying agricultural practices, such as tilling, grazing, and crop rotations. (Robertson et al., 2000, Peterson et al., 1998). A long term controlled burn experiment in Minnesota provided evidence of decadal scale carbon sinks in managed forests (Tillman et al. 2000). These appeared to double the carbon sequestration rate of certain forests over a 50 year time span. It is important to note that these types of results can only be generalized to a certain degree. For example, if a pine forest in western Colorado has been a net carbon sink over the past decade, does not necessarily imply that a pine forest in New Jersey would also be a sink over that time period. Differences between the two forests might include forest management strategies, local climate, and potential fertilization effects from local pollutants.

Despite the implied regional scale of many mechanistically based “missing sink” hypotheses (e.g. nitrogen fertilization, forest management practices, and land use change), there has been little direct research explicitly exploring carbon dynamics at this scale which lies somewhere between the global level and those scales obtainable in eddy covariance studies. One method might be to extrapolate this information from finer scale eddy covariance measurements. For example, one could hypothesize about the impact that nitrogen deposition in conjunction with increased atmospheric carbon dioxide levels might have on the eastern U.S. forests by extrapolation of controlled ecosystem experiments (Oren et al., 2001). The biosphere is heterogenous though and it can be

difficult to predict soil fertility and nitrogen deposition rates such that a proper extrapolation can be performed. Eddy covariance towers are generally representative of a very small, flat, homogeneous area of the biosphere. The tower flux footprints are also often less than one square kilometer, making the general extrapolation of results to other areas uncertain. Furthermore, if an important variable is missing from the extrapolation, such as forest regrowth (proxied by stand age) or warming atmospheric temperatures, the extrapolation can be biased (Schimel et al., 2000). Therefore it is often very difficult to produce an accurate process-based upscaling of fine scale carbon fluxes without extensive knowledge of the underlying processes and how they interact.

Another seemingly plausible, and admittedly cheaper, method would entail interpolating fine scale flux inferences from coarser flux inversion models such as [Gurney et al., 2002]. However, this method is highly sensitive to model assumptions and often leads to biased results (Kaminski et al., 2001). Using a novel receptor-based inversion methodology (Lin et al., 2003, Gerbig et al., 2003) and thoroughly testing the sensitivity of model assumptions, it is possible to perform atmospheric inversions at the “hypothesis” scale previously mentioned. Mechanistic hypothesis of carbon dynamics may be tested by combining atmospheric transport (at a scale comparable to the hypothesis), geostatistical techniques, and aggregation of flux regions into regions in which fluxes may be estimated with some statistical certainty. This represents a unique departure from simply constructing hypotheses by simple geographic regions or biome type. Beyond simply validating or invalidating a hypothesis, which can be done as well, hypotheses may be forged by the ability to estimate fluxes at a variety of scales in time and space, and over a variety of potential relevant variables. An advantage to

atmospheric inversion methodology is that the effect of all variables of importance to flux prediction are implicitly included within the model through the atmospheric carbon dioxide concentrations.

Inversion models generally lack an explicit underlying conceptual model which can cause problems in some scenarios. The *aliasing* of variable estimates is a problem that can occur when two signals are not distinguishable. For example, too much soil respiration or too little plant assimilation during midday summertime conditions can both lead to larger carbon dioxide concentrations in the atmosphere. Therefore if the observations show larger carbon dioxide concentrations than the a priori model does, it is not necessarily easy for the inversion model to distinguish whether it should lessen the gross primary productivity (GPP) or increase the ecosystem respiration (ER) since both have the similar effect of increasing carbon dioxide in the atmosphere. If the height of the planetary boundary layer (PBL), the top of the ‘box’ in which the biosphere carbon flux signals mix effectively on a diurnal basis, is biased too high, then the effect of GPP on the atmosphere in the model will be too weak, forcing the inversion to amplify GPP or reduce ER to match observations. Without a mechanistically based constraint relating all these different variables, it is often difficult to distinguish these signals. Inversion methodology should, in theory, be able to include a very complex process based model for which parameters are estimated during the inversion process. Increasing the complexity of the underlying model generally leads to a need for more parameters and must be balanced by the amount of constraining data that is available.

Atmospheric inversion models are designed to use collected data to capture “snapshots” of source/sink activity in a specified time frame. Although results can be

used to refine biogeochemical or dynamic global vegetation models (DGVM), which in turn are able to forecast into the future and better predict future dynamics, the methodology is inherently based upon collected data. Nevertheless, in a statistical sense, the atmospheric inversion methodology is a framework within which many mechanistically based hypotheses can be invalidated. Before forward-in-time process-based models of carbon transfer can accurately predict future sinks and sources, the exact mechanisms behind the sources and sinks must be illuminated. Statistically defensible atmospheric inversion models have the capability to assist in this process through hypothesis-based learning.

Modeling carbon dioxide dynamics

In the atmosphere

Accurate atmospheric transport is critical to estimating carbon dioxide fluxes via an atmospheric inversion methodology. Inversions rely upon the ability to “connect” upwind carbon fluxes on land, with downwind concentration measurements in the atmosphere. From a modeling standpoint, transport can be provided via a fully prognostic model, such as a global circulation model (GCM) or a regional atmospheric model (e.g. RAMS, MM5, or WRF), or from off-line analyzed winds (e.g. ETA, NCEP, or RUC). The choice of model often depends upon the region and resolution of the interest. Although carbon dioxide is biologically active via the metabolic activities of plants, once in the atmosphere, carbon dioxide is relatively inert (chemically). As a result of this, its forward-in-time or backward-in-time transport in the atmosphere can be

modeled as a simple *tracer*, essentially following the winds produced by a meteorological model.

It is important that the meteorology model chosen for an inversion reflects the scale at which the inversion will be performed and capture important transport dynamics at that scale. To a first order, on the global scale, advective transport is the strongest transporter of atmospheric constituents. This transport, which is dominated by meridional flow, creates a zonal gradient in CO₂ when it is convoluted with seasonally varying carbon fluxes. At this scale, large diurnally-driven biospheric fluxes are smoothed and the seasonal cycle is the main effect seen. A careful interpretation of the Mauna Loa CO₂ record in Fig. 2.2 shows a seasonal cycle at the annual scale, increasing during the northern hemisphere winter and decreasing during the northern hemisphere summer. At a finer scale, synoptic weather patterns including cyclones and anti-cyclones provide the main mechanism for north-south mixing of this seasonally-driven zonal gradient. Recent work has shown that these synoptic patterns provide a significant source of small scale spatial variability in CO₂ concentrations (Wang et al., 2006). In particular, it has been shown that CO₂ can often collect along weather fronts and provides enormous variability in CO₂ concentrations over the matter of hours (Chan et al. 2004, Parazoo 2007) which is critically important when comparing modeled CO₂ to observed CO₂ on sub-diurnal time scales.

Global *inversions* have typically been performed at resolutions of from 3.75 degrees latitude by 5.0 degrees longitude (Michalak, 2004), for geostatistical-based inversions, up to continental scale (Gurney et al. 2002) and larger (Fan et al., 1998) for inversions built upon basis functions (see *Examples*, pg. 30) and aggregation. Inversions

that provide the ability to make inferences about aggregated continental-scale regions (Gurney et al. 2002) still must use gridded transport estimates at a much higher resolution in order to capture atmospheric dynamics correctly. For example, in global transport models it is important to resolve features such as large scale circulation patterns while conversely, some finer-scale features such as vertical mixing processes can be coarsely estimated (i.e. by parameterization). The uncertainty and variability of transport across similar scale transport models must be estimated, and propagated forward into the inversion methodology, in order for one to be confident in inversion-based carbon flux estimates. The variability of global transport models was studied extensively in the Transcom 2 experiment (Denning et al., 1999) using 11 global circulation models with grid sizes between 2.5° latitude by 2.5° longitude to 7.5° latitude by 7.5° longitude. Results showed reasonable success from the models at simulating meridional gradients. Differences in meridional gradients between the global transport models could likely be attributed to vertical transport schemes in the models, particularly over land.

Regional inversions require regional meteorology models. There are similarities and differences when comparing regional and global atmospheric transport models. The resolving of vertical transport, especially near the surface, parameterizations or direct resolution of convective and turbulent processes, and identification of boundary layer heights are problems that are common to both scales of model but are particularly important to finer scale regional models. For example, the comparison of modeled results to observations on hourly time scales requires that vertical mixing processes be resolved at scales much finer than that of global models. An observation of carbon dioxide at the surface during the night may display positive deviations in CO₂ an order of

magnitude higher than what is seen during the daylight periods of carbon drawdown due to the smaller volume (i.e. as a function of height) under which the biospheric fluxes are being mixed. The varying dynamics of vertical mixing under nocturnal and daytime conditions must be captured in order to avoid mischaracterization of fluxes. A bias in boundary layer height, the height at which biosphere carbon fluxes readily mix up to in the atmosphere, can be of great importance to models at all scales, particularly if the bias is not random and persists in time and/or space (McGrath-Spangler et al., 2008). One of the more difficult issues somewhat unique to regional transport modeling is the necessary specification of boundary conditions for the domain, including both atmospheric constraints and carbon dioxide concentrations. This can become very important when the temporal variability of the boundary condition carbon dioxide is as large, or larger, than the variability of carbon dioxide within the domain of interest.

Several difficulties can be encountered in the statistical modeling of atmospheric transport. There is a high probability that errors arising from incorrect models of transport, at any resolution, will be correlated in both time and space. This is due to the continuous nature of atmospheric transport. Assume that one has a transport operator which summarizes transportation of particles in three dimensions. Releasing two particles arbitrarily close in space at time t_1 should result in the two particles being arbitrarily close in space at any time $t_1 + t$. Small errors in initial particle locations, or atmospheric transport fields should give rise to small errors in final particle locations. This error arises in inversion modeling when a *tracer* is released from the surface at some point and carried a distance *downwind* to an observation point. This observation point has some type of sensitivity to the *upwind* flux. There is an error in this sensitivity due to

potential transport errors. Not only must this error term be estimated (for each *upwind* flux region) but also the correlations between this error and the errors in sensitivity between this observation point and other *upwind* flux regions. In general, a lack of accounting for correlation in errors, whether temporal or spatial, will often lead to a false degree of confidence in estimates.

In the biosphere

The biosphere has a strong effect on carbon dioxide concentrations near the ground. Through photosynthetic activities, carbon dioxide is reduced by plants and converted to organic matter. Water is lost in the process of photosynthesis, in turn affecting the overall energy budget at the surface. In order to construct a truly coupled atmosphere-biosphere carbon model that is accurate on fine time scales (e.g. diurnal, for instance), one must capture the carbon and water exchanges correctly while maintaining a correct energy balance. A portion of the carbon that is assimilated into biomass is processed into perennial woody tissue while some of the carbon that is stored in biomass is lost to events such as litterfall and eventually decomposes. Diurnal-scale atmosphere-biosphere interactions are generally not very sensitive to the actual fate of the carbon assimilated. However, on longer timescales, variations in carbon allocation dynamics become more noticeable. Modeling schemes must either explicitly model these dynamics or provide a mechanism through which temporal variations can be parameterized.

Certain facets of carbon dynamics are known better than others. For instance, when the sun comes up in the morning the leaves begin to photosynthesize and generally continue to do so until the sun goes down in the evening. In locations to the north or

south of the equator, and in the warmth of summer, plants are usually healthy and photosynthesizing strongly during the day. Winter conditions are usually colder and less hospitable, many plants lose their leaves and GPP is greatly reduced. These (seasonal and diurnal) are the biggest sources of variability in carbon dioxide concentrations and fluxes and are generally understood and simulated fairly accurately. However, variability in carbon fluxes does not appear on seasonal and diurnal time scales alone. Anthropogenic land-use change (Houghton et al., 1999), variations in the dynamics of long turnover time soil organic matter pools (Zimov et al., 2006), CO₂ fertilization effects of increased atmospheric CO₂ (Oren et al., 2001), effects of nitrogen deposition, changing disturbance regimes such as fire/succession/regrowth dynamics in large expanses of forests (Tillman et al., 2000) all contribute to carbon fluxes on various scales that are often not captured in model simulations. Certain models may accurately predict one or more components while not including others and it is difficult to assume that *all* of these processes can be identified a priori and modeled explicitly. Therefore, deterministic forward simulations of the biosphere often try to capture as many aspects as possible, while focusing more on those with heavier consequences to their particular study, and leave those which are unknown, unexplored, or difficult to model, to atmospheric inversions to capture.

The particular land surface parameterization that is coupled with the RAMS meteorological model for the inversions in this dissertation is based upon the third generation simple biosphere model (SiB3) developed by Piers Sellers (Sellers et al. 1996). The model characterizes carbon, water, and radiation fluxes between the atmosphere and the terrestrial canopy, soil, and snow layers. SiB3 does not explicitly

model the storage of carbon in any reservoir other than the atmosphere. The SiB3 model includes a realistic photosynthesis-conductance model that describes leaf level transfer of CO₂ and water vapor. This is critical not only for the modeling of carbon dioxide but for maintaining realistic surface level energy fluxes of latent and sensible heat. The original SiB3 model used satellite derived NDVI data to derive the fraction of photosynthetically available radiation (FPAR) (i.e. which provides the energy source for photosynthesis) and the one-sided green leaf area per unit ground surface area, leaf area index (LAI), over which the radiation is theoretically applied. For this dissertation, SiB3 code was changed to incorporate satellite-derived Moderate Resolution Imaging Spectroradiometer (MODIS) data, in particular the FPAR and LAI data products (MOD15). Additional modifications to the biosphere scheme in SiB3 include a more detailed soil column consisting of 10 layers, a more detailed snow column consisting of 5 layers, and a more accurate soil water stress response curve. One particularly important characteristic of the model is that it is a net-zero annual flux model, implying that annually summed NEE fluxes in any one cell of the model grid must equal zero. Given the relative magnitude of annual NEE with respect to seasonal maximums and minimums of NEE (Michalak et al., 2004), this zero flux annual requirement is probably valuable in constraining day to day diurnal flux activity when accurate coupling to biogeochemical models is not available. The importance can be conceptualized by considering that systematic biases in ER and GPP on the very fine time scales of a biophysical model, such as SiB, could quickly add up to unrealistic NEE values annually. However, there is a wide body of evidence in support of inter-annual variability in NEE and SiB3 does not currently accommodate this. This illustrates an important requirement of any atmospheric inversion model that is to be

used in conjunction with SiB3. Given the realistic expectation of non-zero annual fluxes, the inversion method must provide flexibility such that the estimated corrected NEE is not constrained to an annual sum of zero. This will be discussed more in Chapter 3.

Inversion Methods

Atmospheric carbon dioxide concentration measurements contain information about carbon fluxes in the terrestrial biosphere and oceans. As an example, assume that the carbon dioxide fluxes of the biosphere and their associated local changes on the surrounding carbon dioxide concentrations are known. Recall that carbon dioxide is essentially chemically inert in the atmosphere. If atmospheric tracer transport of carbon dioxide can be predicted through the use of a meteorological model, then one can predict what carbon dioxide concentrations should be in the atmosphere, at any point in space and time. Alternatively, if the carbon dioxide flux pattern is unknown and perhaps guessed incorrectly, and the transport process is correctly modeled, then one will incorrectly predict carbon dioxide concentrations.

Atmospheric inversion techniques employ this concept to attempt to correct for these initial carbon flux guesses in such a way as to reduce the differences between “expected” modeled carbon dioxide concentrations and actual carbon dioxide measurements. If sufficient carbon dioxide concentration data exists to constrain the problem then a regular least squares, or weighted least squares, approach can be applied. In a statistical regression framework, the design matrix, G , summarizes the atmospheric transport of the fluxes via the Jacobian matrix (partial derivatives of carbon dioxide

concentration at different sampling locations with respect to different carbon dioxide fluxes), β represents a vector of bias factors, and y represents the carbon dioxide observations. The matrix Σ denotes the covariance between the (assumed) mean zero multivariate normal error terms, $\varepsilon = \mathbf{G}\beta - y$. For n carbon dioxide observations and m contributing carbon dioxide flux regions, the model is then

$$y = \mathbf{G}\beta + \varepsilon \quad (1)$$

$$\text{e.g. } \begin{bmatrix} y_1 \\ y_2 \\ \cdot \\ \cdot \\ y_n \end{bmatrix} = \begin{bmatrix} G_{11} & G_{12} & \cdot & \cdot & G_{1m} \\ G_{21} & G_{22} & \cdot & \cdot & \cdot \\ \cdot & \cdot & \cdot & \cdot & \cdot \\ \cdot & \cdot & \cdot & \cdot & \cdot \\ G_{n1} & \cdot & \cdot & \cdot & G_{nm} \end{bmatrix} \begin{bmatrix} \beta_1 \\ \beta_2 \\ \cdot \\ \cdot \\ \beta_m \end{bmatrix} + \begin{bmatrix} \varepsilon_1 \\ \varepsilon_2 \\ \cdot \\ \cdot \\ \varepsilon_n \end{bmatrix}$$

For a full rank matrix \mathbf{G} , the solution to this problem is

$$\hat{\beta} = (\mathbf{G}^T \Sigma^{-1} \mathbf{G})^{-1} \mathbf{G}^T \Sigma^{-1} y \quad (2)$$

and the variance of this estimator is

$$\text{var}(\hat{\beta}) = (\mathbf{G}^T \Sigma^{-1} \mathbf{G})^{-1} \quad (3)$$

This is not necessarily a unique solution. If the row rank of \mathbf{G} is less than the column rank of \mathbf{G} , and \mathbf{G} is full rank, then there will be an infinite number of “least squares” solutions and the solution shown above can appear meaningless in application.

One method to deal with this is to aggregate flux regions (Tans et al., 1990; Enting et al., 1995; Fan et al., 1998;), essentially reducing the column rank of \mathbf{G} so that a unique solution may be constructed. A common way in which flux regions are

aggregated is by fixing a prescribed pattern of fluxes over a region, which is then allowed to increase or decrease linearly in order to fix the observed data. This aggregation could prescribe relative patterns in flux between regions (Fan et al. 1998) or could be a simple *adjoining* of different regions, assuming that their fluxes are the same (Rayner et al. 1999). Temporal patterns, such as seasonal patterns of flux, can also be forced upon the data. These patterns in time and space, are often referred to as basis functions.

[Kaminski et al., 2001] illustrated that if the flux regions are aggregated to form “coarser” inversion regions than those used in the atmospheric transport, then an additional source of error (termed “aggregation error by Kaminski et al., 2001) must be accounted for. There has been subsequent research into the estimation of this error term (Engelen et al., 2002) and as a result, some researchers have moved towards performing inversions based on grids with resolutions similar to that of their transport model (Rodenbeck et al. 2003).

Another technique to dealing with an unconstrained inversion problem is to use Bayesian methodology to constrain the carbon flux estimates to an a priori “best guess” estimate (Gurney et al., 2002). These latter inversions are commonly referred to as Bayesian synthesis inversions (Tarantola 1987). There have also been a variety of recent modifications and extensions of the Bayesian synthesis inversion approach (Michalak et al. 2004). Many inversions have used a combination of the aggregation technique and the Bayesian synthesis inversion (Enting et al., 1995; Rayner et al., 1999; Gurney et al., 2002).

Bayesian Synthesis Inversion

Bayesian methods are used to provide solutions to under-constrained problems in a variety of applied settings (Tarantola, 1987; Gelman et al., 2004; Banerjee et al., 2004). Tarantola (1987) is one of the earliest, and widely cited, references of the Bayesian methodology being applied to the atmospheric chemical transport inversion problem. Recall from the last section, the statistical model and least squares solution to a “well-constrained” inversion problem (one in which the number of unknowns is less than the number of observations). Under the assumption of multivariate normally distributed error terms, the solution can be characterized in terms of the minimization of the following cost function

$$C(\boldsymbol{\beta}) = (\mathbf{G}\boldsymbol{\beta} - \mathbf{y})^T \boldsymbol{\Sigma}^{-1} (\mathbf{G}\boldsymbol{\beta} - \mathbf{y}) \quad (4)$$

If there is not sufficient data to constrain the inversion to a unique solution, then the addition of a “penalty term” to the cost function will have the effect of keeping the solution close to a specified a priori flux, given by $\boldsymbol{\beta}_0$. Assuming the difference between the actual fluxes and a priori fluxes is multivariate normally distributed, this cost function can be written as

$$C(\boldsymbol{\beta}) = (\mathbf{G}\boldsymbol{\beta} - \mathbf{y})^T \boldsymbol{\Sigma}^{-1} (\mathbf{G}\boldsymbol{\beta} - \mathbf{y}) + (\boldsymbol{\beta} - \boldsymbol{\beta}_0)^T \boldsymbol{\Sigma}_0^{-1} (\boldsymbol{\beta} - \boldsymbol{\beta}_0) \quad (5)$$

Notice that as \mathbf{x} moves away from the a priori flux $\boldsymbol{\beta}_0$, the second term in the equation above increases, essentially “penalizing” the solution for moving to far away from $\boldsymbol{\beta}_0$. The covariance of the errors between the actual fluxes and the a priori solution, $\boldsymbol{\Sigma}_0$,

dictate the strength and correlations of the penalty across individual carbon dioxide fluxes.

It is informative to explain the Bayesian statistical model underlying this cost function. Assume that our observations are distributed normally around mean $G\beta$ with known covariance matrix Σ . Furthermore, assume that x is a random variable and it is distributed normally around known mean β_0 with known covariance matrix Σ_0 .

$$\begin{aligned} y | \beta, \Sigma &\sim N(G\beta, \Sigma) \\ \beta &\sim N(\beta_0, \Sigma_0) \end{aligned} \tag{6}$$

The posterior distribution of μ can then be derived and is also normally distributed.

$$\begin{aligned} p(\beta | y, \Sigma) &\propto -\frac{1}{2} \left[(G\beta - y)^T \Sigma^{-1} (G\beta - y) + (\beta - \beta_0)^T \Sigma_0^{-1} (\beta - \beta_0) \right] \\ &= N \left(\left(\Sigma_0^{-1} + G^T \Sigma^{-1} G \right)^{-1} \left(\Sigma_0^{-1} \beta_0 + G \Sigma^{-1} y \right), \left(\Sigma_0^{-1} + G^T \Sigma^{-1} G \right)^{-1} \right) \end{aligned} \tag{7}$$

Thus the posterior mean of the fluxes can be seen to be a precision¹-weighted average of the data and the prior mean. The posterior precision is the sum of the data precision and the prior precision.

Examples

In addition to being a Bayesian synthesis inversion application, the Transcom 3 project provided a transport-sensitive intercomparison of atmospheric carbon dioxide inversions. For each inversion, the earth's surface was divided into 11 land regions and

¹ Precision is the inverse of variance. In Bayesian methodology, precision is often used to characterize variance.

11 ocean regions (Fig. 2.3). Each land region was associated with a “basis function”², a fixed relative pattern of annual flux based upon annual NPP estimates provided by the CASA model (see Fig. 2.4).

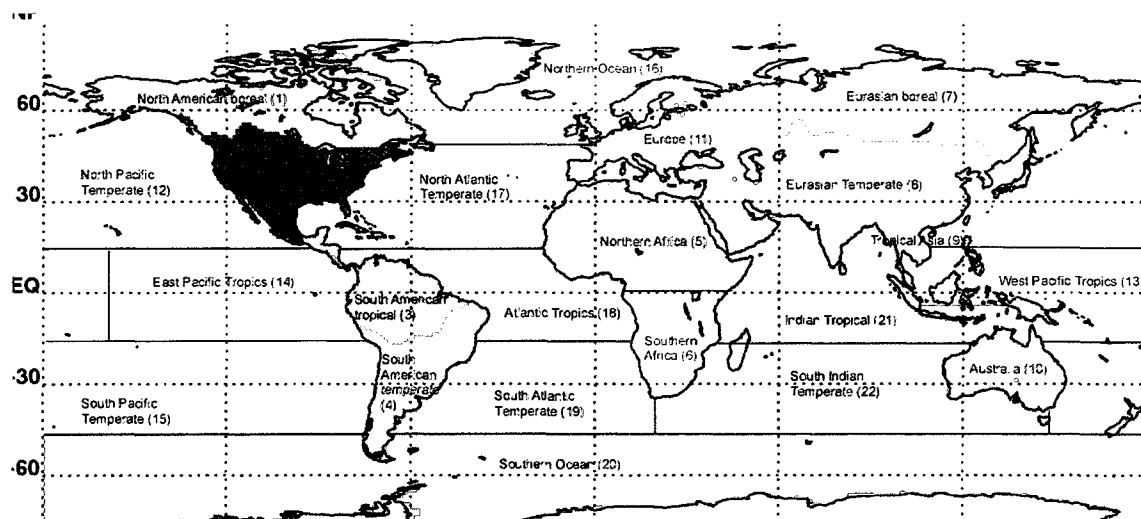


Figure 2.3: Transcom Basis Regions (Gurney et al., 2000)

Similarly, ocean region basis functions were formed based on mean carbon exchange maps and sea-ice patterns. The Jacobian matrix, representing the influence of carbon fluxes to particular observations in time and space, was calculated by simulating independent pulse releases from each basis function. This portion of the inversion was allowed to vary, with different Jacobians calculated for each of 16 different transport models. The prior distributions of the fluxes were constructed from various ocean and terrestrial flux models, and fossil fuel inventory estimates and are shown in Fig. 2.5.

Seventy-six stations provided carbon dioxide observations at various locations around the world for the five year period of 1992-1996 (Fig. 2.5). Important conclusions from the Transcom project included a temperate North American sink estimate that was 60% of that of an earlier study (Fan et al., 1998) and a more uniformly distributed sink over the

² These basis functions form the controversial and aforementioned *aggregation* portion of the inversion (Kaminski et al., 2001)

Northern hemispheric land regions. Given the extensive investigation of transport and the inclusion of several transport models, the flux distribution estimates should be considered robust with respect to transport.

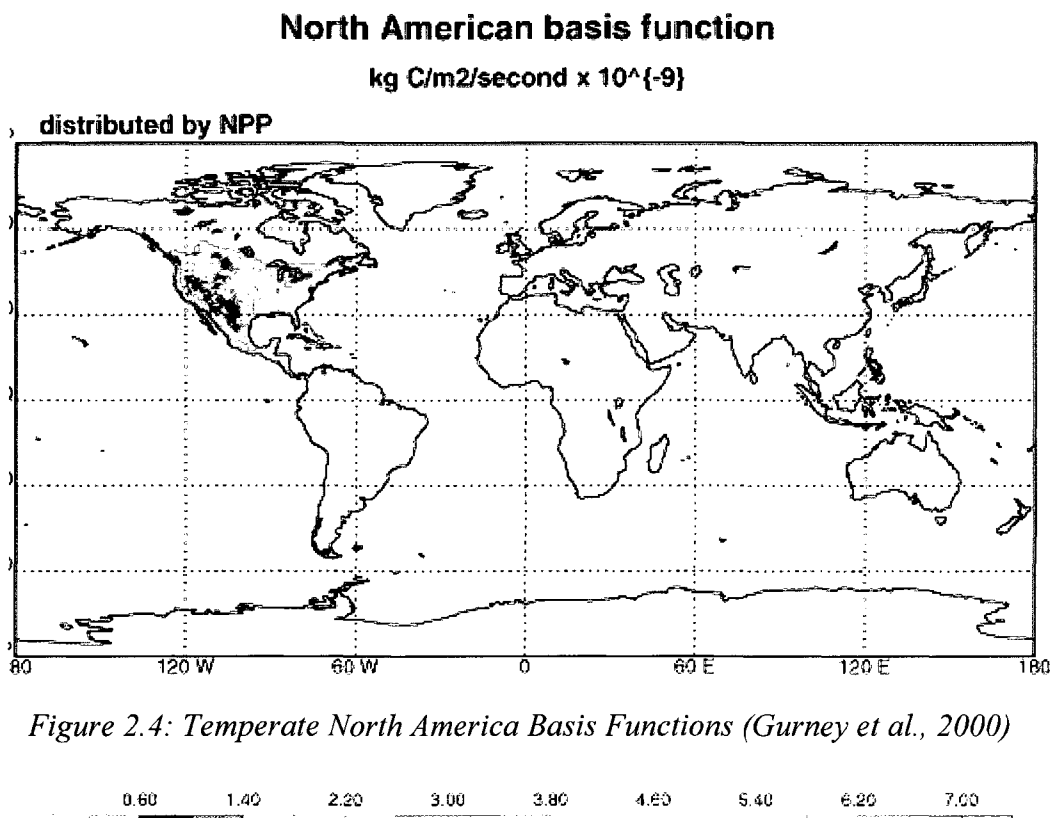


Figure 2.4: Temperate North America Basis Functions (Gurney et al., 2000)

Many of the difficulties surrounding the Bayesian synthesis method concern the specification of the prior flux distribution. In essence, this is the analog of the problems one encounters when aggregating flux regions in order to arrive at a unique solution. Without data to support the pattern of fluxes between flux regions, it is difficult to justify imposing a pattern upon flux regions. Similarly, without explicit a priori knowledge of the nature of the true fluxes, it is difficult to justify a prior flux distribution. External data, independent to the inversion, can often be used to support these prior specifications.

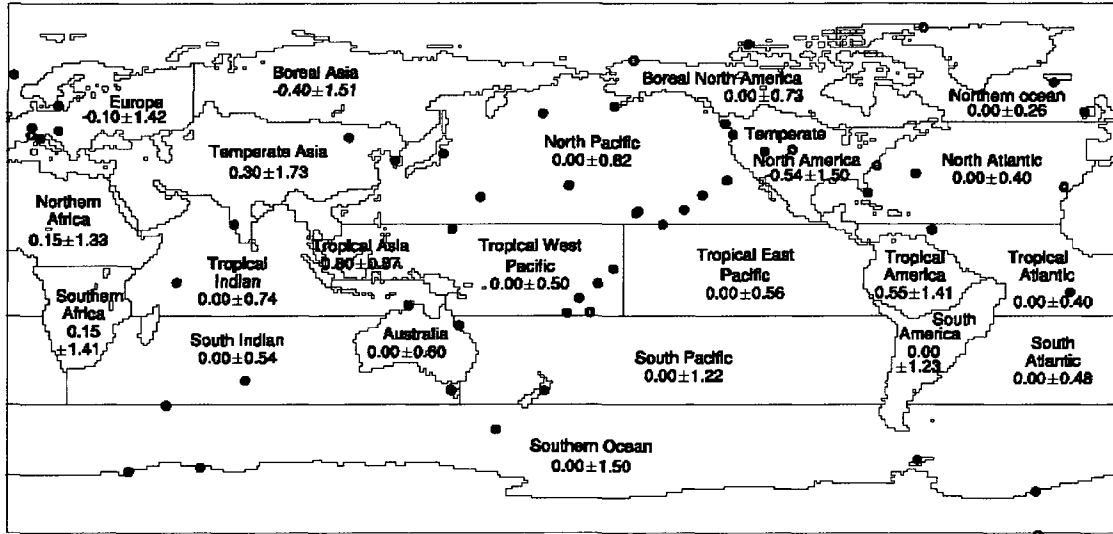


Figure 2.5: Carbon dioxide observing network used in Transcom 3 with normal prior distributions specified (mean \pm s.d.) (Gurney et al., 2003)

Examples include the extrapolation of ground-based measurements of NEE (Enting et al., 1995), modeling of satellite derived vegetation indices (Matross et al., 2006), the use of a fully coupled atmosphere/biosphere model (Wang et al. 2006) . The more difficult, and often more controversial, part of the prior specification involves estimating the covariance matrix which describes the distribution of differences between the actual fluxes and the a priori fluxes. Obtaining an estimate of the variance of these prior flux estimates can be difficult and incorrect specifications can easily lead to unreasonable inversion results. Both of these problems can be mitigated, to some degree, by formalizing the estimation of the prior flux and prior flux variance. This can be done by replacing β_0 in the cost function (Eq. 5) with a statistical model of the prior mean. Michalak (2004) proposed the following model

$$x = D\beta + \varepsilon \quad (8)$$

Where x is a $m \times 1$ vector of the fluxes, D is a known $m \times p$ matrix, β is a $p \times 1$ vector of unknown drift coefficients, and ε is a zero mean multivariate normal random variable

representing the spatially correlated error in the estimate of the fluxes. The **D** matrix might consist of various underlying geographically referenced data, such as satellite-based NDVI and land cover maps, from which the mean flux could be estimated. This method is attractive because it formalizes the estimation process and forces the underlying data to explain the entire flux estimate through a formal statistical spatial model. The estimation and validation of an appropriate spatial covariance structure is important part of this method.

Michalak et al., [2004] presents a sample application of the geostatistical modification to the Bayesian synthesis inversion. The authors employ an annually averaged global carbon flux field with ocean and fossil fuel fluxes from the Transcom 3 project (Gurney et al., 1998) and net ecosystem production (NEP) estimates from McGuire et al. (2001) for the true underlying annual mean fluxes of the inversion. Basis functions which represent the transport component of the inversion were from Rodenbeck (2003). The inversion is performed on a 3.75° by 5.0° longitude grid which yielded a 48×72 grid. Observations are simulated at a site network similar to Transcom 3 (Fig. 2.5). NEP, fossil fuel, and ocean fluxes are estimated in the inversion. Parameters of the spatial covariance structure were estimated by applying maximum likelihood methods to the marginal distributions of the spatial covariance parameters.

Four different cases are considered by **(A)** imposing and then estimating a single spatial covariance structure for the ocean and land regions, **(B)** imposing and then estimating different spatial covariance structures for the ocean and land regions, **(C)** using **(B)** along with a larger observation variance term, and **(D)** using **(C)** along with the specification that fossil fuel fluxes are *known* as opposed to estimating them separately

from the NEP. Estimated variance in case (A) was higher than the actual variance and the estimated correlation length scale was lower. The main consequence was higher variability and lack of “smoothness” in the ocean flux estimates. This in turn led to a large disparity between the estimated ocean fluxes and the true underlying ocean fluxes. This particular situation improved under case (B) and (C). However, the majority of land flux regions still appeared to be statistically insignificant under both of these cases. Case (D) considered the fossil fuel fluxes known. After the removal of fossil fuel fluxes, the only significant NEP annual mean fluxes were in poorly constrained regions of the world. Consequently, there was difficulty in estimating spatial covariance parameters and the land region carbon fluxes. The “power” of the data then went to producing very accurate ocean flux estimates.

This paper represented the first attempt at using geostatistical methods to estimate carbon flux parameters in an inversion framework. It represents a conceptually meaningful and statistically rigorous method with which to add constraints to carbon fluxes in an inversion methodology. The authors noted particular difficulties encountered because of the small relative magnitude of the annually averaged NEP signal. Estimation of the spatial covariance structure appears to be difficult with the variance often being overestimated and the correlation length scale underestimated. The inversion results appear to be sensitive to the discrepancy in the estimated spatial correlation of the errors. There seems to be a need for further investigation of the spatial correlation structure of the errors and the effect upon inversion results. In particular, the pseudo observations do not appear to constrain the inversion well enough which would appear to warrant the oft asked question in science: *“how much data is enough?”*

State-space extension of Bayesian synthesis inversion method

With increasing amounts of data available for atmospheric inversions, researchers have begun investigating new techniques for estimation. A traditional Bayesian synthesis approach makes use of observations and associated carbon fluxes at many locations in time and space concurrently. As available data grows, we would like to estimate fluxes at finer and finer resolutions, both temporally and spatially. Conventional Bayesian synthesis techniques rely upon a single large matrix inversion as part of the solution process which becomes increasingly difficult with the rising dimensionality of the problem. An alternative is to partition the data temporally and estimate the fluxes dynamically in time. While not as rigorous and statistically complete as a theoretical “all at once” synthesis inversion, the technique promises to handle much larger amounts of data while maintaining many of the traits of the conventional inversion techniques.

The first application of the Kalman filter is generally credited to Stanley Schmidt who applied it to the non-linear navigation problems of the manned lunar missions while he was with the NASA Ames Research Center. Today, it is widely used in science and atmospheric inversion problems are no exception. The general idea centers around the recursive estimation of various model parameters which predict, or assist in predicting, carbon fluxes. The main advantage of the framework is that information is passed from one filter step to the next, both in the form of mean estimates of the model parameters as well as the error covariance of those estimates. The propagation of this information allows future estimates of carbon flux to capitalize upon past information already

processed while maintaining the flexibility to capture estimates of model parameters changing in time. There are a variety of adaptations of the filter that are applied to inversion flux problems and it is the basis from which many inversion systems are built. One of the more exciting adaptations is the ensemble Kalman filter (EnKF) (Evensen et al. 1994) which has been shown to have many favorable qualities for inversion problems involving large amounts of data and non-linear dynamics (Peters et al. 2005, Zupanski et al. 2007). These advantages include the fact that the EnKF does not need an explicit adjoint model and that it uses a smaller solution space than a typical Kalman Filter increasing computational efficiency. Many of the current inversion systems draw upon strengths of all of the aforementioned models, simple Bayesian synthesis, spatial correlation assumptions, and the Monte Carlo sampling aspects of the Ensemble Kalman filter.

Adaptation of global inversion methodology to regional scale inversions

While many individuals are interested in global carbon dynamics and the large scale climate effects induced by changes in the carbon cycle, many are also interested in more local effects. There has been increasing interest in regional scale inversions at the scale of a mesoscale meteorology model. Peters et al. [2005] presented an ensemble Kalman filter based system that optimizes NEE estimates over North America by using a combination of the Carnegie Ames Stanford Approach (CASA) Biosphere model and the TM5 atmospheric transport model. Their approach used optimized fluxes over a set of nested grids with increasing resolution centered over North America. Portions of the approach were used to construct the CarbonTracker system developed by National

Oceanic and Atmospheric Administration (NOAA). Peylin et al. [2005] used a somewhat similar nested approach to optimize daily carbon fluxes over Europe for a period of several months in the summer. High resolution regional inversions introduce difficulties not experienced at the global scale, most importantly, the effect of boundary inflow of CO₂ on the inversion. These previous two papers both included optimized global carbon transport models to provide boundary conditions to the smaller regional domain. While the accuracy of global atmospheric transport is a consideration, so are the potential effects of carbon flux optimization outside the regional domain of interest. For example, a deficit of CO₂ recorded in the Mid Northern United States could be a result of a stronger than expected sink of carbon upwind in the boreal forest of Canada or could be a large scale result of drawdown of carbon far upwind over Siberia. Regional inversions are often considered more difficult than larger scale global inversions because of these considerations.

Summary

The terrestrial carbon cycle presents complex biogeochemical dynamics in both time and space which can make estimation of land-atmosphere fluxes difficult. NEE is one of the main interfaces of this biogeochemical cycle with the atmosphere. When NEE is convoluted by atmospheric transport, one gets increasingly complex patterns of CO₂ across the landscape and into the upper air of the atmosphere. These patterns contain very important information about the ground carbon fluxes but are often hidden behind complex atmospheric transport patterns that operate on varying temporal scales. If the atmospheric transport and carbon fluxes can be organized and modeled properly, based

upon the scales at which they operate, then carbon fluxes can be estimated reliably by inverting (with respect to transport) carbon dioxide data collected at various locations in time and space. The inversion-based estimation process is very efficient when compared to brute force ground based sampling, which is very time and cost intensive. These inversion techniques provide an important, resource efficient, independent line of evidence into carbon flux estimation that will help to increase the understanding of the carbon cycle.

LITERATURE CITED

- Andres, R.J., G. Marland, I. Fung, and E. Matthews, 1996: A 10x10 Distribution of Carbon Dioxide Emissions from Fossil Fuel Consumption and Cement Manufacture, 1950-1990. *Global Biogeochemical Cycles*, 10, 419-429.
- Amiro, B. D. (2001), 'Paired-tower measurements of carbon and energy fluxes following disturbance in the boreal forest', *Global Change Biology* 7, 253-268.
- Baker, I.; Denning, A. S.; Hanan, N.; Prihodko, L.; Uliasz, M.; Vidale, P.; Davis, K. & Bakwin, P. (2003), 'Simulated and observed fluxes of sensible and latent heat and CO₂ at the WLEF-TW tower using Sib 2.5', *Global Change Biology* 9, 1262-1277.
- Baldocchi, D. D. (2003), 'Assessing the eddy covariance technique for evaluating carbon dioxide exchange rates of ecosystems: past, present, and future', *Global Change Biology* 9, 479-492.
- Banerjee, S.; Carlin, B. P. & Gelfand, A. E. Isham, V.; Keiding, N.; Louis, T.; Reid, N.; Tibshirani, R. & Tong, H., ed. (2004), *Hierarchical Modeling and Analysis for Spatial Data*, Chapman and Hall/CRC.
- Barford, C. C.; Wofsy, S. C.; Goulden, M. L.; Munger, J. W.; Pyle, E. H.; Urbanski, S. P.; Hutyra, L.; Saleska, S. R.; Fitzjarrald, D. & Moore, K. (2001), 'Factors Controlling Long- and Short-Term Sequestration of Atmospheric CO₂ in a Mid-Latitude Forest', *Science* 294, 1688-1690.
- Barger, N. N.; Ojima, D. S.; Belnap, J.; Shiping, W.; Yanfen, W. & Chen, Z. (2004), 'Changes in Plant Functional Groups, Litter Quality, and Soil Carbon and Nitrogen Mineralization With Sheep Grazing in an Inner Mongolian Grassland', *Journal of Range Management* 57, 613-619.
- Battle, M.; Bender, M.; Tans, P.; White, J.; Ellis, J.; Conway, T. & Francey, R. (2000), 'Global Carbon Sinks and Their Variability Inferred from Atmospheric O₂ and δ¹³C', *Science* 287, 2467-2470.
- Birdsey, R. A. & Heath, L. S. (1995), 'Productivity of America's Forest Ecosystems', *Forest Service General Technical Report RM-GTR-271*, U.S. Forest Service, Fort Collins, CO, 56-70.
- Caspersen, J. P.; Pacala, S. W.; Jenkins, J. C.; Hurtt, G. C.; Moorcroft, P. R. & Birdsey, R. A. (2000), 'Contributions of Land-Use History to Carbon Accumulation in U.S. Forests', *Science* 290, 1148-1150.
- Chan, D., K. Higuchi, C.W. Yuen, J. Liu, A. Shashkov, J. M. Chen, (2004). 'On the CO₂ exchange between the atmosphere and the biosphere: the role of synoptic and mesoscale

processes.' *Tellus B.* 56: 194-212.

Denning, A. S.; Holzer, M.; Gurney, K. R.; Heimann, M.; Law, R. M.; Rayner, P. J.; Fung, I. Y.; Song-Miao Fan, S. T.; Friedlingstein, P.; Balkanski, Y.; Tayler, J.; Maiss, M. & Levin, I. (1999), 'Three-dimensional transport and concentration of SF₆: A model intercomparison study (Transcom 2)', *Tellus* **51B**, 266-297.

Denning, A. S.; Nicholls, M.; Prihodko, L.; Baker, I.; Vidale, P.; Davis, K. & Bakwin, P. (2003), 'Simulated variations in atmospheric CO₂ over a Wisconsin forest using a couple ecosystem-atmosphere model', *Global Change Biology* **9**, 1241-1250.

Elsner J. B., J. P. Kossin, T. H. Jagger (2008), 'The increasing intensity of the strongest tropical cyclones', *Nature* 455, 92-95

Engelen, R. J.; Denning, A. S. & Gurney, K. R. (2002), 'On error estimation in atmospheric CO₂ inversions', *Journal of Geophysical Research* **107**, (10) 1-13.

Enting, I.; Trudinger, C. & Francey, R. (1994), 'A synthesis inversion of the concentration and δ¹³C of atmospheric CO₂', *Tellus* **47B**, 35-52.

Farquhar, G. D.; Caemmerer, S. V. & Berry, J. A. (1980), 'A biochemical model of photosynthetic CO₂ fixation in the leaves of C₃ species.', *Planta* **149**, 78-90.

Gelman, A.; Carlin, J. B.; Stern, H. S. & Rubin, D. B. Chatfield, C.; Tanner, M. & Zidek, J., ed. (2004), *Bayesian Data Analysis*, Chapman & Hall/CRC.

Gerbig, C.; Lin, J. C.; Wofsy, S. C.; Andrews, A. E.; Daube, B. C.; Davis, K. J. & Grainger, C. A. (2003), 'Toward constraining regional-scale fluxes of CO₂ with atmospheric observations over a continent: 2. Analysis of COBRA data using a receptor-oriented framework', *Journal of Geophysical Research* **108**, ACH 6 1-19.

Goodale, C. L.; Apps, M. J.; Birdsey, R. A.; Field, C. B.; Heath, L. S.; Houghton, R. A.; Jenkins, J. C.; Kohlmaier, G. H.; Kurz, W.; Liu, S.; Nabuurs, G.; Nilsson, S. & Shvidenko, A. Z. (2002), 'Forest carbon sinks in the northern hemisphere', *Ecological Applications* **12**(3), 891-899.

Grosso, S. D.; Ojima, D.; Parton, W.; Mosier, A.; Peterson, G. & Schimel, D. (2002), 'Simulated effects of dryland cropping intensification on soil organic matter and greenhouse gas exchanges using the DAYCENT ecosystem model', *Environmental Pollution* **116**, S75-S83.

Gurney, K.; Law, R. & Rayner, P. (2000), 'TransCom 3 Experimental Protocol', Technical report, Colorado State University, Dept of Atmospheric Sciences.

Gurney, K. R.; Law, R. M.; Denning, A. S.; Rayner, P. J.; Baker, D.; Bousquet, P.; Bruhwiler, L.; Chen, Y.; Clals, P.; Fan, S.; Fung, I. Y.; Gloor, M.; Helmann, M.; Higuchi,

- K.; John, J.; Maki, T.; Maksyutov, S.; Masarle, K.; Peylin, P.; Prather, M.; Pak, B. C.; Randerson, J.; Sarmiento, J.; Tagucki, S.; Takahashi, T. & Yuen, C. (2002), 'Towards robust regional estimates of CO₂ sources and sinks using atmospheric transport models', *Nature* **415**, 626-630.
- Houghton, R. A. (1999), 'The annual net flux of carbon to the atmosphere from changes in land use 1850-1990', *Tellus* **51B**, 298-313.
- Houghton, R. A. & Hackler, J. L. (1999), 'Emissions of carbon from forestry and land-use change in tropical Asia', *Global Change Biology* **5**, 481-492.
- Houghton, R. A.; Hackler, J. L. & Lawrence, K. T. (1999), 'The U.S. carbon budget: Contributions from Land-use change', *Science* **285**, 574-578.
- Hurt, G. C.; Pacala, S. W.; Moorcroft, P. R.; Casperson, J.; Shevliakova, E.; Houghton, R. A. & III, B. M. (2002), 'Projecting the future of the U.S. carbon sink', *Ecology* **99(3)**, 1389-1394.
- IPCC (2007), *Climate Change 2007: The Fourth IPCC Assessment Report*, Cambridge, Cambridge University Press.
- Joos, F.; Prentice, I. C. & House, J. I. (2002), 'Growth enhancement due to global atmospheric change as predicted by terrestrial ecosystem models: consistent with US forest inventory data', *Global Change Biology* **8**, 299-303.
- Kaminiski, T.; Rayner, P. J.; Heimann, M. & Enting, I. G. (2001), 'On aggregation errors in atmospheric transport inversions', *Journal of Geophysical Research* **106**, 4703-4715.
- Lin, J.; Gerbig, C.; Wofsy, S.; Andrews, A.; Daube, B.; Davis, K. & Grainger, C. (2003), 'A near-field tool for simulating the upstream influence of atmospheric observations: The Stochastic Time-Inverted Lagrangian Transport (STILT) model', *Journal of Geophysical Research* **108**, ACH 2 1-17.
- S. P. Long, E. A. Ainsworth, A. D. B. Leakey, J. Nosberger, D. R. Ort (2006), 'Food for Thought: Lower-Than-Expected Crop Yield Stimulation with Rising CO₂ Concentrations', *Nature*, 312, 218-221
- Marland, G., T.A. Boden, and R.J. Andres (2003), Global, Regional, and National Fossil Fuel CO₂ Emissions. In Trends: A Compendium of Data on Global Change, Carbon Dioxide Inf. Anal. Cent., Oak Ridge Natl. Lab., U.S> Dep. of Energy, Oak Ridge, Tenn.
- Matross, D. M.; Andrews, A.; Pathmathevan, M.; Gerbig, C.; Lin, J. C.; Wofsy, S. C.; Daube, B. C.; Gottlieb, E. W.; Chow, V. Y.; Lee, J. T.; Zhao, C.; Bakwin, P. S.; Munger, W. & Hollinger, D. Y. (2006), 'Estimating regional carbon exchange in New England and Quebec by combining atmospheric, ground-based and satellite data', *Tellus* **58B**, 344-358.

McGrath-Spangler, E. L.; Denning, A. S.; Corbin, K. D.; and Baker, I. T. (2008): Implementation of a boundary layer heat flux parameterization into the Regional Atmospheric Modeling System (RAMS), *Atmos. Chem. Phys. Discuss.*, 8, 14311-14346.

McGuire, A. D., J. M. Melillo, and L. A. Joyce. 1995. The role of nitrogen in the response of forest net primary production to elevated atmospheric carbon dioxide. *Annual Review of Ecology and Systematics* 26: 472-503.

Michalak, A. M.; Bruhwiler, L. & Tans, P. P. (2004), 'A geostatistical approach to surface flux estimation of atmospheric trace gases', *Journal of Geophysical Research* **109**, 1-19.

Mouillot, F. & Field, C. B. (2005), 'Fire history and the global carbon budget: A 1 deg by 1 deg fire history reconstruction for the 20th century', *Global Change Biology* **11**, 398-420.

Olivier, J.G. J., J.A. Van Aardenne, F. Dentener, L. Ganzeveld, and J.A.H.W. Peters (2005), Recent Trends in Global Greenhouse Gas Emissions: Regional Trends and Spatial Distribution of Key Sources. In *Non-CO₂ Greenhouse Gases (NCGG-4)*, pp. 325-330, Millpress, Rotterdam.

Oren, R.; Ellsworth, D. S.; Johnsen, K. H.; Phillips, N.; Ewers, B. E.; Maler, C.; Schafer, K. V.; McCarthy, H.; Hendrey, G.; McNulty, S. G. & Katul, G. G. (2001), 'Soil fertility limits carbon sequestration by forest ecosystems in a CO₂-enriched atmosphere', *Nature* **411**, 469-471.

Pacala, S. W.; Hurtt, G. C.; Baker, D.; Peylin, P.; Houghton, R. A.; Birdsey, R. A.; Heath, L.; Sundquist, E. T.; Stallard, R. F.; Ciais, P.; Moorcroft, P.; Casperson, J. P.; Shevliakova, E.; Moore, B.; Kohlmaier, G.; Holland, E.; Gloor, M.; Harmon, M. E.; Fan, S. M.; Sarmiento, J. L.; Goodale, C. L.; Schimel, D. & Field, C. B. (2001), 'Consistent Land- and Atmosphere-Based U.S. Carbon Sink Estimates', *Science* **292**, 2316-2320.

Peters, W.; Jacobson, A. R.; Sweeney, C.; Andrews, A. E.; Conway, T. J.; Masarie, K.; Miller, J. B.; Bruhwiler, L. M. P.; Pétron, G.; Hirsch, A. I.; Worthy, D. E. J.; van der Werf, G. R.; Randerson, J. T.; Wennberg, P. O.; Krol††, M. C. & Tans, P. P. (2007), 'An atmospheric perspective on North American carbon dioxide exchange: CarbonTracker', *Proceedings of the National Academy of Sciences of the United States of America* **104**, 18925-18930.

Peterson, G. A.; Halvorson, A. D.; Havlin, J. L.; Jones, O. R.; Lyon, D. J. & Tanaka, D. L. (1998), 'Reduced tillage and increasing cropping intensity in the Great Plains conserves soil C', *Soil & Tillage Research* **47**, 207-218.

Rayner, P. J.; Enting, I. G.; Francey, R. J. & Langenfelds, R. (1999), 'Reconstructing the recent carbon cycle from atmospheric CO₂, δ13C and O₂/N₂ observations', *Tellus* **51B**,

213-232.

Robertson, G. P.; Paul, E. A. & Harwood, R. R. (2000), 'Greenhouse Gases in Intensive Agriculture: Contributions of Individual Gases to the Radiative Forcing of the Atmosphere', *Science* **289**, 1922-1925.

Rodenbeck, C.; Houweling, S.; Gloor, M. & Heimann, M. (2003), 'CO₂ flux history 1982-2001 inferred from atmospheric data using a global inversion of atmospheric transport', *Atmospheric Chemistry and Physics* **3**, 1919-1964.

Schimel, D.; Melillo, J.; Tian, H.; McGuire, A. D.; Kicklighter, D.; Kittel, T.; Rosenbloom, N.; Running, S.; Thornton, P.; Ojima, D.; Parton, W.; Kelly, R.; Sykes, M.; RonNeilson & Rizzo, B. (2000), 'Contribution of Increasing CO₂ and Climate to Carbon Storage by Ecosystems in the United States', *Science* **287(5460)**, 2004-2006.

Schlesinger, W. H. (1977), 'Carbon balance in terrestrial detritus', *Annual Review of Ecology and Systematics* **8**, 51-81.

Schlesinger, W. H. (1997), *Biogeochemistry: An analysis of global change*, Hancourt Brace & Company.

Schlesinger, W. H. (1999), 'Carbon Sequestration in Soils', *Science* **284**, 2095-2098.

Sellers, P. J.; Randall, D. A.; Collatz, G. J.; Berry, J. A.; Field, C. B.; Dazlich, D. A.; Zhang, C.; Collelo, G. D. & Bounoua, L. (1996), 'A Revised Land Surface Parameterization (SiB2) for Atmospheric GCMs. Part I: Model Formulation', *Journal of Climate* **9**, 676-705.

Sellers, P. J.; Los, S. O.; Tucker, C. J.; Justice, C. O.; Dazlich, D. A.; Collatz, G. J. & Randall, D. A. (1996), 'A Revised Land Surface Parameterization (SiB2) for Atmospheric GCMs. Part II: The Generation of Global Fields of Terrestrial Biophysical Parameters from Satellite Data', *Journal of Climate* **9**, 706-737.

SOCCR (2007), 'The first state of the carbon cycle report (SOCCR)', Technical report, U.S. Climate Change Science Program and the Subcommittee on Global Change Research.

Tans, P. P. Macalady, D. L., ed. (1998), *Perspectives in Environmental Chemistry, Chapter 12*, Oxford University Press.

Tans, P. P.; Fung, I. Y. & Takahashi, T. (1990), 'Observational Constraints on the Global Atmospheric CO₂ Budget', *Science* **247**, 1431-1438.

Tarantola, A. (1987), *Inverse Problem Theory: Methods for Data Fitting and Parameter Estimation*, Elsevier Science, New York.

Tilman, D.; Reich, P.; Phillips, H.; Menton, M.; Patel, A.; Vos, E.; Petersion, D. & Knops, J. (2000), 'Fire Suppression and Ecosystem Carbon Storage', *Ecology* **81(10)**, 2680-2685.

Turnbull, J.C. J.B. Miller, S.J. Lehman, P.P. Tans, R.J. Sparks, and J. Southon (2006), Comparison of $^{14}\text{CO}_2$, CO, and SF₆ as Tracers for Recently Added Fossil Fuel CO₂ in the Atmosphere and Implications for Biological CO₂ Exchange.

Wang, J.W., A.S. Denning, L. Lu, I.T. Baker, and K.D. Corbin (2006), Observations and simulations of synoptic, regional, and local variations in atmospheric CO₂. *Journal of Geophysical Research*.112

Zhu, C., Zeng, Q., Ziska, L.H., Zhu, J., Xie, Z., Liu, G. 2008. Effect of nitrogen supply on carbon dioxide-induced changes in competition between rice and barnyardgrass (*Echinochloa crus-galli*). *Weed Science*. 56:66-71.

Zimov, S. A., E. A. G. Schuur, F. S. Chapin III (2006), Permafrost and the Global Carbon Budget. *Science* **312**, 1612-1613

III. Investigation of the sensitivity of Bayesian atmospheric carbon dioxide inversions

Introduction

Bayesian synthesis inversion techniques provide an important tool in the investigation of the spatial and temporal distribution of carbon fluxes on earth. Over the last decade, researchers have been using these techniques to investigate various aspects of the missing sink of carbon (Fan et al., 1998; Rayner et al., 1999; Gurney et al., 2002). This body of research, combined with field research studies (Tilman et al. 2000), provides strong evidence for the existence of a Northern Hemisphere sink of carbon over the last several decades. Nevertheless, little more is known about where, or why, this sink exists. Popular theories include reforestation of previously cleared lands and the effects of fire suppression efforts (Casperson et al., 2000; Hurtt et al., 2002; Mouillot and Field, 2005), and various fertilization scenarios involving carbon fertilization and nitrogen deposition (Oren et al., 2001; Joos et al., 2002).

Many of these global carbon flux inversion studies, including Gurney et al., 2002 and Rayner et al., 1999 have been performed based upon the “basis region” concept of aggregation. This procedure involves the fixing of a prescribed pattern (basis region) of net ecosystem exchange (NEE) for each of 22 partitions of the globe. This type of aggregation of the inversion domain has been necessary in order to render the inversion computationally feasible and “strike a balance” between the available data and the number of parameters in the inversion. The basis region approach to aggregation has been criticized (Kaminski et al., 2001) as producing biased inversion results by not

properly accounting for the possible errors in the basis functions. From a statistical standpoint, this issue arises as a combination of the “hard constraint” nature of the basis functions and unequal sampling coverage or disproportionate “response” functions (as often termed in the geosciences). Besides giving falsely confident estimates of the actual fluxes, the estimates can also be biased.

As a result of these findings, researchers have begun to perform inversions at resolutions closer in scale to that of the underlying transport model (Gerbig et al., 2003, Matross et al., 2006) while specifying covariance structures on the prior guesses for the carbon fluxes (Michalak et al., 2004). While the acknowledgment of variability inherent in the a priori flux and the corresponding specification of a covariance structure on the prior fluxes is likely a step in the right direction, little is known about how the choice of this covariance structure will impact inversion results. Given the fact that atmospheric inversions are generally heavily under-constrained at the transport model resolution, one usually has to make aggressive assumptions about the covariance structure of the prior fluxes. This typically has involved specifying a relatively long decorrelation length and a relatively small overall variance multiplier to the spatial covariance function (generally an exponential covariance structure) for the prior fluxes (Gerbig et al., 2003; Rodenbeck et al., 2003; Michalak et al., 2004). This has the effect of allowing the estimated field to change slowly and in a spatially correlated way, from the prior mean guess. The effects of the choices of the prior covariance structure upon the estimation of the unknown true underlying flux field is not well understood. A thorough investigation of the sensitivity of posterior estimates to a priori assumptions, as well as comparison to other important

error sources, is important in order to have any degree of confidence in the results of an atmospheric inversion.

Sensitivity to variability assumptions is not restricted to spatial dimensions. Treating fluxes independently, an inversion that attempts to solve for m fluxes at p locations and at n points in time, is solving for $m * p * n$ fluxes. In order to combat the increasing parameter space, as a result of estimating fluxes at finer resolutions in either space or time, researchers have begun to use state-space formulations of the inversion problem. In essence, this allows for the restricting of the time dimension of the problem. The methods involved are generally some variant of the Kalman Filter style approach, usually the extended Kalman Filter or ensemble Kalman Filter. In these methods, correction factors are treated as probability distributions (similar to a standard Bayesian Synthesis approach) and are propagated forward through time in a state-space fashion. A period of time must be chosen over which to estimate the correction factors, i.e. the temporal resolution of the state-space formulation. In order to avoid statistical complications, the temporal resolution should be chosen such that the errors in the modeled fluxes are somewhat independently and identically distributed in time. This ensures that an arbitrary sampling of the sequence of fluxes, which is likely under a general inversion setup, will not be biased in its estimate.

In this chapter, simulations of carbon dioxide concentrations are used to investigate the sensitivity of atmospheric inversion results. We focused on the individual estimates of ecosystem respiration and gross primary productivity in particular, while the difference, NEE, will be the focus of Ch. 4. Different components of the inversion are perturbed, such as number of samples, assumed error levels, aggregation of inversion

region, and spatial decorrelation length scale of underlying flux patterns. This testing should be done for any model used in an under-constrained data framework. Many of these components have been investigated in research using other models but the investigation into the sensitivity of the spatial decorrelation length scale is somewhat novel. We tested the ability of the inversion to detect carbon flux patterns that represented varying degrees of *smoothness* even when the smooth pattern was degraded with small scale spatial variability (nugget variance). This work is critical in that it provides an argument for the robustness of the inversion across these inversion components and also shows that the inversion is able to correct for the *individual* flux components, ER and GPP, as opposed to just NEE.

Methods

Inversion Review

Atmospheric carbon dioxide concentration measurements contain information about carbon fluxes in the terrestrial biosphere and oceans. Assume that the carbon dioxide fluxes of the biosphere and their associated local changes on the surrounding carbon dioxide concentrations are known. Recall that carbon dioxide is relatively inert, *chemically*, within the atmosphere. If atmospheric tracer transport of carbon dioxide can be predicted through the use of a meteorological model, then one can predict what carbon dioxide concentrations should be in the atmosphere, at any point in space and time. For example, assume researchers incorrectly modeled an area of land as grasslands when in fact it was composed of heavily managed croplands. One would assume that downwind

CO₂ concentrations would reflect this discrepancy by being lower than what was expected a priori. Therefore, one is able to make inferences about fluxes from this area simply from an a priori flux model and downwind CO₂ measurements. In this fashion, one is able to draw inferences about carbon fluxes by using carbon dioxide concentrations.

Atmospheric inversion techniques employ this concept to attempt to correct for these initial carbon flux guesses in such a way as to reduce the differences between “expected” modeled carbon dioxide concentrations and actual carbon dioxide measurements. If sufficient carbon dioxide concentration data exists to constrain the problem then a regular least squares, or weighted least squares, approach can be applied. In a statistical regression framework, the design matrix, \mathbf{G} , summarizes the atmospheric transport of the fluxes, \mathbf{x} , via the Jacobian matrix (partial derivatives of carbon dioxide concentration at different sampling locations with respect to different carbon dioxide fluxes), to the carbon dioxide observations \mathbf{y} . The matrix $\mathbf{\Sigma}$ denotes the covariance between the (assumed) mean zero multivariate normal error terms, $\boldsymbol{\varepsilon} = \mathbf{G}\mathbf{x} - \mathbf{y}$. For n carbon dioxide observations and m contributing carbon dioxide flux regions, the model is then

$$\mathbf{y} = \mathbf{G}\boldsymbol{\beta} + \boldsymbol{\varepsilon} \quad (1)$$

$$\text{e.g. } \begin{bmatrix} y_1 \\ y_2 \\ \cdot \\ \cdot \\ y_n \end{bmatrix} = \begin{bmatrix} G_{11} & G_{12} & \cdot & \cdot & G_{1m} \\ G_{21} & G_{22} & \cdot & \cdot & \cdot \\ \cdot & \cdot & \cdot & \cdot & \cdot \\ \cdot & \cdot & \cdot & \cdot & \cdot \\ G_{n1} & \cdot & \cdot & \cdot & G_{nm} \end{bmatrix} \begin{bmatrix} \beta_1 \\ \beta_2 \\ \cdot \\ \cdot \\ \beta_m \end{bmatrix} + \begin{bmatrix} \varepsilon_1 \\ \varepsilon_2 \\ \cdot \\ \cdot \\ \varepsilon_n \end{bmatrix}$$

For a full rank matrix \mathbf{G} , the solution to this problem is

$$\hat{\beta} = \left(G^T \Sigma^{-1} G\right)^{-1} G^T \Sigma^{-1} y \quad (2)$$

and the variance of this estimator is

$$\text{var}(\hat{\beta}) = \left(G^T \Sigma^{-1} G\right)^{-1} G^T \Sigma^{-1} y \quad (3)$$

This problem can equivalently be expressed in terms of solving for the minimum of the following cost function (the kernel of the Gaussian likelihood function).

$$C(\beta) = (G\beta - y)^T \Sigma^{-1} (G\beta - y) \quad (4)$$

This is not necessarily a unique solution. If the row rank of \mathbf{G} is less than the column rank of \mathbf{G} , and \mathbf{G} is full rank, then there will be an infinite number of “least squares” solutions and the solution shown above can appear meaningless in application.

If there is not sufficient data to constrain the inversion to a unique solution, then the addition of a “penalty term” to the cost function will have the effect of keeping the solution close to a specified a priori solution. Assuming the difference between the actual fluxes and a priori fluxes is multivariate normally distributed, this cost function can be written as

$$C(\beta) = (G\beta - y)^T \Sigma^{-1} (G\beta - y) + (\beta - \beta_0)^T \Sigma_0^{-1} (\beta - \beta_0) \quad (5)$$

Notice that as \mathbf{x} moves away from \mathbf{x}_0 , the second term in the equation above increases, essentially “penalizing” the solution for moving to far away from \mathbf{x}_0 . The covariance of the errors between the actual fluxes and the a priori solution, Σ_0 , dictate the strength and correlations of the penalty across individual carbon dioxide fluxes.

Main Sources of Inversion Error

The first error term in these methods is summarized via the covariance matrix Σ , i.e. the difference between expected and actual carbon dioxide measurements. Normally specified in an inversion as single error term, it can realistically be allocated to one of the following three categories: (1) aggregation error, (2) representation error, (3) observation error (measurement error), and (4) transport error (Engelen et al 2002). Although fundamentally different, observation error and transport error are very difficult to partition and are usually handled as a sum in the statistical model. Therefore, we will address the sum of these two as *observation* error. It is important to note that the transport portion of the sum is generally believed to be the larger of the two summands. The second error component is error associated with the a priori estimate of the fluxes, which is summarized via the covariance matrix Σ_0 .

Aggregation Error

Aggregation error arises as an effect of running an inversion on a different resolution, either in time or space, or both, than that of the coupled transport model. In a spatial context, this error term has been well documented in the literature (Kaminski, et al., 2001). Kaminski, et al. showed that spatial aggregation errors could be a consequence of the interplay between spatially changing correction factors (for the fluxes) and spatially unbalanced sampling of the surface fluxes.

For tower-based regional inversion schemes, the impact of this error can be somewhat counter intuitive. Assume that there exists a simple stationary isotropic covariance on the prior distribution of fluxes, in other words the variance structure of the

errors in the fluxes (from the prior) is similar with distance between locations. It is then fairly easy to see that the errors in the inversion, in an aggregation-sense, will arise in areas that have the steepest sampling gradients. The most sampled area in tower-based schemes is generally the local area in the vicinity of the tower. The upstream influence drops off considerably with distance from the tower, with the steepest sampling areas being right at the tower. This is somewhat counter intuitive in that the worst aggregation errors, relative to their posterior variances, may very well occur right beneath the sampling towers, where one would expect to get the most reliable results. Adding to the problem, the posterior covariance is usually very small in the vicinity of the tower, owing to the dense sampling, giving a false sense of precision, or confidence.

Less is known about aggregation error from a temporal viewpoint. Temporally, it is generally preferable to assimilate data “on the fly” from within the model, in a Kalman filter (or ensemble Kalman filter) manner, propagating errors forward through the actual model. However, the runtime of many detailed process models is prohibitively expensive and it is generally not feasible to run the multiple parallel instances of the model that are necessary to capture the error distributions. As a result, many inversions are run in an offline manner with a fixed resolution in space and time, choosing to only optimize certain parameters.

Aggregation error in *time* can be illustrated using a hypothetical inversion scenario. Assume one has CO₂ concentration data from a tower that is located 100 km to the south east of an intensively managed corn-dominated agricultural region. Furthermore, assume that the inversion is “blind” to the field of corn, i.e. the prior contains no information on the vigorous summer carbon drawdown located to the

Northwest of the tower. If the winds come from the Northwest in the spring and the Southwest in the summer and a mean correction factor is estimated over the entire summer period, it will likely be biased low because it only “sees” the cornfield during less intense assimilation periods.

A more satisfying solution would be to find a period of time over which the flux correction factors remain somewhat constant. Note that this does not necessarily fix the problem of not “seeing” the cornfields during their most intense drawdown period. The sampling coverage in both space and time is a simple product of the observation network and the meteorology. However, it would be more reasonable to specify large variances in the prior covariance matrices in agricultural regions during periods in which crops are generally growing.

It is very difficult to avoid, or account for, aggregation error. In most cases, researchers attempt to minimize this error by running higher resolution inversions. However, it would be expected that justifying inversion solutions where one has increased the number of parameters in an already under-constrained problem would provide an equally daunting challenge.

Representation Error

Representation error arises from the fact that many carbon dioxide concentration measurements are point measurements in both time and space, but often extrapolated to a grid cell and time frame in an inversion scheme. Essentially the error is a function of sub-grid scale dynamics that are essentially ‘truncated’ in order to perform calculations on a discrete grid. For example, a single measurement of CO₂ at the WLEF tower in

Wisconsin might be used to represent the average of the entire 1600 km² grid cell that contains it in the model. Representation error can be complicated but portions of the error are quantifiable by using correct “change of support” statistical methods (Raftery et al., 2003; Bannerjee et al., 2004). The examples in this paper employ an inverse Lagrangian particle transport approach which should mitigate possible representation errors due to point measurements of carbon dioxide. It is important to note that even though they are related, representation error is distinct from transport error. This is illustrated by the fact that the Lagrangian transport approach is used to provide sub-grid scale transport estimates and remove the representation error. However, this does not necessarily imply that it models the transport *correctly*.

Observation Error

The term “observation error”, derived from the common statistical usage, is a bit of a misnomer for inversion studies since the error term generally combines two error terms, *transport* and *measurement* error, with starkly different magnitudes. The measurement portion of this error term is the actual error in the instrument reading of carbon dioxide. Given reasonably well-calibrated observations, these are small relative to the other error components and generally not of much concern. Transport errors, which arise from errors in the atmospheric transport of NEE fluxes to the tower (observing site), are of a much greater magnitude. Results from the Transcom 3 project (Gurney et al 2002) showed that there are substantial differences in transport dynamics by the leading transport models. It occurs when the transport operator, responsible for moving carbon dioxide in the modeled atmosphere, is incorrectly specified. This can

occur when the actual atmospheric physics are simplified, as in parameterized convection schemes, when the parameters of these simplifications are incorrectly specified, or when actual physics related to transport are excluded, such as the exclusion of convective motion from a transport scheme. The standard methodology in inversion problems is to try to minimize aggregation, representation, and measurement errors, and *specify* transport error, assuming it is the main contributor to the “observation” errors.

Prior Error

Another source of error that must be specified in atmospheric inversions is the manner in which the prior NEE guess differs from the unknown truth. Atmospheric inversion techniques are generally ill-conditioned and thus require prior constraints to constrain the result to a reasonable solution. Therefore, prior constraints force the solution towards an a priori “best guess”. Furthermore, if this prior best guess for the solution is different from the true underlying solution, then errors will result since the estimated solution will be pulled towards an incorrect solution. An error covariance matrix must also be specified that characterizes the variability between this “best guess” and the true underlying solution and this dictates the degree to which the inversion is “pulled” towards the prior estimate.

The rest of this paper will investigate the sensitivity of inversion results to aggregation schemes, prior flux specification, and observation error levels. A pseudo-data case study will be explored for which the *true* fluxes are known and inversion errors can be readily calculated.

North American Case Study

Carbon flux estimates for North America display pronounced variability (Schimel et al., 2001). Atmospheric based inversion studies and ground based upscaling approaches have generally agreed on the *sign* of the NEE flux. However, atmospheric inversion studies have often estimated the flux at levels around twice that of upscaled ground measurement based estimates. Initial atmospheric inversion studies also showed a disproportionate amount of carbon being stored annually within the United States (Fan, et al 1998) while later studies seem to show a more uniform sink mechanism in the northern hemispheres (Gurney, et al 2002).

The estimates are variable, both within each of the methods (atmospheric inversion and ground based) as well as between each. It is not clear what this variability is a function of and how one might proceed to investigate it. Most inversions, to this point, have focused on coupling global biosphere and transport models and inverting fluxes for relatively large areas of land. This has produced meaningful results (Gurney, et al 2002) that tend to agree with ground based observations, to a degree. Furthermore, the results seem to be somewhat robust to simple variability in the priors. Nevertheless, without higher resolution inversion studies, it is difficult to study the robustness of inversion results with respect to finer scale variables like landcover type, nitrogen deposition patterns, and forest stand age.

Forward-in-time NEE Model

The Simple Biosphere model (SiB) is based on a land-surface parameterization scheme originally used to compute biophysical exchanges in climate models (Sellers et

al., 1986), but later adapted to include ecosystem metabolism (Sellers et al., 1996a; Denning et al., 1996a). The parameterization of photosynthetic carbon assimilation is based on enzyme kinetics originally developed by Farquhar et al. (1980), and is linked to stomatal conductance and thence to the surface energy budget and atmospheric climate (Collatz et al., 1991, 1992; Sellers et al., 1996a; Randall et al., 1996). The model has been updated to include prognostic calculation of temperature, moisture, and trace gases in the canopy air space, and the model has been evaluated against eddy covariance measurements at a number of sites (Baker et al., 2003; Hanan et al., 2004; Vidale and Stöckli, 2005; Philpott et al., 2007). SiB has been coupled to the Regional Atmospheric Modeling System (RAMS) and used to study PBL-scale interactions among carbon fluxes, turbulence, and CO₂ mixing ratio (Denning et al., 2003) and regional-scale controls on CO₂ variations (Nicholls et al., 2004; Wang et al., 2006). Other recent improvements include biogeochemical fractionation and recycling of stable carbon isotopes (Suits et al., 2004), improved treatment of soil hydrology and thermodynamics, and the introduction of a multilayer snow model based on the Community Land Model (Dai et al., 2003),

Backward-in-time Mixing Ratio Adjoint Model

High-frequency time variations of photosynthesis and respiration are assumed to be well understood and easily modeled processes (radiation, temperature, soil moisture). Longer-term time variations, such as those potentially caused by very subtle carbon sinks into the soil organic matter of agricultural lands, are estimated by solving for unknown

multiplicative biases in each component flux after smoothing in space and time. This is accomplished by convolving the influence functions generated from a Lagrangian particle dispersion model, LPDM (Uliasz and Pielke, 1991; Uliasz, 1993, 1994; Uliasz et al., 1996), with gridded net photosynthesis (ASSIMN, gross primary production (GPP) – leaf level autotrophic respiration) and ecosystem ground respiration (RESPG, heterotrophic respiration in the soil and root respiration) at each time step in SiB-RAMS. The net ecosystem exchange (NEE) is composed of these two component fluxes:

$$NEE(x,y,t) = RESPG(x,y,t) - ASSIMN(x,y,t) \quad (6)$$

where x and y represent grid coordinates and t represents time. Sub-hourly variations in the simulated component fluxes in time are primarily controlled by the weather (especially changes in radiation due to clouds and the diurnal cycle of solar forcing), whereas seasonal changes are derived from phenological calculations parameterized from satellite imagery. Fine-scale variations in space are driven by variations in vegetation cover, soil texture, and soil moisture. To estimate regional fluxes from atmospheric mixing ratios, we assume that the model of the component fluxes is biased, and that the biases are smoother in time and space than the fluxes themselves.

$$NEE(x,y,t) = (1 + \beta_{RESPG}(x,y,t))RESPG(x,y,t) - (1 + \beta_{ASSIMN}(x,y,t))ASSIMN(x,y,t) \quad (7)^1$$

A persistent bias in photosynthesis might result from underestimation of leaf area, available nitrogen, or soil moisture, whereas a persistent bias in respiration might result from overestimation of soil carbon or coarse woody debris. In any case, it is reasonable that such biases vary much more slowly in time than the fluxes themselves.

¹ Note that $NEE(x,y,t)$ is constructed so that the bias correcting betas are estimated relative to ‘1’ and represent the deviation from the a priori flux estimates)

To estimate slowly varying biases β_{RESPG} and β_{ASSIMN} using SiB-RAMS and LPDM, we first generate surface flux influence functions by integrating the backward-in-time particle trajectories from LPDM. Using these, we can represent the carbon dioxide mixing ratio observed at a given station k at time m as

$$C_{k,m} = \sum_{x,y,n} \left(\beta_{R,x,y} RESPG_{x,y,n} - \beta_{A,x,y} ASSIMN_{x,y,n} \right) C^*_{k,m,x,y,n} \Delta t_f \Delta x \Delta y + C_{BKGD,k,m} \quad (8)$$

where x and y are grid indices in the zonal and meridional directions, n is the time at which ASSIMN and RESPG occurred (not usually the time at which the resulting change in mixing ratio was measured!). The influence function $C^*_{k,m,x,y,n}$ is then the discrete form of the partial derivative of the observed mixing ratio with respect to the NEE at grid cell (i,j) at time step n . The length scales Δx and Δy are the sizes of the grid cells in the zonal and meridional direction, and Δt_f is the time step over which the fluxes are applied. The term $C_{BKGD,k,m}$ represents the contribution of “background” CO₂ flowing into the model domain from the larger scales. Summing where possible, this becomes:

$$C_{obs} = \sum_{cell=1}^{nCell} \beta_{RESP,cell} C^*_{RESP,obs,cell} + \sum_{cell=1}^{nCell} \beta_{ASSIMN,cell} C^*_{GPP,obs,cell} + C_{BKGD,obs} \quad (9)$$

where obs is an observation number (combines indices k and m), and $cell$ is a grid cell number (combines indices i and j). The influence functions have been convolved with the ASSIMN and RESPG terms from the forward model and integrated over the time period over which the bias terms are assumed to apply:

$$\begin{aligned} C^*_{RESPG,obs,cell} &= \Delta t_f \Delta x \Delta y \sum_n RESPG_{cell,n} C^*_{obs,cell,n} \\ C^*_{ASSIMN,obs,cell} &= -\Delta t_f \Delta x \Delta y \sum_n ASSIMN_{cell,n} C^*_{obs,cell,n} \end{aligned} \quad (10)$$

Experiments have been run successfully with 10-day time scales for the bias terms, which allow influence functions on hourly fluxes and observations to be integrated for 240 hours. This approach has two important advantages: (1) the area and strength of upstream influence over 10 days is much greater than for a single hour, so the inverse problem of estimating the bias terms, β , is much better constrained than the estimation of the fluxes themselves; and (2) the storage of the influence functions (in eq 10) is 240 times smaller than would be required to store all the $C_{obs,cell,n}$!

The result of equation (10) is basically a statistical regression problem that can, under the appropriate Gaussian assumptions, be solved using linear regression. However, the number of observations is usually small relative to the number of bias parameters to be estimates, leaving a very unconstrained regression problem. Fortunately, as was discussed earlier, there are some avenues of recourse to constrain this problem.

On the justification of prior spatial covariance assumptions

It has become increasingly fashionable to run inversions at increasingly fine resolutions and then apply a spatial correlation structure to the errors in one's prior flux estimate. This applies a very strong constraint to a generally unconstrained inversion problem and tends to "stabilize" (Kaminski et al., 2001) the solution. In a statistical sense, this essentially means that the solution space is very multi-modal (for an unconstrained problem) and that the spatial covariance constraint tends to constrain the problem well enough to focus in on a single mode in the space of the posterior pdf. There are countless solutions to unconstrained solutions, so although the utility can not be questioned, the justifiability of this solution as *the solution* is a separate matter.

Providing evidence of some degree of spatial correlation in the errors for the prior flux would be needed to provide a more justified solution. However, neither the covariance structure of the underlying carbon fluxes nor the related covariance structure of the errors in the prior flux are yet well understood and thus it is not clear whether this spatial correlation structure in the prior errors is justified.

In this inversion scenario, SiB3 is being used to capture fine temporal scale fluxes. It is not expected to include longer term, more persistent flux differences. There are many mechanistic hypotheses for these *unresolved* longer time-frame flux differences. For example, on larger regional scales, atmospheric warming may increase the soil temperature in the boreal forest regions which would likely increase the activity of heterotrophs in the soil and subsequently provide an increase in respiration and carbon dioxide to the atmosphere (Zimov et al., 2006). Given the large amount of relatively labile carbon that is stored away in boreal soils, this would seem a plausible hypothesis. Given the “zero annual NEE” constraint in SiB, this may not be captured in the prior. Furthermore, it has already been shown that a warming atmosphere is correlated to a lengthening growing season (refs) in the far north. This might indicate the presence of relatively new carbon sinks, especially along an expanding forest-tundra ecotone. It is not certain to what extent the prior would account for this expansion. Certainly the use of satellite vegetation data is beneficial in this aspect. Disturbance is also a major driver of carbon fluxes and it is not well understood how complex disturbance regimes, such as fire, may change under the current trajectory. These persistent flux differences may operate on a number of different spatial and temporal scales, making them difficult to

estimate. The time frame of this case study precludes the ability to analyze disturbance regimes, however it may allow for *snapshot* views of them at a certain point in time.

Many of the important variables which may influence the errors in the prior do appear to be spatially correlated themselves. Relevant information might include variables describing soil moisture levels and satellite derived LAI. Naively assuming some sort of linear relationship between flux corrections and these variables would imply a somewhat spatially correlated correction pattern. Unfortunately there appears to be little current evidence that the effect of biases may be so simple, even if they are spatial in nature. Nevertheless, we can move forward by examining if there is any apparent “cost” to including this prior if it is incorrect.

Inversion region and prior mean

In the following example, pseudo data is used to investigate a 6000km by 3600km region of land encompassing much of North America (Fig. 3.1). The prior mean for the carbon fluxes is calculated by running the fully coupled SiB-RAMS biosphere-atmosphere model. The model was run on a 150 x 100 cell grid with a resolution of 40km, and covers the majority of North America. The time period was from May 1, 2004 through August 31, 2004. RAMS was nudged to ETA reanalysis data to provide improved transport. The code in SiB was modified to accept MODIS landcover data which provided 8-day estimates of fPAR and LAI. The transport from RAMS was then processed into the LPDM model to provide source based estimates of sensitivity to upwind fluxes. To reiterate its utility, the main reason for using this particle model was

to avoid the explicit calculation of a full adjoint to SiBRAMS which would have been prohibitively expensive.

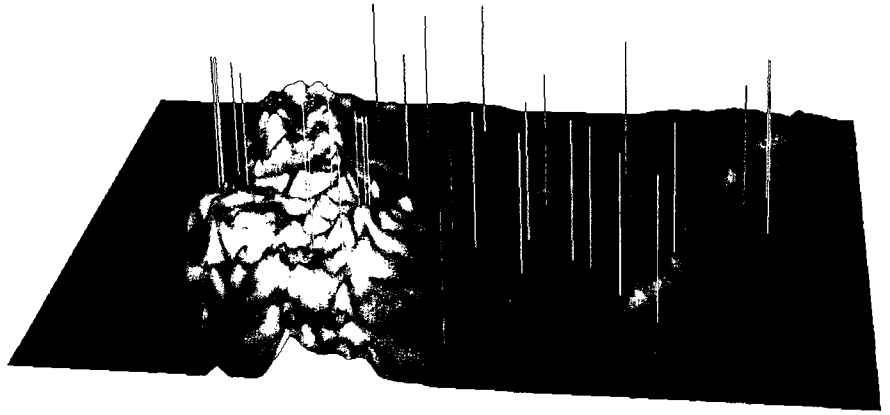


Figure 3.1: Inversion region and calibrated carbon dioxide observing towers Eight towers in red available for 2003/2004, remaining green towers available in 2007/2008.

For this particular example, the initial 40 km SiBRAMS grid was

aggregated up to 100km grid cells to facilitate covariance matrix inversions. Flux uncertainty is only considered over the land cells of the aforementioned 60 x 36 - 100km x 100km grid, meaning that simulated flux biases were applied uniformly across individual 100km x 100km grid cells. Fluxes outside of this domain, as well as variation in inflow concentrations, fossil fuels fluxes, and ocean fluxes are prescribed and are considered fixed and without uncertainty in this example.

CO₂ measurements

Eight flux towers are located in the region, at the WLEF site, the ARM site, the KWKT site, the Western Peatland site, the BERMS site, the NOBS site, and Harvard site, and the Argyle, ME site (shown in red in Fig 3.1). All of the sites have collected well calibrated carbon dioxide measurements since 2003. It is also anticipated that over 30 towers will be available for the same region for the summer of 2007 (shown in green in Fig 3.1). Before inverting real concentration data, it must be determined how well these eight

towers will constrain an atmospheric inversion and how sensitive these results will be to inversion assumptions.

Model Assumptions

An assumption for this experiment is that the true carbon fluxes, both from the respiration of heterotrophic organisms and plant assimilation, are proportional to the prior fluxes estimated by the coupled biosphere-atmosphere model. It can not be reasonably assumed that all errors in the fluxes can be corrected via this mechanism. However, it will allow a first-order correction to the fluxes that might provide insight into model deficiencies as well as potentially provide for the independent correction of GPP and respiration fluxes which is necessary in an annually carbon balanced model. The crux of the inversion is to estimate the multiplicative biases, $\beta_{i,j,RESPG}$ and $\beta_{i,j,ASSIMN}$, as was shown in Equation 9.

The inversion will be calculated in a more or less traditional Bayesian synthesis fashion. As was shown before (Equation 5), the inversion can be solved by minimizing the following cost function.

$$C(\beta) = (G\beta - y)^T \Sigma^{-1} (G\beta - y) + (\beta - \beta_0)^T \Sigma_0^{-1} (\beta - \beta_0)$$

where,

$$\Sigma = \sigma_{obs}^2 I$$

$$\Sigma_0 = \begin{bmatrix} \Sigma_{Respg, prior} & 0 \\ 0 & \Sigma_{Assimn, prior} \end{bmatrix}.$$

For the case of correlated errors in the prior flux, the respiration and assimilation covariance matrices are each formed from the exponential covariance function, where t_{ij} is the distance between points β_i and β_j .

$$Cov(\beta_i, \beta_j) = \begin{cases} \sigma_0^2 (1 - \alpha_0) \exp\left(\frac{-t_{i,j}}{h_0}\right), & i \neq j \\ \alpha_0 \sigma_0^2, & i = j \end{cases}$$

The h_0 parameter is the range (or decorrelation length) parameter, giving the distance at which the covariance between two points is equal to $\sigma_0^2 (1 - \alpha_0) e^{-1}$. The parameter α_0 controls what percentage of the covariance can be attributed to spatial covariance and allows for easy interpretation.

The transport portion of the inversion is fixed and the underlying true flux distributions are, in theory, unknown. In order to objectively test the sensitivity of the inversion to different spatial prior covariance assumptions, a reasonable range of *true* underlying covariance structures must be considered. Spatially correlated bias fields are generated by sampling from a multivariate normal distribution, with a spatially correlated variance, and using smoothing techniques to ensure small-scale continuity of the surface. The smoothing of the field generally results in a small dampening of the assumed variance.

Observations are simulated 4 times a day at the eight sites over a 113-day period. Afternoon observations are simulated to lessen the impact of low precision measurements

made during times of extremely stable and stratified nighttime atmospheric conditions near the ground. In total, there are 3616 observations covering the period May 1, 2004 to August 20, 2004 (14916 for the 33 towers expected in 2007). CO₂ observations were simulated by multiplying net photosynthesis and ground respiration influence functions by the bias factors in Figure 3.2 and adding a 1-2 ppm normal i.i.d. error term. This error term accounts for the observation and transport error previously discussed in section 2. This is a fairly unrealistic and simplistic error term for transport. For example, two observations taken 2 hours apart on the same tower most likely have very similar footprints of influence and thus are very likely strongly correlated. However, given the relatively even distribution of observations for each day and tower available in a pseudo data experiment, the effect of temporally correlated observations is likely small. We note, however, that this is probably an important component of inversions operating on real CO₂ observations and is likely an area in which further research is

needed.

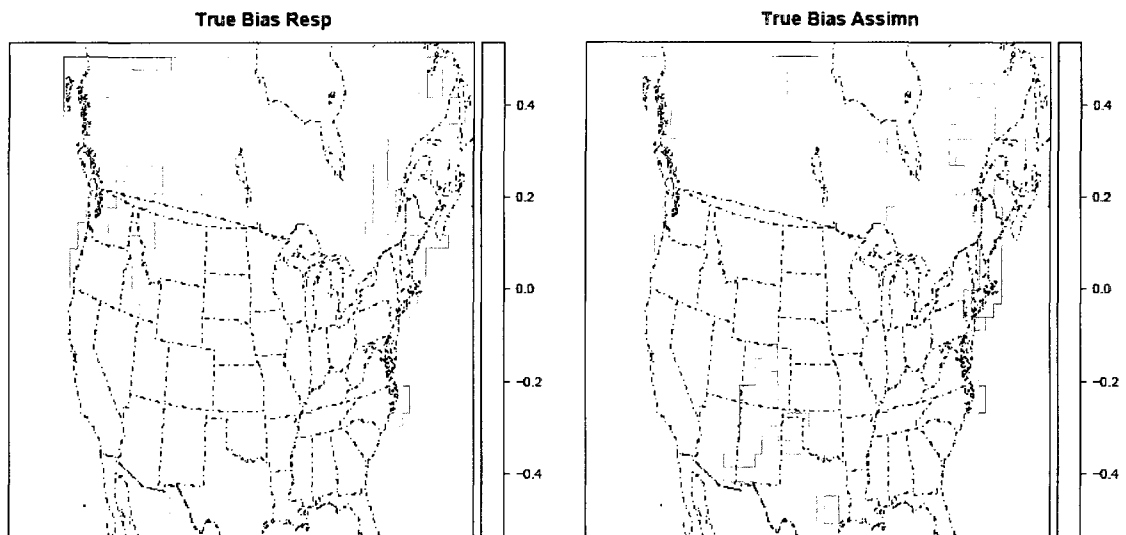


Figure 3.2: Example bias fields for net photosynthesis (ASSIMN) and ground respiration (RESPG).

To summarize the point of this exercise, we are interested in estimating the correction factors, β_{RESP} and β_{ASSIMN} , indicated in Equation 9 (and shown in Figure 3.2), using knowledge of atmospheric transport and simulated downwind carbon dioxide mixing ratio observations at the towers shown in Figure 3.1. Additionally, we will test the sensitivity of the inversion to many different variables in the inversion.

Results

Metric for gauging the inversion success

In unconstrained regressions in which one has many more parameters than unknowns, it can be expected that observations will be fit very well. In other words, a plot of simulated CO_2 and inversion-estimated CO_2 at the towers should show very good

agreement with a very high R^2 value. This is to be expected and would likely only be noted if it produced a *suspect* fit to the observations. This is quite different from the prediction ability of the inversion, which is how well the inversion recovers the underlying bias parameters. A useful measure of the prediction ability is the root mean squared error (RMSE), which is the square root of the mean squared error between the predicted biases and the underlying biases used in the simulation. So for most examples in the paper, a reduction in RMSE, from the prior to the posterior, is chosen as the metric of comparison (which is generally applied as an average over the entire domain),

$$1 - \frac{RMSE_{POSTERIOR}}{RMSE_{PRIOR}}.$$

This statistic tends to one, as the posterior fit gets increasingly better. A zero value indicates that the posterior fit is of the same prediction quality as the prior, and accordingly, a negative value indicates that the posterior fit is a worse fit than the prior. It is important to note that inversions such as this will generally have greater success at capturing larger scale mean flux biases. As a result of the inability to capture fine scale flux biases perfectly, maximum reductions of the prior RMSE tend to be around 60% for these examples.

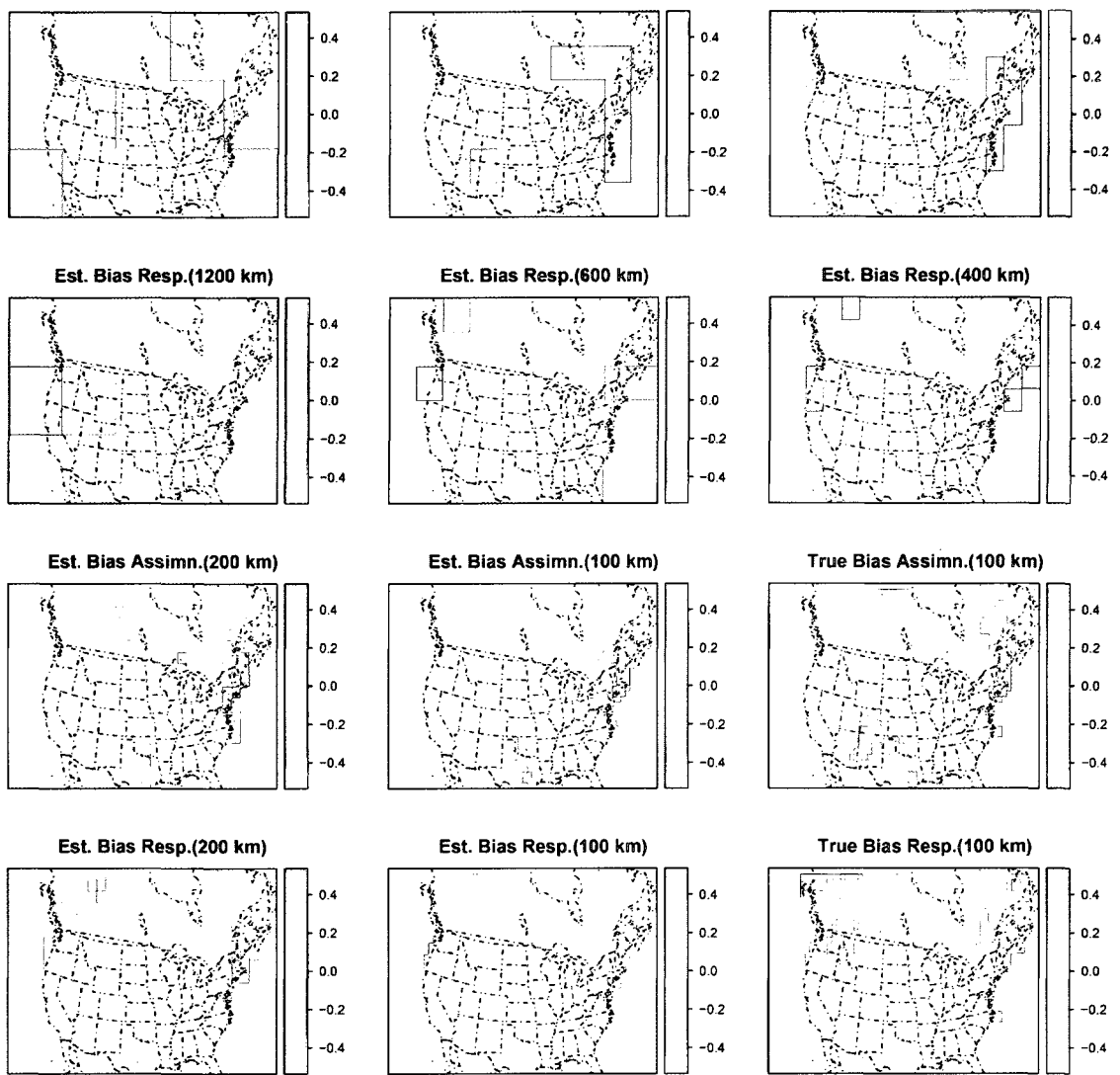


Figure 3.3: Evolution of inversion with increasing resolution of inversion, from 1200 km to 100 km. Plot generated by aggregating up assimilation and respiration influence functions and performing inversion on that 'coarser' aggregated domain. Underlying bias patterns were simulated by using exponential spatial covariance structure with a decorrelation length scale of 500 km length scale with 0.2 standard deviation and performing a post-hoc smoothing. Notice the last panels, bottom right and the plot above that, indicate the targeted corrections.

Sensitivity to Inversion Domain Aggregation Errors

The effect of aggregating the 60x36 grid by a factor of 2,3,4,6, and 12 leading to grids of size 30x18, 20x12, and 15x9, 10x6, and 5x3 is investigated first. Inversion estimates for correction factors for ground respiration and net photosynthesis are shown in Figure 3.3. Given the relatively unconstrained nature of the problem, it was not surprising that the inversion-based bias estimates predicted CO₂ observations at the towers matching the simulated observations very well ($R^2 > 0.95$ for all aggregations, not shown). It is

important to note that this does not necessarily imply that the correction factors accurately predict the true underlying bias, which is the variable that needs to be recovered by the inversion. An overall measure of the ability to predict the underlying bias field is summarized in Fig. 3.4. One will notice that GPP is corrected better than respiration in Fig. 3.4 and this is likely a result of stronger GPP fluxes in summer (when the tests were run) and daytime observations of carbon dioxide being more representative of terrestrial uptake conditions.

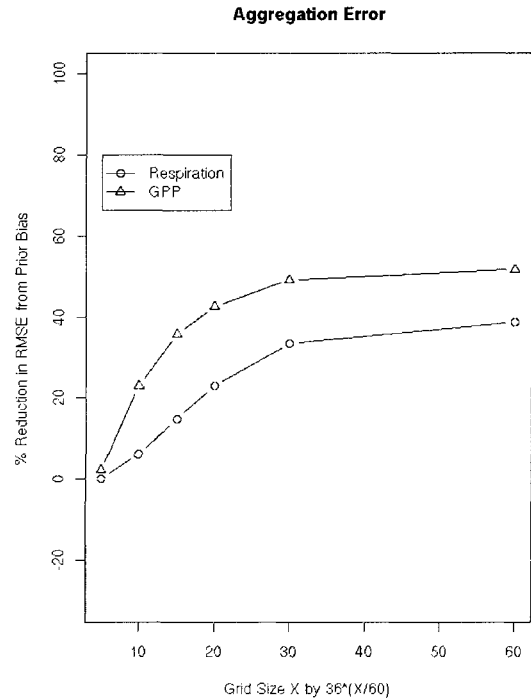


Figure 3.4: Aggregation Error Plot. Simulated effect of aggregating inversion domain upon a prediction ability, as summarized by $1 - RMSE_{posterior} / RMSE_{prior}$. Underlying bias patterns are smooth 500km length scale with 0.2 standard deviation. Note that X-axis value of '30' equates to a 30 by 36 * (30/60) = 30 by 18 grid. A 1.4 ppm observation error

It can be seen that aggregations resulting in an order of magnitude less inversion cells still are able to provide a significant amount of improvement over the prior in predicting biases. Given this fact, and taking into account computational concerns, a 30 x 18 grid will be used in place of a 60 x 36 for sensitivity tests involving many inversion realizations.

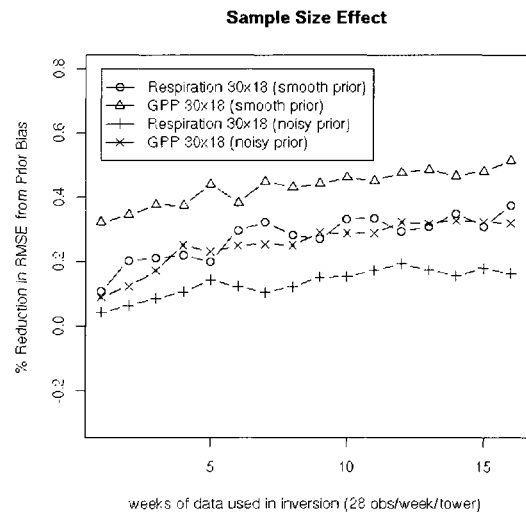


Figure 3.5. Inversion effectiveness as a function of sample size. Lack of smoothness is due to independent random draws of observation error for each 'weeks of data' data point. Averaging across multiple simulations would provide smoother curves.

Sensitivity to the Number of Samples

Increasing the number of samples available to any statistical estimation technique will improve the estimation. However, investigation of this is very important on a problem-by-problem basis. This example constrains the corrected ground respiration and net photosynthesis to be proportional to prior estimates. This is not necessarily a bad assumption, given the data, but is a very strong assumption to make. Short-term temporal variations in NEE fields will be smoothed out by this approach, which may be beneficial for identifying trends in areas such as large relatively uniform expanses of native prairie or forest. This method is not wholly appropriate for regions with temporally rapidly changing NEE, such as might be experienced in the period before, during, and after the harvesting of a winter wheat field in Oklahoma. Thus identifying a point of diminishing return in sample size is important. Inversions can then be discretized by this time period. This will allow the inversion to be more responsive to local temporal changes in NEE, such as those often induced by intensive agricultural operations.

Results are shown in Fig. 3.5. It appears that the inversion might make more significant gains in prediction power during the first 4 or 5 weeks of data, after which it still gains power but at an increasingly slower rate. More

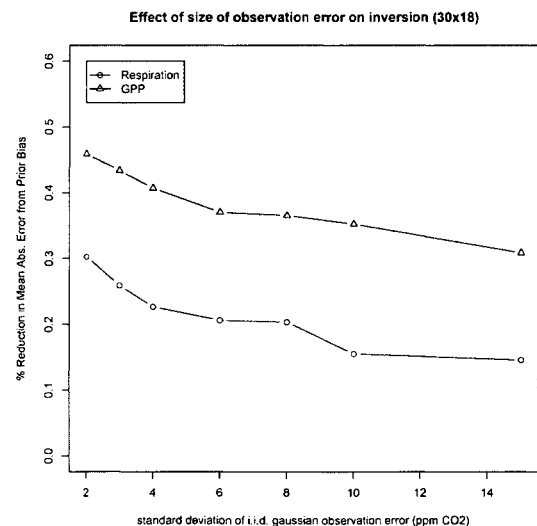


Figure 3.6: Effect of increasing “observation error” on inversion. Underlying bias patterns are created from an exponential spatially covariance structure with 500 km decorrelation length scale with 0.2 standard deviation. An ensemble of 10 simulations for each ‘standard deviation’ on the x-axis, is used to smooth the effect of a particular observation error pattern on result.

importantly, results seem to imply that a spatially correlated prior for the biases can be beneficial in prediction when the true underlying biases are spatially correlated.

Sensitivity to the transport error

This is one of the most important parameters in the inversion. If aggregation error can be minimized, transport error will be the main source of error in the observational portion of the cost function. It is a function of the true fluxes and it is one of the most likely errors to be incorrectly specified or over simplified. Assume that one has a reasonable idea of how their prior flux may vary from the true flux, i.e. through exploration of modeled and observed NEE at observation sites such as the Ameriflux network. The observation error covariance matrix, which is likely dominated by transport error, than completely dictates the balance of the power of the estimation between the data and the prior constraint. For this example, an independent and identically distributed Gaussian error term has been chosen to describe the observation error term. Results are shown in Figure 3.6. For the aggregate 30x18 grid, it appears that predictive ability drops off significantly over the range of 2 to 4 ppm while losses are not as great for increases beyond this range.

Sensitivity of correction to variability in underlying NEE patterns

While the NEE patterns illustrated in Figure 3.2 represent plausible patterns of bias for correcting the coupled SiB-RAMS model, it is important to investigate how the variability in possible underlying bias fields might influence the inversion estimates. Systematic and quickly generated bias fields are needed in order to methodically test this sensitivity. Randomly generated, spatially correlated fields will be generated as

candidate NEE correction fields from a multivariate normal distribution with mean zero and correlation matrix Σ_{True} . This method is employed in order to speed computations and preserve the overall variability of the bias fields. It is important to note, that as a consequence, these fields have somewhat more small scale variability than smoothed fields and the maximum “recovery” of the inversion may be less than for smoothed biases. Therefore a locally weighted regression smoother (LOCFIT, <http://www.cs.bell-labs.com/cm/ms/departments/sia/project/locfit/index.html>) is used to provide a slight degree of smoothing to the candidate fields, resulting in bias fields with slightly less variability than “advertised”.

$$\Sigma_{True} = \begin{bmatrix} \Sigma_{Respg,true} & 0 \\ 0 & \Sigma_{Assimn,true} \end{bmatrix}$$

$$Cov(\beta_i, \beta_j) = \begin{cases} \sigma_{true}^2 (1 - \alpha_{true}) \exp\left(\frac{-t_{i,j}}{h_{true}}\right) + \sigma_{true}^2 \alpha_{true}, & i \neq j \\ \sigma_{true}^2, & i = j \end{cases}$$

Sensitivity of the prediction accuracy to the three parameters of the spatial covariance function is investigated. In particular, we investigate sensitivity to σ_{true}^2 the variance of the NEE correction field, α_{true} the percentage of this variability allocated to independent small spatial-scale *nugget* variance (the rest allocated to spatial covariance), and h_{true} the *range* parameter of the spatial covariance, i.e. the distance between cells at which the spatial correlation has decreased to approximately 0.36 (e^{-1}). It has been noted that a spatially correlated prior seems beneficial overall, given the superior predictive

ability when the true underlying biases are spatially correlated. In order to keep the results tractable, a *reasonable* prior distribution is fixed with a variance of 0.04, a range (decorrelation length) of 500km, and no nugget variance. This variance corresponds to a prior standard deviation of 0.2, representing a reasonable prior variance for correcting many biases in the range of -50% to 50%.

The degree to which the true underlying variability in the correction factors partitions between independent *nugget* variance and variance due to spatial patterns in the data can be shown to be very important. Figure 3.7 shows results of the inversion performed on random spatially correlated Gaussian surfaces with varying decorrelation length scales and *nugget/spatial* variance partitioning. The most accurate inversions result from fields that are correlated over long distances, several hundred kilometers. Correspondingly, the prediction ability depends even more strongly on the amount of variability partitioned to the spatial component of the variance. It can be seen that the flux correction fields, over which the inversions provide the most correction, have correlation length scales on the order of 500km or more, with at least 25% of the variability being attributable to spatial

covariance.

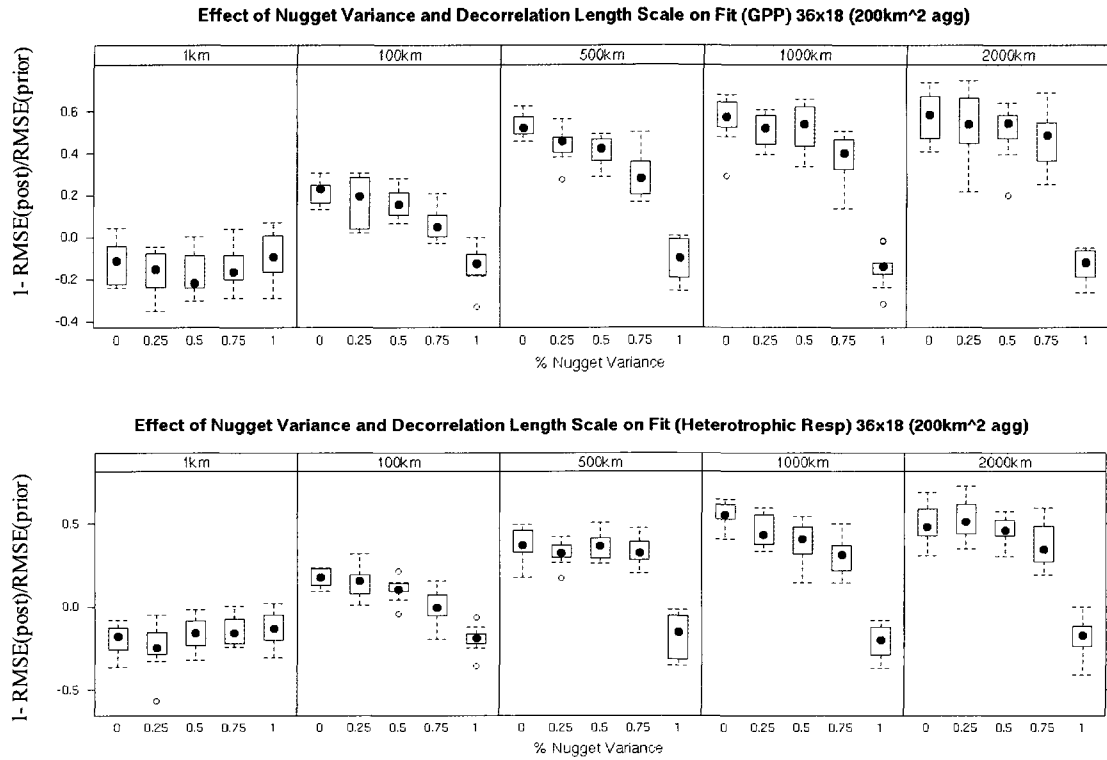


Figure 3.7: Effect of spatial correlation length scale and percentage of variability assigned to “nugget” variance on the inversion fit to simulated true underlying flux bias. A 1 ppm observation error term was used for the results shown here..

Discussion

Due to the increasing use of spatially constrained priors in carbon flux inversion problems, there has been a mounting interest in the sensitivity of inversion results to prior specifications of covariance structure. Results from this study seem to imply that prediction ability is far more dependent upon the existence of a smooth mean spatial pattern, at some spatial scale, than any spatial specification in the prior covariance structure. While inversions such as this are not designed to capture flux estimates at the scale of crop fields, it would be reasonable to expect the inversion to capture a large spatial scale mean trend over intensely managed agricultural lands. A spatially correlated

prior does not seem to damage the prediction ability of the inversion, regardless of the true covariance structure of the errors. However, in an under constrained inversion problem, improving prediction ability is very dependent upon smooth covariance structure to the errors in the biases. In essence, one only has the statistical power to extract large scale mean patterns from the data. Additionally, it would seem that the correlations need to be fairly persistent over long spatial scales. Fig. 3.7 indicates that, for this study, this might be in the range of several hundred kilometers for a decorrelation length scale, or range. These type of persistent (in space) biases would likely include effects such as those stemming from solely from large climatic changes while the *nugget* variance would likely represent effects such as land use change and natural sub-grid scale variability. This would seem to provide evidence to support the construction of a good prior which is relatively close to the truth but possibly more importantly, whose error structure is spatial in nature and therefore provides a bias that can be recovered. For example, with the ability to more accurately model fine scale carbon flux processes in agricultural lands, one may be able to recover more subtle processes such as changes in soil organic matter. A more accurate depiction of forest ages and species distributions in the North Eastern United States might provide the ability to see subtle underlying large spatial scale effects of nitrogen deposition. With an increasing number of flux stations coming online, one should soon be able to more accurately estimate this covariance structure. Results from this study seem to show that without this structure it may be very difficult to recover flux estimates accurately without an essentially brute-force upscaled estimate from a plethora of spatially distinct CO₂ observing sites.

The Kalman-filter based inversions seemed remarkably robust to gaussian transport error specification. However, it is unlikely that errors are distributed exactly in this fashion. More research is needed to determine how relaxing this assumption will affect inversion results.

Aggregation did not seem to affect the prediction ability of the inversion as much as was expected, a priori. This is somewhat of a surprising result but has to be tempered by the fact that the covariance structure in these examples is somewhat simple. More complicated non-stationary and “patchy” covariance structures, that might be a function of more than simply distance, might provide more aggregation-based difficulties.

The maximum reduction in RMSE achieved during any of these simulations was about 60% for assimilation and 35% for respiration. This resulted from the full kalman filter operating on the unaggregated 60 x 36 100km grid. Sequentially applying the filter over time, along with a variation inflation scheme, and assuming a temporally changing underlying bias field would likely result in more modest gains in prediction. The study used only afternoon observations which probably had a direct impact on GPP being predicted better than respiration. The high level of correlation between GPP and respiration influence functions is a concern and might have additionally created difficulties for the inversion. It might be possible to formally test this by separating (GPP and respiration) and reshuffling the influence functions (in time) in order to break this correlation and rerunning the inversions, but this has not been done. Furthermore, the inversion results will likely be much better when aggregated up to larger regions.

LITERATURE CITED

Baker, I.; Denning, A. S.; Hanan, N.; Prihodko, L.; Uliasz, M.; Vidale, P.; Davis, K. & Bakwin, P. (2003), 'Simulated and observed fluxes of sensible and latent heat and CO₂ at the WLEF-TW tower using Sib 2.5', *Global Change Biology* **9**, 1262-1277.

Caspersen, J. P.; Pacala, S. W.; Jenkins, J. C.; Hurtt, G. C.; Moorcroft, P. R. & Birdsey, R. A. (2000), 'Contributions of Land-Use History to Carbon Accumulation in U.S. Forests', *Science* **290**, 1148-1150.

Collatz, G. J.; Ball, J. T.; Grivet, C. & Berry, J. A. (1991), 'Physiological and environmental regulation of stomatal conductance, photosynthesis, and transpiration: a model that includes a laminar boundary layer', *Agricultural and Forest Meteorology* **54**, 107-136.

Dai, Y.; Zeng, X.; Dickinson, R.; Baker, I.; Bonan, G.; Bosilovich, M.; Denning, S.; Dirmeyer, P.; Niu, P. H. G.; Oleson, K.; Schlosser, A. & Yang, Z. (2003), 'The common land model (CLM)', *Bulletin of the American Meteorological Society* **84**, 1013-1023.

DePury, D. & Farquhar, G. (1997), 'Simple scaling of photosynthesis from leaves to canopies without the errors of big-leaf models', *Plant, Cell, and Environment* **20**, 537-557.

Evensen, G. (2004), 'Sampling strategies and square root analysis schemes for the EnKF', *Ocean Dynamics* **54**, 539-560.

Fan, S.; Gloor, M.; Mahlman, J.; Pacala, S.; Sarmiento, J.; Takahashi, T. & Tans, P. (1998), 'A large terrestrial carbon sink in North America implied by atmospheric and oceanic carbon dioxide data and models', *Science* **282**, 442-446.

Gelman, A.; Carlin, J. B.; Stern, H. S. & Rubin, D. B. Chatfield, C.; Tanner, M. & Zidek, J., ed. (2004), *Bayesian Data Analysis*, Chapman & Hall/CRC.

Gerbig, C.; Lin, J. C.; Wofsy, S. C.; Andrews, A. E.; Daube, B. C.; Davis, K. J. & Grainger, C. A. (2003), 'Toward constraining regional-scale fluxes of CO₂ with atmospheric observations over a continent: 2. Analysis of COBRA data using a receptor-oriented framework', *Journal of Geophysical Research* **108**, ACH 6 1-19.

Gerbig, C.; Lin, J. C.; Wofsy, S. C.; Daube, B. C.; Andrews, A. E.; Stephens, B. B.; Bakwin, P. S. & Grainger, C. A. (2003), 'Toward constraining regional-scale fluxes of CO₂ with atmospheric observations over a continent: 1. Observed spatial variability from airborne platforms', *Journal of Geophysical Research* **108**.

Gurney, K. R.; Law, R. M.; Denning, A. S.; Rayner, P. J.; Baker, D.; Bousquet, P.; Bruhwiler, L.; Chen, Y.; Clals, P.; Fan, S.; Fung, I. Y.; Gloor, M.; Helmann, M.; Higuchi, K.; John, J.; Maki, T.; Maksyutov, S.; Masarle, K.; Peylin, P.; Prather, M.; Pak, B. C.; Randerson, J.; Sarmiento, J.; Tagucki, S.; Takahashi, T. & Yuen, C. (2002), 'Towards robust regional estimates of CO₂ sources and sinks using atmospheric transport models', *Nature* **415**, 626-630.

Hanan, N. P.; Berry, J. A.; Verma, S. B.; Walter-Shea, E. A.; Suyker, A. E.; Burba, G. G. & Denning, A. S. (2004), 'Model analyses of biosphere-atmosphere exchanges of CO₂, water and energy in Great Plains tallgrass prairie and wheat ecosystems', *Agricultural and Forest Meteorology*.

Hurt, G. C.; Pacala, S. W.; Moorcroft, P. R.; Casperson, J.; Shevliakova, E.; Houghton, R. A. & III, B. M. (2002), 'Projecting the future of the U.S. carbon sink', *Ecology* **99**(3), 1389-1394.

Joos, F.; Prentice, I. C. & House, J. I. (2002), 'Growth enhancement due to global atmospheric change as predicted by terrestrial ecosystem models: consistent with US forest inventory data', *Global Change Biology* **8**, 299-303.

Kaminiski, T.; Rayner, P. J.; Heimann, M. & Enting, I. G. (2001), 'On aggregation errors in atmospheric transport inversions', *Journal of Geophysical Research* **106**, 4703-4715.

Matross, D. M.; Andrews, A.; Pathmathevan, M.; Gerbig, C.; Lin, J. C.; Wofsy, S. C.; Daube, B. C.; Gottlieb, E. W.; Chow, V. Y.; Lee, J. T.; Zhao, C.; Bakwin, P. S.; Munger, W. & Hollinger, D. Y. (2006), 'Estimating regional carbon exchange in New England and Quebec by combining atmospheric, ground-based and satellite data', *Tellus* **58B**, 344-358.

Michalak, A. M.; Bruhwiler, L. & Tans, P. P. (2004), 'A geostatistical approach to surface flux estimation of atmospheric trace gases', *Journal of Geophysical Research* **109**, 1-19.

Mouillot, F. & Field, C. B. (2005), 'Fire history and the global carbon budget: A 1 deg by 1 deg fire history reconstruction for the 20th century', *Global Change Biology* **11**, 398-420.

Nicholls, M. E.; Denning, A. S.; Prihodko, L.; Vidale, P.; Davis, K. & Bakwin, P. (2004), 'A multiple-scale simulation of variations in atmospheric carbon dioxide using a coupled biosphere-atmospheric model', *Journal of Geophysical Research* **109**.

Oren, R.; Ellsworth, D. S.; Johnsen, K. H.; Phillips, N.; Ewers, B. E.; Maler, C.; Schafer, K. V.; McCarthy, H.; Hendrey, G.; McNulty, S. G. & Katul, G. G. (2001), 'Soil fertility limits carbon sequestration by forest ecosystems in a CO₂-enriched atmosphere', *Nature*

411, 469-471.

Philpott, A. W.; Denning, A. S.; Baker, I. T.; Corbin, K.; Hanan, N. P.; Hargrove, W. W.; Berry, J. A. & Schaefer, K. (2007), 'Simulated surface energy budget at the site level in the southern Great Plains using the Simple Biosphere Model, version 3 (SiB3).', *Journal of Geophysical Research*.

Randall, D. A.; Sellers, P. J.; Berry, J. A.; Dazlich, D. A.; Zhang, C.; Collatz, G. J.; Denning, A. S.; Los, S. O.; Field, C. B.; Fung, I.; Justice, C. O.; Tucker, C. J. & Bounoua, L. (1996), 'A Revised Land-Surface Parameterization (SiB2) for Atmospheric GCMs. Part 3: The Greening of the CSU General Circulation Model', *Journal of Climate* **9**, 738-763.

Rayner, P. J.; Enting, I. G.; Francey, R. J. & Langenfelds, R. (1999), 'Reconstructing the recent carbon cycle from atmospheric CO₂, d13C and O₂/N₂ observations', *Tellus* **51B**, 213-232.

Rodenbeck, C.; Houweling, S.; Gloor, M. & Heimann, M. (2003), 'CO₂ flux history 1982-2001 inferred from atmospheric data using a global inversion of atmospheric transport', *Atmospheric Chemistry and Physics* **3**, 1919-1964.

Schimel, D. S.; House, J. I.; Hibbard, K. A.; Bousquet, P.; Ciais, P.; Peylin, P.; Braswell, B. H.; Apps, M. J.; Baker, D.; Bondeau, A.; Canadell, J.; Churkina, G.; Cramer, W.; Denning, A. S.; Field, C. B.; Friedlingstein, P.; Goodale, C.; Heimann, M.; Houghton, R. A.; Melillo, J. M.; Moore III, D. M.; Noble, I.; Pacala, S. W.; Prentice, I. C.; Raupach, M. R.; Rayner, P. J.; Scholes, R. J.; Steffen, W. L. & Wirth, C. (2001), 'Recent patterns and mechanisms of carbon exchange by terrestrial ecosystems', *Nature* **414**, 169-172.

Sellers, P. J.; Randall, D. A.; Collatz, G. J.; Berry, J. A.; Field, C. B.; Dazlich, D. A.; Zhang, C.; Collelo, G. D. & Bounoua, L. (1996), 'A Revised Land Surface Parameterization (SiB2) for Atmospheric GCMs. Part I: Model Formulation', *Journal of Climate* **9**, 676-705.

Suits, N. S.; Denning, A. S.; Berry, J. A.; Still, C. J.; Kaduk, J. & Randerson, J. T. (2004), 'Seasonal and spatial variations in carbon isotopic ratios of plant biomass, terrestrial CO₂ fluxes and atmospheric CO₂', *Global Biogeochemical Cycles*.

Tarantola, A. (1987), *Inverse Problem Theory: Methods for Data Fitting and Parameter Estimation*, Elsevier Science, New York.

Tilman, D.; Reich, P.; Phillips, H.; Menton, M.; Patel, A.; Vos, E.; Petersen, D. & Knops, J. (2000), 'Fire Suppression and Ecosystem Carbon Storage', *Ecology* **81(10)**, 2680-2685.

Uliasz, M. (1996), Lagrangian particle modeling in mesoscale applications, in P. Zannetti,

ed., 'Environmental Modeling III', Computational Mechanics Publications, , pp. 145-182.

Ulliasz, M. (1994), Lagrangian particle modeling in mesoscale applications, in P. Zannetti, ed., 'Environmental Modeling II', Computational Mechanics Publications, , pp. 71-102.

Ulliasz, M. (1993), 'The atmospheric mesoscale dispersion modeling system (MDMS)', *Journal of Applied Meteorology* **32**, 139-149.

Ulliasz, M. & Pielke, R. A. (1991), 'Application of the receptor oriented approach in mesoscale dispersion modeling', in H. Van Dop & D. G. Steyn, ed., 'Air Pollution Modeling and its Applications VIII', Plenum Press, New York, 399-408.

Wang, J. W.; Denning, A. S.; Lu, L.; Baker, I. T. & Corbin, K. D. (2006), 'Observations and simulations of synoptic, regional, and local variations in atmospheric CO₂', *Journal of Geophysical Research* **112**.

IV. Seeing the forest through the Trees: Recovering large-scale carbon flux biases in the midst of small-scale variability

Abstract

Results from eddy covariance flux towers, such as those in the Chequamegon Ecosystem-Atmosphere Study (ChEAS), have shown that significant small scale spatial variability can exist in annual NEE due to factors such as forest age and structure. It is uncertain how the spatial variability seen in eddy covariance flux measurements, often applicable to areas less than one square kilometer, scales up in space but these studies certainly provide reason to believe that significant small scale spatial variability may exist in NEE. Biosphere-atmosphere models typically are run on grid spacings anywhere from several square kilometers to several square degrees and many of these models are not able to accurately capture the kind of carbon dynamics responsible for the small scale spatial variance seen in eddy covariance tower networks like those in ChEAS. Furthermore, even if models are available to capture dynamics at a point in space like a flux tower, it is unlikely that it can be confidently applied across continental sized regions at that scale. The question then becomes how does this small scale spatial variability scale up space and to what degree is this variability tolerable when using atmospheric inversion techniques to recover large regional carbon flux estimates. This paper investigates the effect of this variability upon regional carbon flux inversion estimates in North America using simulated data from May 1, 2004 through Aug 31, 2004 and a sparse network of 8 towers in North American. Inversion techniques use carbon dioxide concentrations to improve a priori carbon flux estimates and in situations where regional scale spatial variability contributes at least 33% to 50% of the variability in the carbon flux errors, we find significant improvements in the RMSE of the model are possible across a wide range of spatial decorrelation length scales, with post aggregation providing even more dramatic corrections, in spite of a very sparse network of observing towers.

INTRODUCTION

During the last decade, Bayesian-based atmospheric inversion techniques have emerged as a viable tool to investigate the spatio-temporal pattern of terrestrial carbon fluxes (Enting et al. 1995; Fan et al., 1998, Gurney et al. 2002). Earlier research has been focused on large continental-sized regions of the earth, using coupled general circulation models (GCM). Lately, researchers have begun applying these techniques to regional flux domains with increasingly finer resolution inversion domains.

In general, regional scale inversions focusing on temporal biases that are of a seasonal length, or longer, are possible because biosphere models have become adept at capturing the majority of carbon exchange that occurs on diurnal and seasonal time scales. The effects of the temperature, available soil water, and sunlight have been modeled extensively and predictions have become reasonably accurate over a variety of conditions and scales (Baker et al., 2003, Hanan et al., 2004; Vidale and Stöckli, 2005). However, the necessary components to model longer term processes such as nitrogen deposition, land management, and other biogeochemical dynamics are often missing from these advanced biophysical models and thus lead to errors in the model. These effects may be unrecognizable at the diurnal scale but may dominate over longer spatial and temporal scales. Thus, researchers can begin to estimate these unknown processes by effectively removing the high frequency diurnal signals at fine scales and estimating the residuals over longer time and space scales.

The biggest hurdle to these inversions is insufficient carbon dioxide concentration data to constrain the flux inversion problem. Therefore, various additional constraints must be added. Two major methodologies have been employed to deal with this problem.

The first of these two methods, which was employed in earlier inversion papers (Enting et al. 1995; Fan et al., 1998, Gurney et al. 2002, Peters et al. 2007) involved the pre-aggregation of large flux regions, generally according to prior guesses of flux patterns based upon global spatial net primary production (NPP) estimates. Largely in response to criticisms of this method (Kaminski et al, 2001; Engelen et al, 2002), geostatistical techniques were employed (Michalak et al. 2004) to constrain the inversion problem. Michalak et al. [2004] used maximum likelihood techniques to estimate spatial covariance parameters (of the carbon flux error component) and then applied the resulting smooth covariance matrices to the errors between the underlying fluxes and the a priori fluxes. As a consequence of these additional constraints, inversion resolutions could be used that were much closer to that of the underlying forward transport and carbon flux models. Zupanski et al [2007] used techniques similar to Michalak et al. 2004, with the exception that they used Monte Carlo style ensemble Kalman filters to track the covariance structure dynamically instead of using more traditional geostatistical point-based estimates of spatial covariance parameters. Peylin et al. [2005] explored the effect of two different error correlation length scale assumptions when estimating daily fluxes over a large portion of Europe.

It seems reasonable to hypothesize that large scale patterns may exist in the errors for many models. For example, assume that one is modeling a large continental region such as North America. If the underlying flux model consistently under-predicts gross primary productivity (GPP) over forest regions and over-predicts over grassland regions over a given time interval such as a day or a year, then a map of the errors will likely show small positive errors in GPP over the grasslands and larger negative errors over the

forested regions. Since grasslands and forested regions tend to exist in “clumps” on larger scales, this has the effect of inducing a spatially correlated structure to the errors. It is difficult to exactly predict the structure, but it is reasonable to believe that correlations might exist on the order of several hundred kilometers or more. It is important to realize that this does not imply that the structure will be simple to recover. For instance, along ecotones such as the transition from the western to eastern slope of the Rocky Mountains and into the Great Plains of the central United States, one might not expect errors in fluxes to be strongly correlated. It is also reasonable to believe that the covariance function may not simply be a function of distance and may involve some kind of structuring around covariates such as biome classification.

Small scale spatial variability has been a recurrent theme of eddy flux measurement towers. For instance, data from the Chequamegon Ecosystem Atmospheric Study (<http://cheas.psu.edu>) showed significant variability in annual NEE between mature hardwood forests and old growth hardwood forests (Desai et al., 2005). Disturbance histories and the associated age structure has also been shown to be important to carbon dynamics in ponderosa pines of the Western United States (Thornton et al., 2002, Law et al., 2003). Important factors explored in these papers, such as stand age and land management, are generally only coarsely modeled, or not modeled at all in larger scale inversion studies. Of course the sampling footprints of the towers that generate these estimates of variability are generally on the order of a square kilometer or two and thus aggregated flux results at, for instance, 40 kilometers might be expected to show less variability than that because of the averaging effect of aggregation. Regional inversions generally provide NEE corrections which exhibit features on much larger

scales than 40 kilometers (Gerbig et al., 2003; Peylin et al. 2005). The effect this has on fluxes is to introduce a layer of “noise” relative to potentially larger spatial scale error signals, such as continental scale sinks or large scale agricultural expansion.

For example, assume that the flux model providing the prior estimates underpredicts GPP, on average, for a large forested area of North America. It is reasonable, if not expected, that this bias would vary spatially over this area on fine scales as a function of local land management practices, natural fire regimes, climate, and anthropogenic fertilization effects. These types of effects have different magnitudes and can be persistent at different temporal scales. This small scale spatial variability has not typically been included as part of the prior error covariance structure (Michalak et al, 2004, Peylin et al., 2005, Peters et al., 2005, Peters et al., 2007, Zupanski et al., 2007), where it would be represented by a independent variance component that is typically termed the “nugget” in geostatistical literature (Cressie 1993). In general, it is unclear how the existence and/or exclusion of this error term in the inversion will affect inversion results.

In this paper we investigate the effect of fine scale spatial variability upon large spatial scale improvements in estimated NEE and show that regional inversions are robust to fine scale spatially independent variance in the flux errors. These inversions are performed in a manner in which assumptions need not be made about a fixed “pattern” of fluxes across large regions. In particular, we vary both the level of small scale independent variance (noise) as well as the decorrelation length scale of the spatially correlated portion of the bias which has a covarying effect upon the success of the inversion. A sparse network of 8 towers in North America is used and the effects of

varying these two quantities are tested using simulated fluxes and corresponding simulated measurements from a biosphere-meteorological model.

METHODS

Model

The Simple Biosphere model (SiB) is based on a land-surface parameterization scheme originally used to compute biophysical exchanges in climate models (Sellers et al., 1986), but later adapted to include ecosystem metabolism (Sellers et al., 1996a; Denning et al., 1996a). The parameterization of photosynthetic carbon assimilation is based on enzyme kinetics originally developed by Farquhar et al. (1980), and is linked to stomatal conductance and hence to the surface energy budget and atmospheric climate (Collatz et al., 1991, 1992; Sellers et al., 1996a; Randall et al., 1996). The model has been updated to include prognostic calculation of temperature, moisture, and trace gases in the canopy air space, and the model has been evaluated against eddy covariance measurements at a number of sites (Baker et al., 2003; Hanan et al., 2004; Vidale and Stöckli, 2005). SiB has been coupled to the Regional Atmospheric Modeling System (RAMS) and used to study PBL-scale interactions among carbon fluxes, turbulence, and CO₂ mixing ratio (Denning et al., 2003) and regional-scale controls on CO₂ variations (Nicholls et al., 2004; Wang et al., 2006). Other recent improvements include biogeochemical fractionation and recycling of stable carbon isotopes (Suits et al., 2004), improved treatment of soil hydrology and thermodynamics, and the introduction of a multilayer snow model based on the Community Land Model (Dai et al., 2003). This

latest version of SiB is termed SiB3.

In SiB3, the net ecosystem exchange (NEE) is composed of two component fluxes, gross primary productivity (GPP) and ecosystem respiration (RESP), which includes autotrophic and heterotrophic respiration terms.

$$NEE(x, y, t) = RESP(x, y, t) - GPP(x, y, t) \quad (1)$$

where x and y represent grid coordinates and t represents time. High-frequency time variations of photosynthesis and respiration are assumed to be well understood and easily modeled processes, i.e. due to changes in radiation, temperature, soil moisture, etc. Long-term, more persistent biases are estimated (Eq. 2) by solving for unknown multiplicative biases in each component flux after smoothing in space and time. This is accomplished by convolving the influence functions generated from a lagrangian particle dispersion model, LPDM (Uliasz and Pielke, 1991; Uliasz, 1993, 1994; Uliasz et al., 1996), with GPP and RESP at each time step in SiB-RAMS. It is noted that at the present time convection is not included in the LPDM and it is uncertain what effect this will have on inversion results.

To summarize, we estimate regional fluxes from atmospheric mixing ratios by assuming that the model of the component fluxes is biased, and that the biases are smoother in time and space than the fluxes themselves:

$$NEE(x, y, t) = (1 + \beta_{RESP}(x, y))RESP(x, y, t) - (1 + \beta_{GPP}(x, y))GPP(x, y, t) \quad (2)$$

The model domain, shown in Fig. 1, consists of most of the United States as well as a large portion of Canada and the northern portions of Mexico. SiB3-RAMS was run on a single 150 x 90 grid of 40 kilometer cells. RAMS meteorology was nudged with NCEP

ETA 40km analysis data throughout the domain using the 4DDA scheme (Walko et al., 2002) to produce more reliable wind fields. SiB3 was run with 8-day fractional photosynthetically available radiation (FPAR) and leaf area index (LAI) fields derived from the MODIS MOD15 product. This was provided from the Numerical Terradynamics Simulation Group at the University of Montana who generated it for use in constructing the official MOD17 GPP product (Mu et al., 2007). The focus of this study was on the regional domain and therefore boundary inflow of CO₂ was assumed fixed, without uncertainty, for the term of the study. An inversion of North America using real data would likely follow a nested coarse-inversion concept, similar to that presented by Peylin et al. 2005.

Synthetic Data

CO₂ observations are simulated hourly at eight measuring sites (WLEF, Harvard Forest, ARM, BERMS, Fraserdale, Western Peatland, WKWT, and Argyle (ME), see Fig. 3.1 for locations) over a 113-day period. These were produced by first running a realistic model run of SiB for the period and domain of interest to serve as our a priori biosphere flux model. Then we convolved specified pseudo bias fields for net photosynthesis and ground respiration with LPDM derived inverse transport fields. Gerbig et. al. [2003] found mean standard deviations on the order of 0.6 to 1 ppm when viewing morning and afternoon vertical profiles of CO₂. As a consequence, robust afternoon hourly average observations, at 12PM, 2PM, 4PM, and 6PM local time, are used to lessen the impact of low quality modeled measurements made during times of extremely stable and stratified

nocturnal atmospheric conditions near the ground. The effect of a simulated inversion is a perfect flux correction model, i.e. a well behaved error structure, as well as a data set with no missing values, which lessens the potential impact of using a patchwork of sub-daily CO₂ observations. The use of real data would certainly lead to a more thorough investigation of time averaging CO₂ hourly concentrations to obtain more robust observations. In total, there are 3616 observations covering the period May 1, 2004 to August 20, 2004. An independent mean-zero 2 ppm standard deviation Gaussian error term is added to the CO₂ observations to provide a crude estimate of transport errors.

In summary, we used a realistic continental scale model run of SiB, based upon a 113-day period in the summer of 2004, to provide realistic GPP and respiration fluxes. We also used a realistic model run of RAMS during the same period to provide transport fields. We then assume ‘truth’ is actually represented by these biosphere fluxes multiplied by synthetic, simulated, bias fields. We then simulated what the carbon dioxide concentrations would be at the observing towers give these biases. Finally, we performed the inversion to see how well we can estimate the biases from the carbon dioxide concentration observations.

Inversion Procedure

Standard multivariate normal assumptions are made and data are assimilated using a Bayesian synthesis inversion, or equivalently, a single standard Kalman-filter updating step. The resolution of the inversion domain (36 X 60, 200km grid spacing) and the number of measurements (3616) were selected such that the needed matrix inversions

could be calculated relatively quickly and without the aid of additional covariance sub-sampling procedures such as the Ensemble Kalman Filter methods (Evensen et al. 1994, Zupanski et al. 2007) employ. While sufficient for theoretical exercises, it is noted that additional measurements and increased inversion domain resolution would require more involved sub-sampling procedures such as those used in the ensemble methods as well as a filter mechanism to propagate information forward. In particular, for a length n CO_2 measurement vector y , length m CO_2 flux bias vector β , $n \times n$ observation error covariance matrix Σ , $n \times m$ Jacobian transport matrix G , length m prior flux estimate β_0 , and $m \times m$ model-prior mismatch covariance matrix Σ_0 , the Bayesian statistical assumptions are¹:

$$\begin{aligned} y | \beta, \Sigma &\sim N(G\beta, \Sigma) \\ \beta &\sim N(\beta_0, \Sigma_0) \end{aligned} \quad (3)$$

The posterior distribution of the flux vector can be solved for analytically and is:

$$\begin{aligned} p(\beta | y, \Sigma) &\propto -\frac{1}{2} \left[(G\beta - y)^T \Sigma^{-1} (G\beta - y) + (\beta - \beta_0)^T \Sigma_0^{-1} (\beta - \beta_0) \right] \\ &\sim N \left(\left(\Sigma_0^{-1} + G^T \Sigma^{-1} G \right)^{-1} \left(\Sigma_0^{-1} \beta_0 + G^T \Sigma^{-1} y \right), \left(\Sigma_0^{-1} + G^T \Sigma^{-1} G \right)^{-1} \right) \end{aligned} \quad (4)$$

With a little bit of algebra, one can rewrite the mean/expectation of the posterior distribution of the mean, giving the familiar Kalman-filter updating equation.

$$E[\beta_{posterior}] = \beta_0 + \left(G^T \Sigma^{-1} G + \Sigma_0^{-1} \right)^{-1} G^T \Sigma^{-1} (y - G\beta_0) \quad (5)$$

With respect to constraining the problem with spatially correlated errors, the covariance matrix Σ_0 will take on the following form.

$$\Sigma_0 = \begin{bmatrix} \Sigma_{RESP, prior} & 0 \\ 0 & \Sigma_{GPP, prior} \end{bmatrix} \quad (6)$$

¹ $N(\mu, \Sigma)$ represents a multivariate Gaussian/Normal distribution with mean vector μ and covariance matrix Σ .

For the case of correlated errors in the prior flux, the respiration and GPP covariance matrices are each formed from the exponential covariance function, where $t_{i,j}$ is the distance between points x_i and x_j .

$$Cov(\beta_i, \beta_j) = \begin{cases} \sigma_0^2 (1 - \alpha_0) \exp\left(\frac{-t_{i,j}}{h_0}\right), & i \neq j \\ \alpha_0 \sigma_0^2, & i = j \end{cases} \quad (7)$$

The h_0 parameter is the range, or decorrelation length scale parameter, giving the distance at which the covariance between two points is equal to $\sigma_0^2 (1 - \alpha_0) e^{-1}$. The σ^2 parameter is the scalar variance parameter and determines the variance of the marginal distribution of the particular flux component. The parameter α_0 controls what percentage of the covariance can be attributed to spatial covariance, as opposed to spatially independent errors.

Given a posterior mean NEE $x_{posterior}$ of length n , a posterior mean NEE variance estimate $\Sigma_{posterior}$ of dimension $n \times n$, and a scalar vector b of length n that maps higher resolution fluxes to coarser resolution fluxes, the following result from multivariate Gaussian statistics (Johnson and Wichern, 1988) can be employed to compare mean NEE at larger post-aggregated scales:

$$\overline{NEE}_b = b' x_{posterior} \sim N(b' \bar{x}_{posterior}, b' \Sigma_{posterior} b) \quad (8)$$

The scalar vector b can be chosen as a sequence of 1/k's and 0's where one is estimating the mean of a block of k cells together. In essence, this is mapping the higher resolution posterior mean fluxes to coarser resolution mean fluxes. Given that we are considering

NEE as the sum of GPP and RESP, the above result can first be employed to sum GPP and RESP correctly and then employed again to aggregate up resulting NEE. In this example, our finest resolution was 100km, a grid of 60 by 36. Values of k were chosen to be 4, 9, 16, 36, 144, and 2160, which represent aggregations to 400 km, 900 km, 1600 km, 3600 km, 14400 km, and the entire domain. In order to compare to the prior, this calculation was performed on both the distribution of the mean of the posterior fluxes as well as the assumed distribution of the mean of the prior fluxes.

This is a fairly long period of time over which to consider the flux biases absolutely constant. From initial forays into real data inversions under this same inversion setup, it appears that temporal coherence in the biases might be shorter than our current inversion timescale, on the scale of a month or two, or shorter, likely tracking a seasonally-dominated temporal error structure. For a filtering-style setup, e.g. Kalman filter, results should be similar to those shown in Fig. 2 but the absolute amount of the NEE correction might be expected to be different due to (1) lesser amounts of useable data per filtering step and (2) additional numbers of fitting parameters afforded by using a filter.

Experiments

In order to test the sensitivity of the inversion to fine scale spatial noise, we introduce a set of Monte Carlo inversion experiments. The point of the paper is to vary small scale spatial noise, however given the uncertainty surrounding the effect of the prior decorrelation scale length of the flux errors, we will include that as an adjustable

parameter in the inversion as well. The forward model of both fluxes (SiB3) and transport (RAMS) operates on 40 km and is post aggregated to 100 km for computational reasons.

An intercomparison of atmospheric CO₂ inversion models (Transcom3, Gurney et al., 2002) provided source/sink estimates on the order of a few tenths of a Pg of carbon per inversion region per year. When compared to the actual net photosynthesis or ground respiration fluxes for this region, this results in uncertainties on the order of 10 – 30% in either direction, on a cumulative basis. Mean-zero Gaussian-based biases for individual 100 km grid cell GPP and respiration using 20% standard deviation appear reasonable given the model constraints. These biases also seem to be a reasonably conservative (broad, encompassing) a priori specification for the scalar multiplier on the spatial portion of the prior Gaussian covariance. Small scale spatial noise of the same order also seems reasonable, and in combination with the spatial component generates a reasonably wide range of potential biases, on the order of 40% standard deviation for the individual 100 km grid cells for which they are applied.

In particular, decorrelation length scale is investigated at levels of 100 km, 500 km, 1000 km, and 2000 km. Small scale Gaussian flux noise will be allowed to vary between standard deviation levels of 1%, 5%, 10%, 20%, and 40% of the a priori fluxes. The a priori scalar standard deviation on the spatial covariance term is set to 20% and the prior inversion decorrelation length scale will be set to 500km, a reasonably conservative prior compromise between similar parameters used in some recent papers (Michalak et al. 2004, Peylin et al. 2005). For each combination of these two levels, 20 realizations of each scenario will be run using randomly generated pseudodata corresponding to the

levels used. Since the temporally varying sampling pattern of the 8 towers is somewhat stationary with respect to their locations, we must ensure that many different potential flux patterns are realized by the experiments so that the results are not dependent upon the sampling footprint of the towers.

A specific example is presented to show the methodology of one realization. Fig. 1 shows the spatial noise pattern, the longer scale spatially correlated signal, as well as the summed bias and the inversion estimate for both GPP and respiration fluxes. This particular example employed a noise level of 20%, equivalent to the scalar variability of the spatially correlated signal. The spatial decorrelation length scale used to create the correlated flux errors was 500 km, equal to that used as the a priori estimate. Table 1 shows summary statistics for the mean flux estimates of upscaled, increasingly coarse, gridded flux regions for this example. These statistics will be used as the measure of fit for inversions based upon the complete set of levels mentioned above.

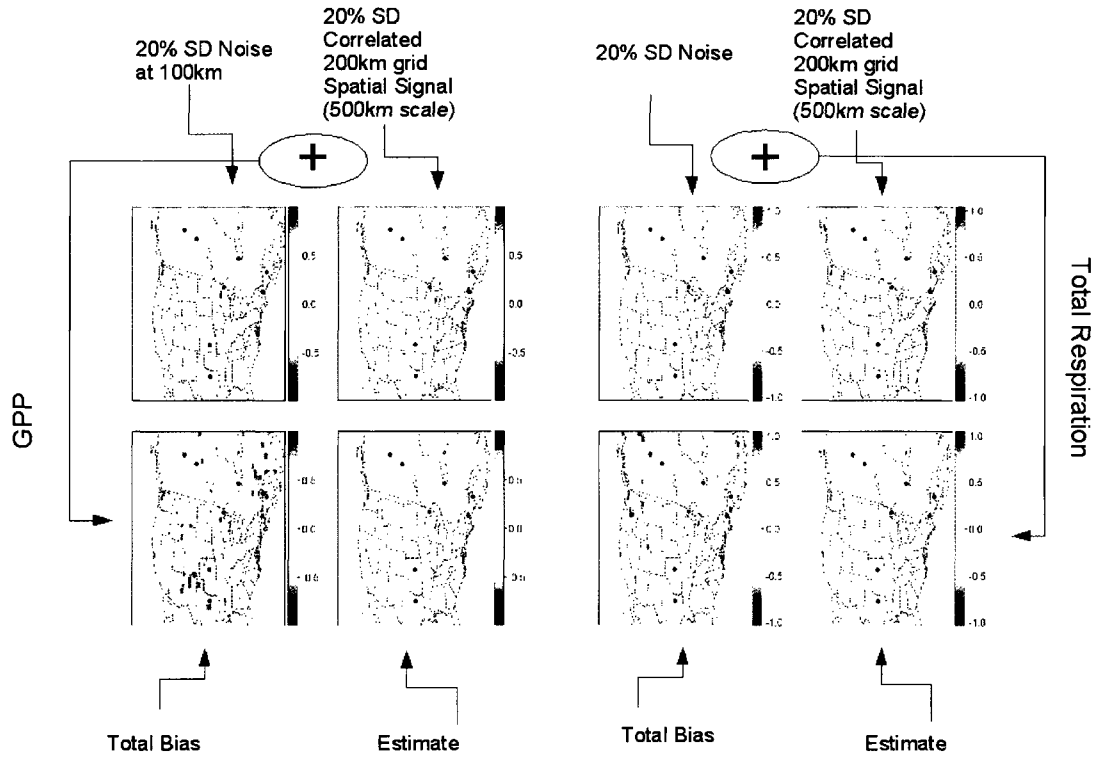


Figure 4.1: Example correction of GPP and total respiration signal. 4 Panel Plots: Upper left: small spatial scale bias applied over model domain, upper right: large scale bias over model domain which we would like to recover, lower left: total signal (sum of small and large), lower right: posterior estimate of mean bias. The eight CO₂ observing towers are

Table 4.1. Summary statistics for example inversion shown in Fig. 1.

Flux-based Statistics	200km	400km	600km	1200km	Domain
Prior Mean RMSE (g/m ²)	45.3	38.4	35.3	26.8	2.6
Posterior Mean RMSE (g/m ²)	28.2	20.5	16.4	8.0	1.7
Percent Improvement over Prior	39.2%	49.1%	56%	72.3%	57.1%
Percent improvement in mean SD for grid cell mean over Prior (crude measure of tightening of posterior)	32.5%	40%	45.8%	59.1%	77.9%

Note: This result is based upon a simulated observation error and thus changes slightly with different realizations. Third row of table is what is presented in Fig. 2 for multiple inversion study.

Results

Results from the sample realization, shown in Fig. 1, indicate that the posterior improves fluxes considerably over the a priori estimates. Improvement in the spatial average RMSE over the prior fluxes is from 40% to 90% depending upon the post aggregation level. This is promising, considering that the level of small scale noise (20% at 100 km) is equivalent to that of the spatially correlated portion of the flux errors (20%) for this example.

Figure 2 shows these results over the entire range of small scale variability and decorrelation length scale parameters given in Sect. 2.4. The aggregated results, based upon 100 km resolution inversions, are shown in blue. Variability within each panel of the image is due to the fact that the underlying bias field is not known and therefore has to be sampled over the set of all possible bias fields. The improvement in the spatial average RMSE over the prior is generally in the range of 20% to 90% over all combinations. The results show that the inversion is robust to small scale spatial noise over a wide range of noise levels and decorrelation length scales. Although it may seem at first glance that these results contradict findings of others, such as Peylin et al. [2005] who found that changing a priori covariance assumptions impacts the strength and location of corrections, spatially, it must be understood that these results are presented as large scale spatial averages. The degree and location of correction is likely to change with varying a priori spatial assumptions on the errors but as one post aggregates results to larger scales, corrections appear more robust. This is likely a result of varying a priori spatial assumptions driving correlated posterior flux estimates.

The power of higher resolution inversions versus lower resolution “pre-aggregated” inversions is shown in Fig. 2 as well. Inversions performed on the grid cell size shown in the x-axis are shown in red. For instance, at the point in an individual panel at which the x-axis indicates 600 km, the blue results give aggregated results based upon 100 km inversions while the red results give results based upon 600 km inversions. The difference is clearly most sensitive to the spatial correlation length scale of the bias pattern while much less sensitive to the layer of noise added to the flux biases. This is as one would expect, very smooth bias fields require less precise spatial estimates of the biases while less smooth bias fields require more precise spatial estimates.

Figure 3 shows the “contraction” of the cumulative NEE integrated over the entire domain from the a priori cumulative flux to the posterior cumulative flux, centered around the assumed true cumulative NEE. The a priori NEE is the same for all the inversions while the posterior NEE distribution is based upon the example inversion given previously. The posterior cumulative flux estimates are much closer to the truth, displaying significantly less variability. Furthermore, the a priori spatially integrated cumulative fluxes appear to show a reasonable range of possible deviations, +/- 3PgC per year, from the a priori assumed mean-zero annual NEE balance of SiB3, representing the potential to encompass many realistic source/sink scenarios.

Inversion Sensitivity to 100km Noise

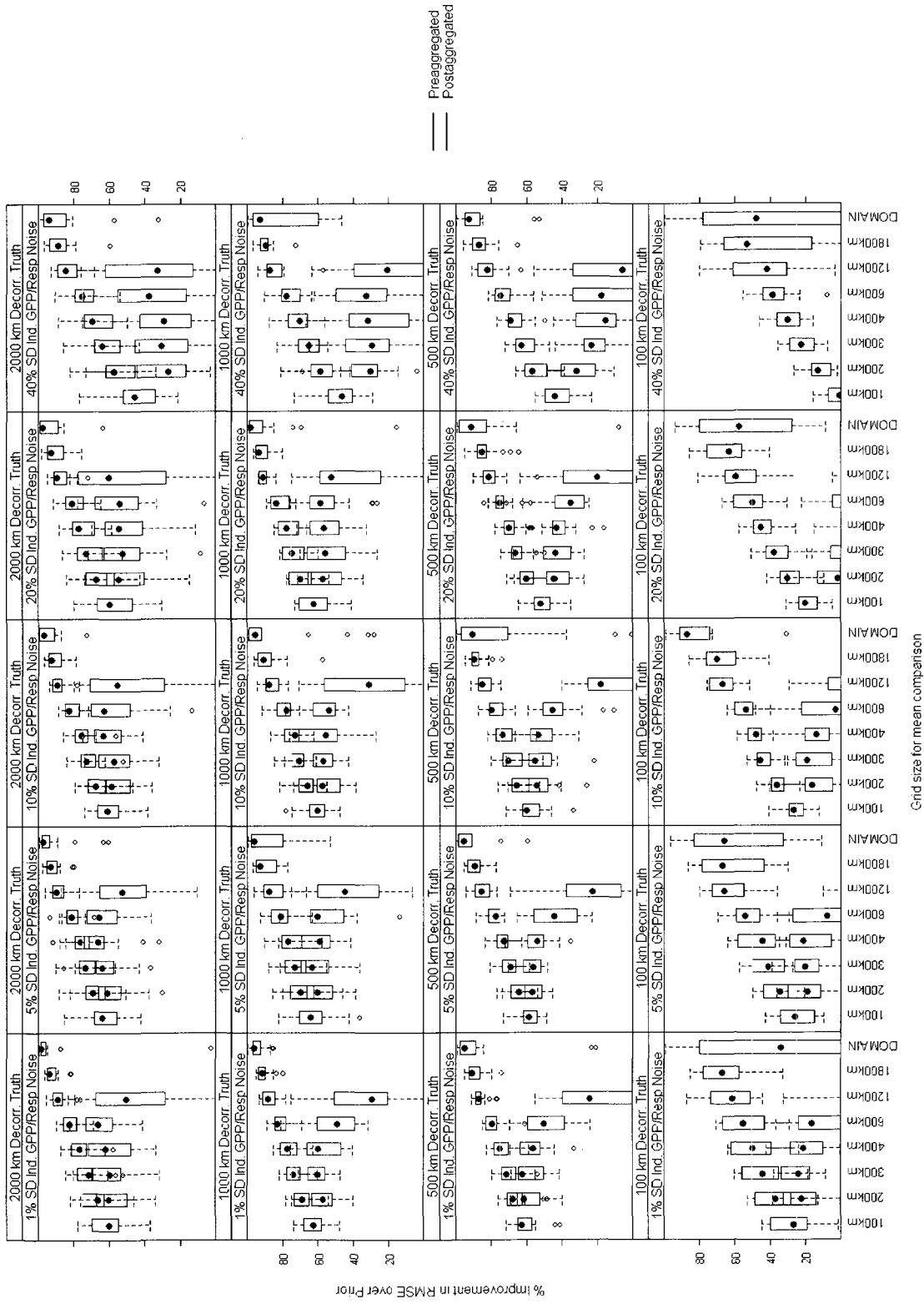


Figure 4.2: Improvement of posterior with respect to prior, for pre-aggregated (red) and post-aggregated (blue) inversion grid, factored over noise level and decorrelation length scale of true pattern used. Pre-aggregated (red) inversions are only performed for grid sizes between 200 km and 1200 km.

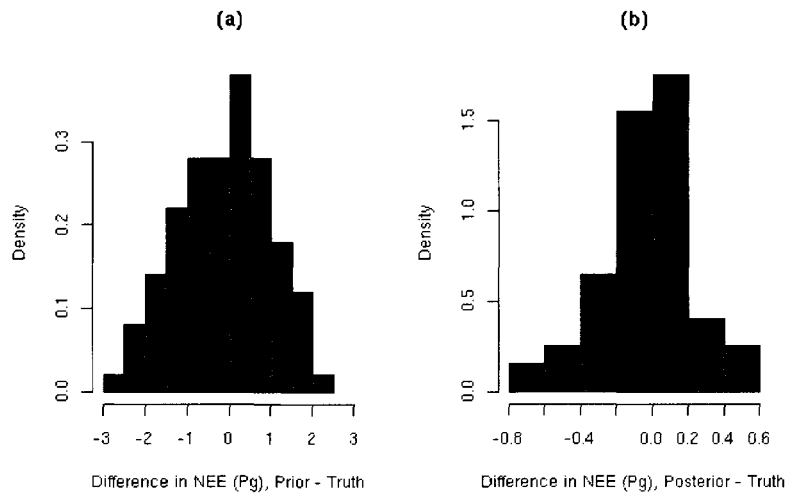


Figure 4.3: Prior(a) and posterior(b) cumulative NEE over period of 5/11/2004 – 8/31/2004 for example shown in Fig. 4.1 and Table 4.1.

Conclusions

The results of this paper show that NEE predictions can be significantly improved when large scale spatial bias patterns exist in the GPP and respiration estimates. Predictions are improved across a range of possible spatial decorrelation length scales. Furthermore, and most importantly, these relatively large-scale post-aggregated fluxes are robust to significant small scale spatial noise that may exist in the flux biases at resolutions that are commonly used for regional inversion studies.

One might have predicted that the inversion would be influenced heavily by small scale variability in a few grid cells surrounding the towers where the CO₂ observations were made. However, even when only 33% of the overall variability is on the larger scales, improvements of greater than 40% (RMSE) can be made, dependent upon the post aggregation unit. In general, this is not true of eddy-covariance-based flux tower measurements which often capture the effect of a small flux footprint (a few km). These measurements may not be very representative of surrounding fluxes, even those in close proximity to the tower and shows the value of collecting and analyzing CO₂ mixing ratio measurements.

There are several components of a standard regional inversion which are not addressed in this paper due to the nature of the hypothesis and result. For example, the choice of temporal averaging time for observations is not necessarily needed for this paper but needs investigation in an applied regional inversion. Boundary inflow of CO₂ also plays a very critical role in regional inversions but is not needed for this paper. These will be investigated and included in a paper utilizing real 2004 tower observation data in the next chapter.

Literature Cited

- Baker, I.; Denning, A.; Prihodko, L., Schaefer, K., Berry, J.; Collatz, G., Suits, N., Stockli, R., Philpott, A. & Leonard, O.: Global Net Ecosystem Exchange (NEE) of CO₂, Available on-line [<http://www.daac.ornl.gov>] from Oak Ridge National Laboratory Distributed Active Archive Center, Oak Ridge, Tennessee, U.S.A., 2007
- Baker, I., Denning, A. S., Hanan, N., Prihodko, L., Uliasz, M., Vidale, P., Davis, K. & Bakwin, P.: Simulated and observed fluxes of sensible and latent heat and CO₂ at the WLEF-TW tower using Sib 2.5, *Global Change Biology* 9, 1262-1277, 2003
- Chevallier, F., N. Viovy, M. Reichstein, and P. Ciais, On the assignment of prior errors in Bayesian inversions of CO₂ surface fluxes, *Geophys. Res. Lett.*, 33, L13802, doi:10.1029/2006GL026496, 2006
- Collatz, G. J., Ball, J. T., Grivet, C. & Berry, J. A.: Physiological and environmental regulation of stomatal conductance, photosynthesis, and transpiration: a model that includes a laminar boundary layer, *Agricultural and Forest Meteorology* 54, 107-136, 1991
- Collatz, G. J., Ribas-Carbo, M. & Berry, J. A.: Coupled photosynthesis-stomatal conductance model for leaves of C₄ plants, *Aust. J. Plant Physiol.* 19, 519-538, 1992
- Cressie, N., *Statistics for spatial data*, Wiley Interscience, 1993.
- Dai, Y., Zeng, X., Dickinson, R., Baker, I., Bonan, G., Bosilovich, M., Denning, S., Dirmeyer, P., Niu, P. H. G., Oleson, K., Schlosser, A. & Yang, Z.: The common land model (CLM), *Bulletin of the American Meteorological Society* 84, 1013–1023, 2003
- Denning, A. S., Collatz, J. G., Zhang, C., Randall, D. A., Berry, J. A., Sellers, P. J., Colello, G. D. & Dazlich, D. A.: Simulations of terrestrial carbon metabolism and atmospheric CO₂ in a general circulation model. Part 1: Surface carbon fluxes, *Tellus* 48B, 521-542, 1996
- Denning, A. S., Nicholls, M., Prihodko, L., Baker, I., Vidale, P., Davis, K. & Bakwin, P.: Simulated variations in atmospheric CO₂ over a Wisconsin forest using a couple ecosystem-atmosphere model, *Global Change Biology* 9, 1241-1250, 2003
- DePury, D. & Farquhar, G.: Simple scaling of photosynthesis from leaves to canopies without the errors of big-leaf models, *Plant, Cell, and Environment* 20, 537-557, 1997
- Desai, A. R., Bolstad, P. V., Cook, B. D., Davis, K. J. & Carey, E. V.: Comparing net ecosystem exchange of carbon dioxide between an old-growth and mature forest in the upper Midwest, USA, *Agricultural and Forest Meteorology* 128, 33-55, 2005
- Enting, I., Trudinger, C. & Francey, R.: A synthesis inversion of the concentration and d13C of atmospheric CO₂, *Tellus* 47B, 35-52, 1994
- Evensen, G.: Sequential data assimilation with a nonlinear quasi-geostrophic model using Monte Carlo methods to forecast error statistics, *Journal of Geophysical Research* 99, 143-162.

- Fan, S., Gloor, M., Mahlman, J., Pacala, S., Sarmiento, J., Takahashi, T. & Tans, P. (1998): A large terrestrial carbon sink in North America implied by atmospheric and oceanic carbon dioxide data and models, *Science* 282, 442-446, 1994
- Farquhar, G. D., Caemmerer, S. V. & Berry, J. A.: A biochemical model of photosynthetic CO₂ fixation in the leaves of C₃ species., *Planta* 149, 78-90, 1980
- Gurney, K. R., Law, R. M., Denning, A. S., Rayner, P. J., Baker, D., Bousquet, P., Bruhwiler, L., Chen, Y., Clais, P., Fan, S., Fung, I. Y., Gloor, M., Helmann, M., Higuchi, K., John, J., Maki, T., Maksyutov, S., Masarie, K., Peylin, P., Prather, M., Pak, B. C., Randerson, J., Sarmiento, J., Taguetti, S., Takahashi, T. & Yuen, C.: Towards robust regional estimates of CO₂ sources and sinks using atmospheric transport models, *Nature* 415, 626-630, 2002.
- Hanan, N. P., Berry, J. A., Verma, S. B., Walter-Shea, E. A., Suyker, A. E., Burba, G. G. & Denning, A. S.: Model analyses of biosphere-atmosphere exchanges of CO₂, water and energy in Great Plains tallgrass prairie and wheat ecosystems, *Agricultural and Forest Meteorology*, 2004.
- Johnson, R. A. & Wichern, D. W., *Applied Multivariate Statistical Analysis*, Prentice Hall, 1988.
- Kaminiski, T., Rayner, P. J., Heimann, M. & Enting, I. G.: On aggregation errors in atmospheric transport inversions, *Journal of Geophysical Research* 106, 4703-4715, 2001.
- Law, B. E., Sun, O. J., Campbell, J., Tuyl, S. V. & Thornton, P. E.: Changes in carbon storage and fluxes in a chronosequence of ponderosa pine, *Global Change Biology* 9, 510-524, 2003.
- Michalak, A. M., Bruhwiler, L. & Tans, P. P.: A geostatistical approach to surface flux estimation of atmospheric trace gases, *Journal of Geophysical Research* 109, 1-19, 2004.
- Mu, Q., F. A. Heinsch, M. Zhao, S. W. Running. Development of a global evapotranspiration algorithm based on MODIS and global meteorology data. *Remote Sensing of Environment*, 111: 519-536., 2007.
- Nicholls, M. E., Denning, A. S., Prihodko, L., Vidale, P., Davis, K. & Bakwin, P.: A multiple-scale simulation of variations in atmospheric carbon dioxide using a coupled biosphere-atmospheric model, *Journal of Geophysical Research* 109, 2004.
- Parazoo, N.: Investigating synoptic variations in atmospheric CO₂ using continuous observations and a global transport model, Master's thesis, Colorado State University., 2007
- Peters, W., Miller, J. B., Whitaker, J., Denning, A. S., Hirsch, A., Krol, M. C., Zupanski, D., Bruhwiler, L. & Tans, P. P.: An ensemble data assimilation system to estimate CO₂ surface fluxes from atmospheric trace gas observations, *Journal of Geophysical Research* 110, D24304, 2005.
- Peylin, P., Rayner, P. J., Bousquet, P., Carouge, C., Hourdin, F., Heinrich, P., Ciais, P. & contributors, A.: Daily CO₂ flux estimates over Europe from continuous atmospheric measurements: 1, inverse methodology, *Atmospheric Chemistry and Physics* 5, 3173-3186, 2005.
- Randall, D. A., Sellers, P. J., Berry, J. A., Dazlich, D. A., Zhang, C., Collatz, G. J., Denning, A. S., Los, S. O., Field, C. B., Fung, I., Justice, C. O., Tucker, C. J. & Bounoua, L.: A Revised Land-Surface Parameterization (SiB2) for Atmospheric GCMs. Part 3: The Greening of the CSU General Circulation

Model, *Journal of Climate* 9, 738-763, 1996.

Sellers, P. J., Mintz, Y., Y. C. Sud & Dalcher, A.: A simple biosphere model (SiB) for use within general circulation models, *Journal of Atmospheric Sciences* 43, 505-531, 1986.

Sellers, P. J., Randall, D. A., Collatz, G. J., Berry, J. A., Field, C. B., Dazlich, D. A., Zhang, C., Collelo, G. D. & Bounoua, L.: A Revised Land Surface Parameterization (SiB2) for Atmospheric GCMs. Part I: Model Formulation, *Journal of Climate* 9, 676-705, 1996.

Suits, N. S., Denning, A. S., Berry, J. A., Still, C. J., Kaduk, J. & Randerson, J. T.: Seasonal and spatial variations in carbon isotopic ratios of plant biomass, terrestrial CO₂ fluxes and atmospheric CO₂, *Global Biogeochemical Cycles*, 2004.

Thornton, P. E., Law, B. E., Gholz, H. L., Clark, K. L., Falge, E., Ellsworth, D. S., Goldstein, A. H., Monson, R. K., Hollinger, D., Falk, M., Chen, J. & Sparks, J. P.: Modeling and measuring the effects of disturbance history and climate on carbon and water budgets in evergreen needleleaf forests, *Agricultural and Forest Meteorology* 113, 185-222, 2002.

Uliasz, M., Lagrangian particle modeling in mesoscale applications, in P. Zannetti, ed.: *Environmental Modeling III*, Computational Mechanics Publications, , pp. 145-182, 1996.

Uliasz, M., Lagrangian particle modeling in mesoscale applications, in P. Zannetti, ed.: *Environmental Modeling II*, Computational Mechanics Publications, , pp. 71-102, 1994.

Uliasz, M.: The atmospheric mesoscale dispersion modeling system (MDMS), *Journal of Applied Meteorology* 32, 139-149, 1993.

Ulliasz, M. & Pielke, R. A.: Application of the receptor oriented approach in mesoscale dispersion modeling, in H. Van Dop & D. G. Steyn, ed., *Air Pollution Modeling and its Applications VIII*, Plenum Press, New York, 399-408, 1991.

Vidale, P. L. & Stockli, R.: Prognostic canopy air space solutions for land surface exchanges., *Theoretical Applied Climatology* 80, 245-257, 2005.

Wang, J. W., Denning, A. S., Lu, L., Baker, I. T. & Corbin, K. D.: Observations and simulations of synoptic, regional, and local variations in atmospheric CO₂, *Journal of Geophysical Research* 112, 2006.

Zupanski, Dusanka, Denning, A. Scott, Marek Uliasz, Zupanski, Milija, Schuh, Andrew E., Rayner, Peter J., Peters, Wouter & Corbin, Katherine D.: Carbon flux bias estimation employing Maximum Likelihood Ensemble Filter (MLEF), *Journal of Geophysical Research* 112, 2007.

V. A REGIONAL HIGH-RESOLUTION CARBON FLUX INVERSION OF NORTH AMERICA FOR 2004.

Abstract

Resolving the discrepancies between NEE estimates based upon (1) ground studies and (2) atmospheric inversion results, demands increasingly sophisticated techniques. In this paper we present a high-resolution inversion based upon a regional meteorology model (RAMS) and an underlying biosphere (SiB3) model, both running on an identical 40 km grid over most of North America. Previous papers have utilized inversion regions formed by collapsing biome-similar grid cells into large aggregated regions. The effect of this is that the NEE *correction* imposed on forested regions on the east coast of the United States might be the same as that imposed on forests on the west coast of the United States while there likely exist subtle differences in the two areas, both natural and anthropogenic. Our current inversion framework utilizes portions of the geostatistical approach taken by Michalak et al. [2004] and others and also allows carbon flux corrections to be biome independent. Temporally and spatially high-resolution results utilizing biome-independent corrections provide insight into carbon dynamics in North America.

In particular, we analyze hourly CO₂ mixing ratio data from a sparse network of eight towers in North America for 2004. A prior estimate of carbon fluxes due to gross primary productivity (GPP) and ecosystem respiration (ER) is constructed from the SiB3 biosphere model on a 40 km grid. A combination of transport from the RAMS and PCTM models is used to forge a connection between upwind biosphere fluxes and downwind observed CO₂ mixing ratio data. A Kalman filter procedure is used to estimate weekly corrections to biosphere fluxes based upon observed CO₂. RMSE-weighted annual NEE estimates, over an ensemble of potential inversion parameter sets, show a mean estimate 0.57 Pg/yr sink in North America. We perform the inversion with two independently derived boundary inflow conditions and calculate jackknife-based statistics to test the robustness of the model results. We then compare final results to estimates obtained from Level-4 Ameriflux data and the INTEx aircraft campaign. Results are promising, showing the ability to grossly correct carbon fluxes from the biosphere models over annual and seasonal time scales, as well as over the different GPP and ER components, and also providing interesting hypotheses for future work.

Introduction

Carbon dioxide inversion studies have generally been focused on improved estimation of terrestrial carbon fluxes such as ecosystem respiration (ER), gross primary

production (GPP), and net ecosystem exchange (NEE) as a means to better understand the carbon cycle of the earth. Researchers have progressively increased the resolution, in both time and space, and accuracy of the carbon flux estimates over the past decade. Early inversion studies were focused primarily with finding an explanation for the missing sink of carbon that can be easily identified from calculating a budget from annual fossil fuel emissions to the atmosphere, the effect of land use changes, and the oceanic carbon sink and comparing it to annual records of increasing atmospheric carbon dioxide concentrations. Given that it often represents a third of the annual fossil fuel emissions, it is of great interest to scientists and policy makers alike. Inversion results have been very effective at identifying large defining features of the terrestrial portion of the carbon sink (Fan et al., 1998, Gurney et al., 2002) although much debate remains even at extremely large scales (Stephens et al., 2007). However, the debate on a global scale has not deterred researchers from focusing these techniques on finer scale problems. In fact, criticism has been aimed at large scale global inversions because of the fact that their estimates can be biased on finer regional scales (Kaminski et al., 2001). The data available for regional inversion studies is increasing rapidly year after year, primarily within the developed industrial nations of the Northern Hemisphere. This provides researchers with some of the first opportunities to perform inversion studies in a very high-resolution setting.

Gerbig et al. 2003 provided the first major regional inversion paper. They used a receptor-oriented inversion approach to investigate a series of flights from the CO₂ Budget and Rectification Airborne (COBRA) study conducted in 2000. Results showed that the effect of biosphere carbon fluxes could be seen at altitude in mixed layer CO₂

observed by aircraft. The paper pointed out several areas for future improvements in regional inverse modeling including improving biosphere-atmosphere exchange and convective transport modeling. Peylin et al. 2005 followed this with a regional inversion based on western Europe in which he estimated daily fluxes for a month using relatively continuous measurements of CO₂ from towers in the inversion domain. The most similar effort made for North America comes from the ongoing CarbonTracker project (Peters et al., 2007). Peters et al. used a nested transport structure (TM5) with a relatively high-resolution 1-degree inner grid over North America. A priori carbon fluxes were estimated by modifying 1-degree by 1-degree monthly output from the Carnegie Ames Stanford Approach (CASA) model to provide diurnal variability by incorporating a Q₁₀ temperature relationship for respiration and a linear scaling of GPP with solar radiance. NEE estimates were optimized by estimating linear correction factors for NEE for each of 17 ecoregion-based (Olsen et al., 1992) sub-areas of North America based upon a 5-week smoothing window. The coarseness of the inversion over North America is required in order to be able to solve biases simultaneously across the globe on the coarser nested grids.

Our inversion framework has drawn upon certain techniques from previous inversions while including some new features. The aim of the inversion is to provide fine scale inversion results over North America for 2004. A novel feature of this inversion is the distinct estimation of GPP and ER instead of just NEE, which to our knowledge has not previously been performed, at least in the regional framework. We have drawn upon the spatial correlation constraints used by Rodenbeck et al. 2003 and Michalak et al. 2004, largely in order to regularize the inversion problem. Large matrix inversions,

required of nearly all inversion techniques, limited the inversion grid size to approximately 10,000 km² (100 km by 100 km cells). For sensitivity studies involving numerous inversion runs, a 40,000 km² grid (100 km by 100 km cells) is used. Most previous global inversions have been performed upon grid areas of around 5 to 10 times that size. In order to provide some contrast, CarbonTracker optimizes 17 bias correction factors for NEE while this inversion typically optimizes 540 each for ER and GPP. However, this does not come without a cost since we can't simultaneously optimize fluxes outside of North America. Therefore we used offline-derived boundary conditions and provided these as fixed contributions to the tower CO₂ budget.

Previous work (Ch. 3) showed that considerable success could be achieved in estimating large spatial scale ER and GPP signals in the midst of small spatial scale variability in fluxes. We leveraged this result and put the problem in a Kalman filter framework in order to allow higher resolution spatial estimation. This filter is of a somewhat simple variety and allowed us to work with all portions of the inversion, such as complete prior and posterior covariance matrices, explicitly. We then tested sensitivity to a number of pieces of the inversion considered uncertain, including parameters in the actual inversion as well as fixed contributions to the modeled CO₂ such as fossil fuel and boundary inflow. As far as we know this is also the first paper providing a comparison of inversion results derived by using two independent boundary inflow estimates. Additionally, the effect of including recently available high-resolution fossil fuel inventory data is quantified.

Methods

Prior flux model and transport

The Simple Biosphere model (SiB) is based on a land-surface parameterization scheme originally used to compute biophysical exchanges in climate models (Sellers et al., 1986), but later adapted to include ecosystem metabolism (Sellers et al., 1996a; Denning et al., 1996a). SiB has been coupled to the Brazilian version of the Regional Atmospheric Modeling System (RAMS, Pielke et al., 1992; Frietas et al., 2006) and used to study PBL-scale interactions among carbon fluxes, turbulence, and CO₂ mixing ratio (Denning et al., 2003) and regional-scale controls on CO₂ variations (Nicholls et al., 2004; Wang et al., 2006). This latest version of SiB is termed SiB3.

In SiB3, net ecosystem exchange (NEE) is composed of two component fluxes, gross primary productivity (GPP) and ecosystem respiration (ER), which includes autotrophic (canopy respiration and root respiration) and heterotrophic respiration terms (due to decomposition of dead organic matter),

$$NEE(x,y,t) = ER(x,y,t) - GPP(x,y,t) \quad (1)$$

where x and y represent grid coordinates and t represents time. High-frequency time variations of photosynthesis and respiration are assumed to be well understood and easily modeled processes, i.e. due to diurnally varying quantities such as radiation, temperature, or longer term variations in modeled quantities such as soil moisture etc. Photosynthesis and assimilation are derived using a coupling of equations based upon the work of Farquhar, Collatz, and Ball (Farquhar et al., 1980; Collatz et al., 1992; Ball et al., 1987) while soil respiration is based upon a rather simple function of temperature and soil moisture and constrained in such a way that annual NEE is equal to zero (Raich et al., 1991; Denning et al., 1996)

Several papers have provided comparisons of models to observations, largely by using eddy flux towers to estimate true fluxes of water, carbon, and energy (Baker et al., 2003; Hanan et al., 2005; Baker et al., 2008). Longer-term, more persistent biases are estimated by solving for unknown multiplicative biases in each component flux after smoothing in space and time. While these biases could result from incorrectly modeled short term processes, such as errors in the daily development of the planetary boundary layer, or short-term processes not in the model such as seasonal fertilization and irrigation, the main purpose is to capture longer-term processes not explicitly modeled such as land use change (Robertson et al., 2000, Peterson et al., 1998), disturbances, anthropogenic fertilization effects (Oren et al., 2001), managed forestry (Tillman et al. 2000), and large scale carbon removal (Ciais et al., 2007). This modeling is accomplished by convolving the *influence* functions generated from a lagrangian particle dispersion model, LPDM (Uliasz and Pielke, 1991; Uliasz, 1993, 1994; Uliasz et al., 1996; Zupanski, 2007), with gridded gross primary productivity (GPP) and total ecosystem respiration (ER) at each time step in SiB3-RAMS. The LPDM transport scheme reverses advection derived from RAMS at very fine time scales and parameterizes vertical turbulent diffusion according to a Gaussian process. A large advantage of this model is the ability to simulate transport of atmospheric constituents at sub grid scales, reducing representation error that might be caused by associating an observing tower with a 40 km grid cell in the model. By tracking particles upwind, backward in time, from the towers, one may make inferences about the contribution of upstream GPP and ER sources.

In particular, we have estimated regional fluxes from atmospheric mixing ratios

by assuming that the model of the component fluxes is biased, and that the biases are smoother in time and space than the fluxes themselves:

$$NEE(x,y,t) = (1 + \beta_{RESP}(x,y))ER(x,y,t) - (1 + \beta_{GPP}(x,y))GPP(x,y,t) \quad (2)$$

The model domain, shown in Fig. 5.1/Fig. 5.2, consists of most of the United States as well as a large portion of Canada and the northern portions of Mexico. Both SiB3 and RAMS were run on a single 150 x 90 grid of 40 kilometer cells, with SiB3 utilizing 3 patches per cell to

capture subgrid-scale variability in land cover.

RAMS

meteorology was nudged

with 40 kilometer

forecast meteorology

from the National Center

for Environmental

Protection's Eta model

throughout the domain

using a 4 dimensional data assimilation (4DDA) scheme to produce more reliable wind

fields. Soil classes were calculated from 5 minute "% clay / % sand / % silt" soil data

from the International Geosphere-Biosphere Programme (IGBP) (Fig. 5.1). Biomes were

extracted from the UMD classification scheme of the MODIS 12 Landcover 1 km

product and mapped to the most similar SiB biome class for all cells and for each of the

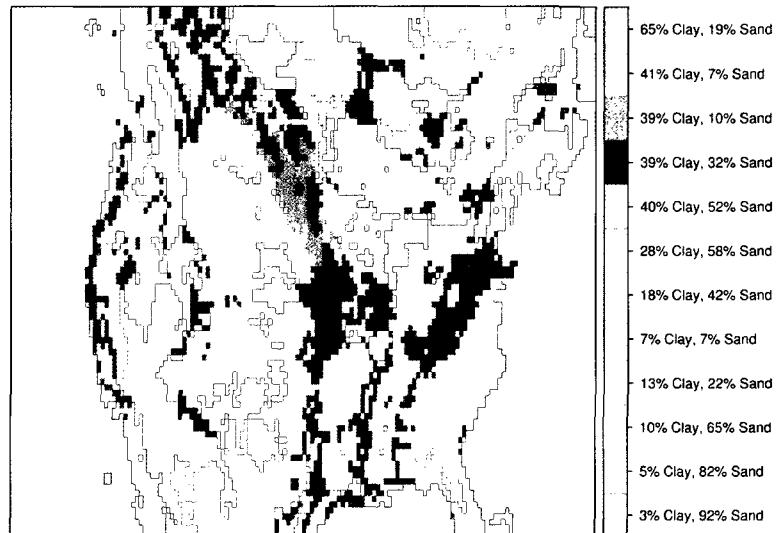


Fig 5.1. Soil classes (IGBP) used for SiB3

three patches used (Fig. 5.2). An exception are the C₄ vegetation classes, grasses and crops, which were projected onto the MODIS biomes from [Wang et al. 2006]. The crop characterization is admittedly simple and more work is currently being done to incorporate more accurate crop maps and more realistic crop modeling into SiB (Lokupitiya et al., 200*).

SiB has traditionally calculated fPAR, which defines the fraction of photosynthetically available radiation that is absorbed by the plant canopy, and leaf area index (LAI) using

satellite derived NDVI fields. The code was

changed to use fPAR and LAI fields derived by the Moderate Resolution Imaging Spectroradiometer (MODIS) (Mu et al., 2007) and averaged over appropriate biome-areas based upon the three patch scheme. SiB3 was run with these 8-day fPAR and LAI products that were provided by the Numerical Terradynamics Simulation Group at the University of Montana who generated it for use in constructing the official Moderate Resolution Imaging Spectroradiometer GPP product.

Modeled carbon dioxide at the tower is calculated as the sum of 3 component fluxes convoluted by *time* and *tower* dependent transport.

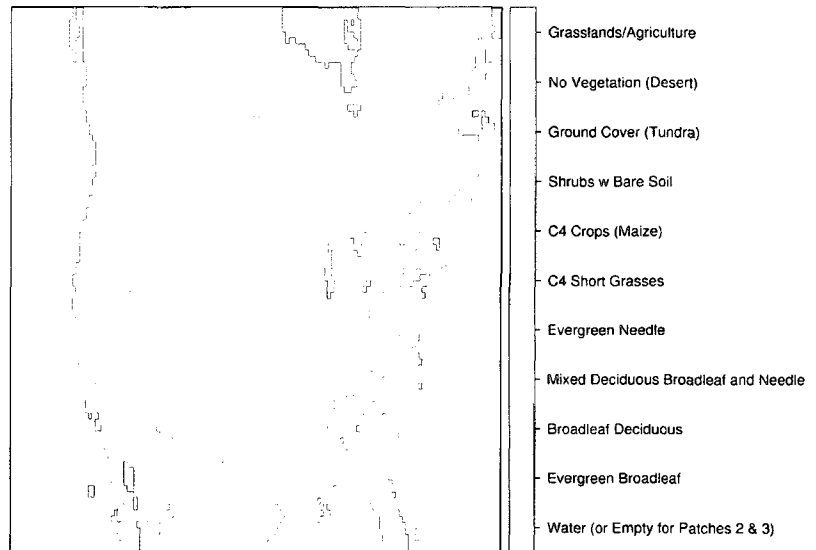


Fig 5.2. Dominant SiB3 biome classes for the first biome patch derived from MODIS 12 Landcover product

$$CO_2(\text{time}, \text{tower}) = \text{Transport}_{\text{time}, \text{tower}} \left(\begin{array}{l} \text{Boundary Inflow}(x, y, \text{time}) \\ + \text{Fossil Fuel}(x, y, \text{time}) \\ + \text{Domain Biogenic Fluxes}(x, y, \text{time}) \end{array} \right) \quad (3)$$

The boundary inflow component was calculated by convolving the influence functions from the LPDM model over boundary CO₂ fields derived using a global biosphere-transport model. At any point in time, the boundary inflow is the average of all upstream particles located in a 3 dimensional 40 km thick rectangular “ring” around the domain. CO₂ resulting from the transport of fossil fuels to the towers is calculated by convolving the influence functions from the LPDM model with surface fossil fuel flux estimates. In particular, the boundary CO₂ fields were calculated by combining transport from the parameterized chemistry transport model (PCTM) (Kawa et al., 2004; Parazoo, N.C. 2007) and pre-calculated archived hourly SiB3 fluxes (Baker et al., 2007) on a 1.25-degree by 1-degree global grid. The model was spun up for 2000-2004 and the CO₂ was centered around the Northern Hemispheric mean CO₂ for 2004. In addition to this, results from the CarbonTracker project, which provide globally optimized CO₂ concentration fields, are used for comparison purposes.

Fossil fuel fields were constructed using recently available high resolution Vulcan fossil fuel inventory fields (Gurney et al., 2008), at a 10 km horizontal spatial scale and hourly temporal scale. Previously available fossil fuel flux fields were derived by distributing country-level fossil fuel sources spatially as a function of population at a 1-degree resolution (Andres et al., 1995). The Vulcan fields provide many improvements including the incorporation of mobile emission sources and power plants, often located in areas distant from high density population centers, increased temporal resolution

allowing the modeling of diurnal variability, and increased spatial resolution allowing better delineation of high density population centers. The sensitivity to the new fossil fuel fields is tested by running inversions using both the Vulcan fields as well as the Andres et al. 1995 fields.

SiB3 balances carbon annually by assuming that ER is in approximate balance with GPP on an annual time frame for each surface location and therefore annual NEE is zero for each surface location or grid cell (Raich et al., 1991; Denning et al., 1996). While this is accurate to a large degree and provides reasonable approximations of respiration on diurnal time scales, it ignores annual imbalances in carbon due to a number of external factors such as land use, fertilization effects, disturbance history, etc. For example, aerial photos and satellite images of the coastal mountains of Oregon show a patchwork of forest ages largely dictated by forest management practices. Under standard models of forest regrowth, a regenerating forest will eventually enter a long period in which carbon is being drawn from the atmosphere and stored in wood and roots, thereby providing a sink of carbon from the atmosphere to the biosphere. Conversely, recently burned forests usually enter a short-term period in which they represent a significant carbon source to the atmosphere. Processes such as these that are largely responsible for annual imbalances in NEE are not characterized in SiB3.

The effect of this on boundary inflow estimates is that the PCTM-SiB3 calculated boundary CO₂ fields lacks the effect of sources or sinks in 2004. Given the consensus opinion of an annual mean sink for carbon resulting from the biosphere, this means that the CO₂ fields used will be biased somewhat by the effect of not including this expected global sink. We investigate the effect of this by including a comparison of the inversion

using CarbonTracker optimized CO₂ concentration fields for boundary inflow, which provides an estimate of sources/sinks. As of this time, carbon dioxide resulting from forest fires is not included in the global PCTM-SiB3 inflow or domain SiB3 runs, but is included in the CarbonTracker inflow providing one more contrast between the two fields.

Observational Data

Calibrated CO₂ observations were provided half-hourly at eight measuring sites (WLEF, Harvard Forest, ARM, BERMS, Fraserdale, Western Peatland, WKWT, and Argyle (ME)) for 2004 (Parazoo, 2007). Gerbig et al. [2003] found mean standard deviations on the order of 0.6 to 1 ppm when viewing morning and afternoon vertical profiles of CO₂ in the mixed layer. As a consequence, robust afternoon snapshot observations, at 12PM, 2PM, 4PM, and 6PM local time, are used to lessen the impact of low quality modeled measurements made during times of extremely stable and stratified nocturnal atmospheric conditions near the ground. One exception is the WKWT tower in Moody, TX. Data at this tower consistently showed high diurnally-influenced CO₂ concentrations in the 12PM records for most days. It is uncertain exactly what the cause of this is but it appears that it may be due to some kind of systematic late venting of nocturnal respiration-based CO₂ buildup. For this tower, mixed boundary layer conditions appeared to be better represented by snapshot observations shifted by 2 hours: 2PM, 4PM, 6PM, and 8PM. The first 10 days of the year are not comparable due to a lack of transport preceding 2004. In all there were 2433 missing observations, resulting in $4 \text{ (observations/day)} * 8 \text{ (towers)} * 355 \text{ (days)} - 2433 \text{ (missing)} = 8927 \text{ observations}$.

In a previous pseudo-data inversion using a very similar model (Zupanski et al., 2007), the errors on the observations were assumed to be 1 ppm for afternoon observations. Nevertheless, relative to the inversion techniques presented in the next section, the errors on these observations should include errors due to calibration error, mapping error, transport error, and representation error. For this inversion, transport error and representation error are likely the largest components which are notoriously tricky to quantify. Investigations into the sensitivity of inversion test results combined with initial maximum likelihood estimation results suggest errors in the range of 5-6 ppm are appropriate for this particular inversion. For the remaining inversions, the errors are assumed to be identical and independently distributed (i.i.d.) mean zero errors with standard deviation set to 5.5 ppm. It should be noted that while it is possible to run inversions with artificially low prescribed “observation” errors, this will generally manifest itself in a need to “over tighten” the a priori covariance structure.

Climatic Conditions for 2004

The 2004 year was the 6th wettest in the contiguous United States over the preceeding 110 years (1894-2004). It was also warmer than on average. Nevertheless, there was a great amount of variability in precipitation and temperature as a function of location and season. Drought continued in the west through the summer of 2004, essentially prolonging a multi-year period of drought conditions. The spring was also very dry for the southeast, extending a period of dry conditions from late in 2003. However, summer brought increased precipitation to the east and southeast, culminating in enormous amounts of rain in late summer and early fall due to an extremely active

hurricane season. The south (Texas, Louisiana, Mississippi, Arkansas, Oklahoma, and Kansas) had the wettest summer on record and was much cooler than average. These conditions were important as they provided initial conditions for the inversion that involved soil moisture induced plant stress over large areas of the United States.

Inversion Technique

Standard multivariate Gaussian assumptions are made and data are assimilated using a modified Kalman Filter algorithm (Kalman 1960). In particular, for an initial length n CO₂ measurement vector y representing the first set of measurements, length m unknown CO₂ flux bias vector β , $n \times n$ observation error covariance matrix Σ , $n \times m$ *Jacobian* transport matrix G , length m prior flux estimate β_0 , and $m \times m$ model-prior mismatch covariance matrix Σ_0 , the Bayesian statistical assumptions are:

$$\begin{aligned} y | \beta, \Sigma &\sim N(G\beta, \Sigma) \\ \beta &\sim N(\beta_0, \Sigma_0) \end{aligned} \quad (4)$$

The posterior distribution of the flux vector can be solved for analytically and is:

$$\begin{aligned} p(\beta | y, \Sigma) &\propto -\frac{1}{2} \left[(G\beta - y)^T \Sigma^{-1} (G\beta - y) + (\beta - \beta_0)^T \Sigma_0^{-1} (\beta - \beta_0) \right] \\ &\sim N \left((\Sigma_0^{-1} + G^T \Sigma^{-1} G)^{-1} (\Sigma_0^{-1} \beta_0 + G^T \Sigma^{-1} y), ((\Sigma_0^{-1} + G^T \Sigma^{-1} G))^{-1} \right) \end{aligned} \quad (5)$$

With a little bit of algebra, one can rewrite the mean of the posterior distribution of the mean, giving the Kalman-filter updating equation for the mean.

$$E[\beta] = \beta_0 + (G^T \Sigma^{-1} G + \Sigma_0^{-1})^{-1} G^T \Sigma^{-1} (y - G\beta_0) \quad (6)$$

The posterior mean and variance of x are then fed into the next filter step with a new set of measurements. This particular inversion estimates biases over 7-day periods using available data from that 7-day period of time. Therefore, bias estimates for both

ecosystem respiration and GPP as well as corresponding variance estimates are available for all of 2004 with the bias estimates changing with a weekly resolution.

Two difficulties often arise when using filter-style correction schemes. The filter estimates can drift away from realistic values if the data are not plentiful or precise enough to constrain it. Secondly, the nature of the Kalman filter at each step is to create posterior variance estimates that are in general smaller than the prior estimates. This can essentially cause the filter to get “stuck” and also produce unrealistically small posterior variance estimates around the biases. There is generally no easy solution to this problem. Artificially inflating the posterior variance at each filter step is one method in which one can try to circumvent (Zupanski et al. 2007). This accommodates the fact the biases are likely to change in reality and it allows the filter to consider a wider range of possibilities for the bias factors. However, it does not necessarily constrain the biases to any particular “reasonable” region of values allowing the bias estimates to drift into unrealistic parameter space. Therefore, we have chosen to weight the filter at each step with a “grand” prior. This effectively handles both of the preceding problems. With respect to our inversion, there will be three pieces of information at each step, the grand prior which is derived from the forward SiB3-RAMS model with an error assumption, the local prior which is derived from the previous filter step’s posterior flux bias distribution, and the data which forms the statistical likelihood function. In some sense, this new piece of the covariance structure provides a bound upon how much the inversion can “learn” about the bias structure.

In order to quantify, we denote the grand prior as a multivariate Gaussian distribution around β_{grand} with covariance matrix $\sigma_{grand}^2 \Sigma_{grand}$, and additional weight factor w , and we rewrite the expression given in (4) as:

$$p(\beta | y, \Sigma) \propto -\frac{1}{2} \left[(G\beta - y)^T \sigma_{obs}^{-2} I (G\beta - y) + (\beta - \beta_0)^T \sigma_0^{-2} \Sigma_0^{-1} (\beta - \beta_0) + (\beta - \beta_{grand})^T w \sigma_{grand}^{-2} \Sigma_{grand}^{-1} (\beta - \beta_{grand}) \right] \quad (7)$$

Thus β is distributed as a multivariate Gaussian with parameters:

$$Mean(\beta) = E[\beta] = \left(w^{-1} \sigma_{grand}^{-2} \Sigma_{grand}^{-1} + \sigma_0^{-2} \Sigma_0^{-1} + G^T \sigma_{obs}^{-2} I G \right)^{-1} \left(w \sigma_{grand}^{-2} \Sigma_{grand}^{-1} \beta_{grand} + \sigma_0^{-2} \Sigma_0^{-1} \beta_0 + G^T \sigma_{obs}^{-2} I y \right) \quad (8)$$

$$Variance(\beta) = E[\beta^2] - (E[\beta])^2 = \left(\left(w \sigma_{grand}^{-2} \Sigma_{grand}^{-1} + \sigma_0^{-2} \Sigma_0^{-1} + G^T \sigma_{obs}^{-2} I G \right) \right)^{-1} \quad (9)$$

Eq. 7 specifically separates out the variance scalars, σ_{grand}^2 , σ_0^2 , and σ_{obs}^2 from the covariance matrices, leaving the covariance matrices essentially scaled to 1. The w weight is a redundant factor and is simply included to facilitate easier interpretation of tightening/loosening of the grand prior covariance (around the SiB3 derived a priori carbon fluxes). Unless otherwise specified, this weight, w , on the grand covariance matrix is set to 2. This means that the initial variance around the grand prior is increased, thus providing a weaker constraint. For the initial filter step, only the grand prior is used. After that point, there exist both a grand prior and a prior (from the posterior of the previous filter step). The inversion is further constrained by the assumption of spatially

correlated errors in the grand prior, i.e. the covariance matrix Σ_{grand} will take on the following form.

$$\Sigma_{grand} = \begin{bmatrix} \Sigma_{Resp.,prior} & 0 \\ 0 & \Sigma_{Assimn.,prior} \end{bmatrix} \quad (10)$$

The respiration and GPP covariance matrices are each formed from the exponential covariance function, where $t_{i,j}$ is the distance between points β_i and β_j .

$$Cov(\beta_i, \beta_j) = \begin{cases} \sigma_0^2 (1 - \alpha_0) \exp\left(\frac{-t_{i,j}}{h_0}\right), & i \neq j \\ \alpha_0 \sigma_0^2, & i = j \end{cases} \quad (11)$$

The h_0 parameter is the range, or decorrelation length scale parameter, giving the distance at which the covariance between two points is equal to $\sigma_0^2 (1 - \alpha_0) e^{-1}$. The σ^2 parameter is the scalar variance parameter and determines the variance of the marginal distribution of the particular flux component. The parameter α_0 controls what percentage of the covariance can be attributed to spatial covariance, as opposed to spatially independent errors.

Inversion techniques can be extremely sensitive to assumptions. It was shown in Chapter 3 that this inversion model is robust to small spatial scale random deviations in flux bias and that post-aggregated (in space) estimates can be very good even when using a fairly sparse network of towers observing CO₂. Nevertheless, given the unconstrained nature of the inversion problem, it is always important to assess the impact of varying certain unknown parameters in the inversion, such as spatial decorrelation length scales, the weight given to the “grand” prior, and the fixed CO₂ contributions from both the boundary inflow and fossil fuel sources.

Sensitivity

The inversion essentially guarantees some improvement in prediction of observed CO₂ (Eq. 5). However, when using a regression style approach in a heavily unconstrained environment, this improvement can often be overstated because of the great freedom the inversion has to fit the data. Therefore, it is often desirable to go beyond simply comparing observed carbon dioxide at the towers to model-based predicted carbon dioxide. Comparing model observations to independent observations not used in the inversion, comparing models which predict similar quantities, as well as testing the sensitivity of the model to variations in unknown parameters are all methods of generating more confidence in estimates.

We used a variety of different procedures to test the sensitivity of the inversion. Regional inversions have been shown to be very sensitive to boundary inflow variations. Therefore, we first test the sensitivity of the inversion to varying the inflow of CO₂ at the boundaries. To do this, we derive boundary inflow to the 8 towers using the LPDM model and optimized carbon dioxide concentration fields from the CarbonTracker project (Peters et al., 2007). Inversion results are then compared with the results derived from the LPDM model and the PCTM inflow. Secondly, we vary several different variance parameters and derive annual domain-summed NEE and tower observation based RMSE based upon the varied parameters. Thirdly, we use a re-sampling procedure in which we create 100 different observation data subsets by holding out a randomly selected 50% of the observation data for each. Each set of data is run through the weekly inversion scheme and the sensitivity of the predicted CO₂ at the towers and the estimated flux biases is explored. This provides estimates of the variability of the flux correction factors

and can be used to assess the sensitivity of the source/sink to the constraint provided by the data. Using the held out data as independent evaluation data and the complementing data as training data for the inversion, one may also derive a more accurate estimate of root mean-squared error (RMSE) of the inversion-optimized fluxes. We test the impact of the high resolution Vulcan fossil fuel inventory on the inversion results by comparing inversion results relying upon Vulcan to those results utilizing the Andres et al. [1995] fossil fuel inventory.

SiB3 has been evaluated at many sites and over many time periods, nevertheless, the particular model run used for the a priori flux estimates was not optimized to fit the flux data at any site in particular. Even though there is a mismatch in representation, with the flux towers representing footprints of less than a square kilometer and the inversion results representing flux estimates on the scale of thousands of square kilometers, we believe that these comparisons are of value, especially in locations that are more spatially homogeneous than others, such as grasslands and large forest reaches. This is then the fourth comparison we make.

Results

As was indicated in the previous section, there are a number of variables that the inversion will likely be sensitive to and therefore the results are expected to be quite variable. For results, we choose to present one particular case with a fixed set of inversion inputs as an initial case study and then use it to compare the effect of varying the boundary inflow and the source of the domain fossil fuel fluxes. With reference to the preceding section and Eq. 7 in particular, the following values are used for these

inversions: $\sigma_{\text{grand}} = 0.15$, $\sigma_0 = 0.15$, $\sigma_{\text{obs}}^2 = 5.5$ ppm, $w = 2$, $h_0 = 250$ km. In particular, a value of $\sigma_{\text{grand}} = 0.15$ would mean that we expect that approximately 68% of the GPP and ER biases are within +/- 15% of the original SiB3 estimated fluxes, with 95% within +/- 30%. This variation when combined with positive spatial correlations was shown to provide a reasonable a priori range of annual domain-summed NEE. These deviations must generally be kept to less than 30% - 40% to ensure that posterior ER and GPP fluxes are not reduced by more than 100 percent, which makes no conceptual sense. We then test the sensitivity of the results over a number of varying inversion inputs using the PCTM boundary conditions and the Vulcan fossil fuel flux field.

General Structure of Results

CO₂ can be predicted by invoking the relationship shown in Eq. 3. The predicted mean observed CO₂ is derived as $G\hat{x}$ where \hat{x} represents one (for the prior fluxes) plus the inversion-optimized flux biases. Using the PCTM boundary conditions and the Vulcan fossil fuel inventory, a comparison of the inversion-corrected posterior predictions at the towers to the observations is shown in Fig. 5.3. For domain-summed temporal plots, NEE is calculated via Eq. 2 while ER and GPP are calculated via the two respective summands on right hand side of that equation. These domain-summed temporal results are shown in Fig. 5.4.

The observed carbon dioxide concentrations contain information that infers a dampening of the a priori annual GPP cycle, and hence the a priori annual ER cycle (due to the strong correlation of the annual sums of each). Since both GPP and ER are significantly dampened, it is not surprising that the NEE signal is dampened as well.

Furthermore, the data suggest a weak temporal shift in the prior NEE signal. This manifests itself as a stronger, but more gradual onset of spring, followed by a weaker overall carbon sink over the middle and late summer periods.

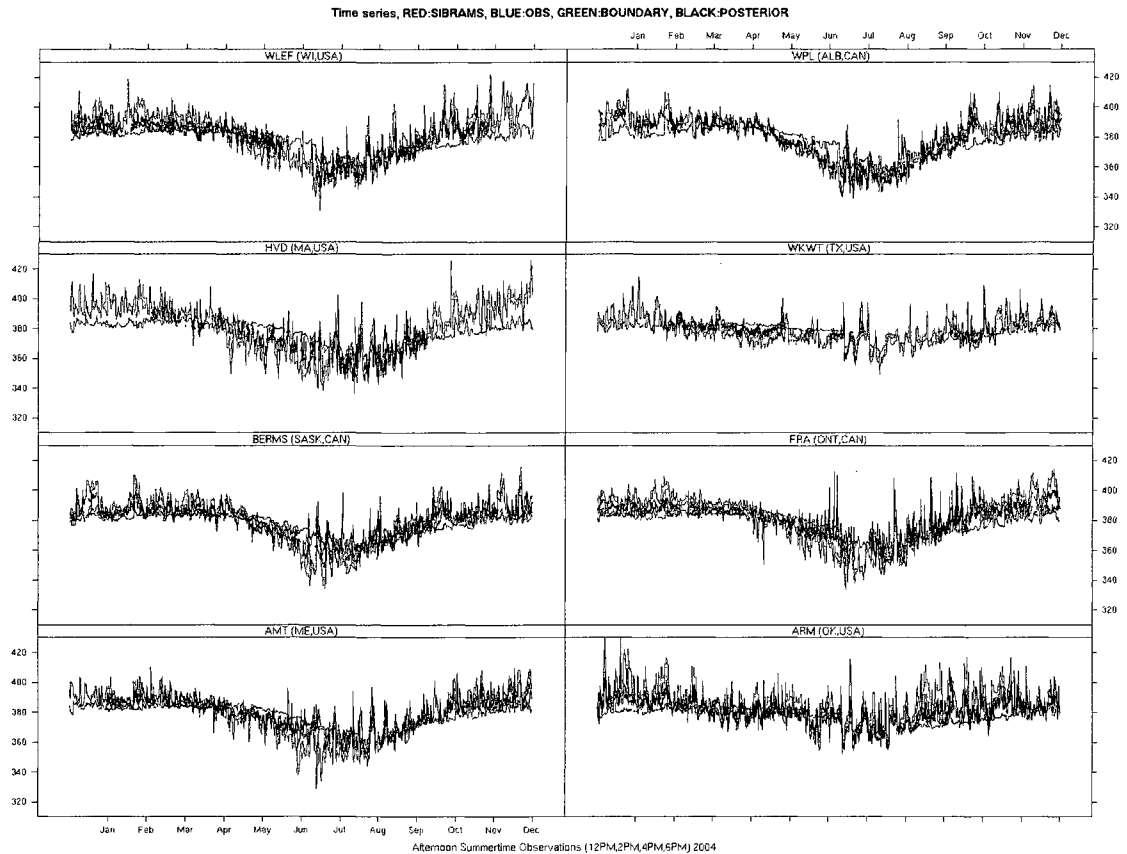


Figure 5.3: Time series plots of carbon dioxide observations (blue), SiBRAMS prior (red), boundary inflow estimate (green), and posterior prediction (black).

We use a resampling procedure to account for variability that might be associated with over fitting the model and which provides additional variability to the standard covariance estimates of the biases given in Eq. 6. One hundred different inversions are run, each based upon a different subsample of the observations. Assuming temporal independence of the errors in the filter, one may simulate properties of the annual NEE probability density functions (pdf) for each of these 100 inversions by using the posterior

covariance provided at each step of the Kalman Filter for each inversion. A 95% confidence interval (CI) for the entire domain can be calculated at each step of the filter for each of the 100 inversions. The CI shown in Figure 5.4 then characterizes variability in the NEE by selecting the 95% CI of each set of 95% CIs for each weekly time step.

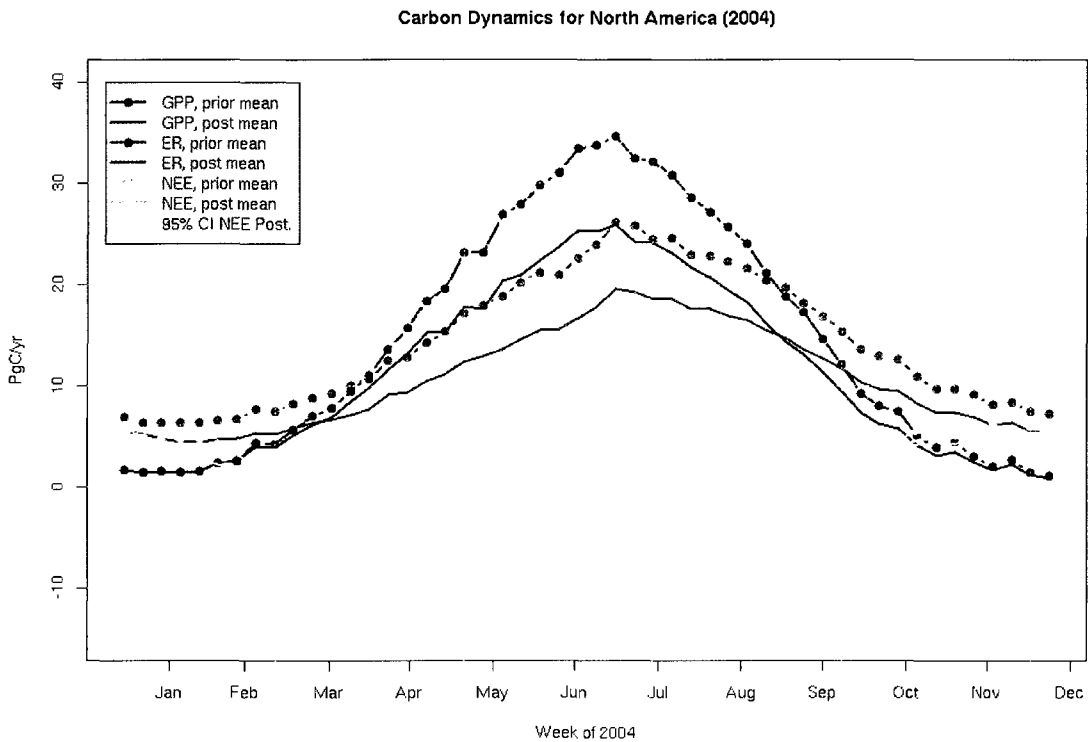


Figure 5.4: Plots of prior and posterior estimates for GPP, ER, and NEE. Results are shown for a single inversion while the confidence intervals are derived from an ensemble of 100 inversions.

The ensemble mean of the domain summed annual NEE flux is approximately -0.5 Pg/yr while the standard deviation of this estimate is about 0.15 Pg/yr. It is important to note that this standard deviation estimate does appear to be too small, giving tighter bounds on the flux than found in other inversion papers (Gurney et al. 2002; Peters et al. 2007). An additional source of variability in the estimate is discussed later (section on *Sensitivity and Robustness of Results to Prior Variance Structure*) and likely provides another 0.1 Pg/yr – 0.15 Pg/yr to this standard deviation estimate. The spatial representation of these

sources and sinks can be seen in the first panel of Fig. 5.7. Depictions of this variability in a spatial framework are shown in Fig. 5.5. This variability is partitioned into two pieces, variability associated with the spread of mean estimates over the 100 inversions (measure of over fitting) and variability associated with summing up the posterior variances at each filter step (regular KF variance) evaluated over all 100 inversions. Besides the spatial display of posterior variance information for NEE, which roughly tracks the convolution of the sampling footprint of the network and the prior ER/GPP signals, the results show that over fitting the model may provide a significant source of variability comparable to that which is normally constructed from each filter step's posterior covariance matrix.

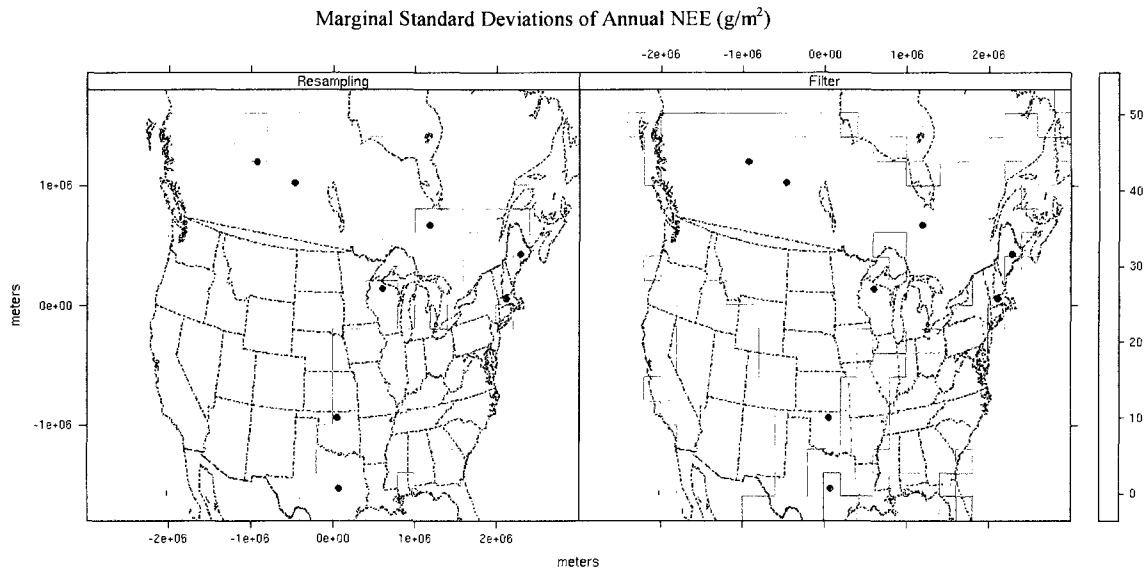


Figure 5.5: Uncertainty measures in annual NEE. The left panel is the result of running 100 inversions each using a randomly selected 50% of the data and then calculating the variance of each cell's mean estimate, over the 100 inversions, and summing over each of the weekly filter cycles. Finally, the square root of this summed variance (standard deviation) is displayed and is a measure of the uncertainty of the mean estimate due to model overfitting. For the right panel, the summed annual variance in NEE is calculated for each inversion, from the weekly filter estimates, and the the square root of this (standard deviation) is shown for each cell. These plots aim to provide a measure of the uncertainty of each cell's NEE estimate, incorporating the correlation between ER and GPP in each cell, but not incorporating the spatial correlation in the covariance matrices.

CarbonTracker Optimized CO₂ Inflow - Unoptimized PCTM Inflow

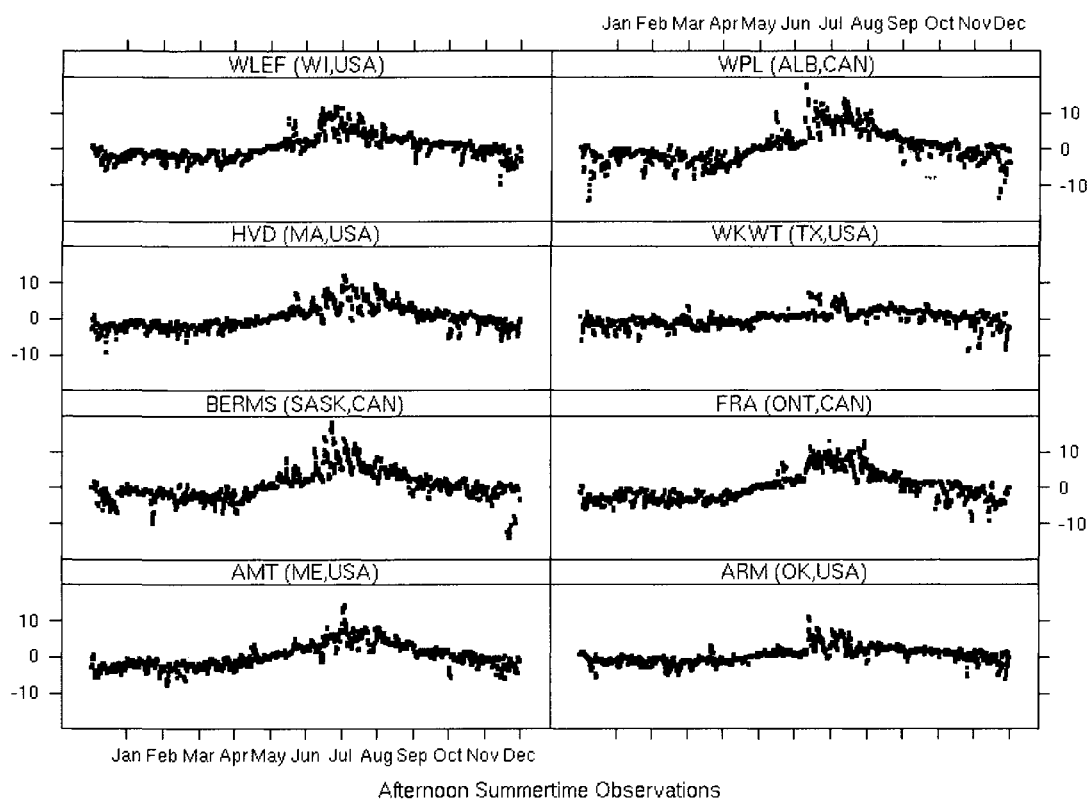


Figure 5.6: Difference of boundary inflows (1420 sequential '12/2/4/6PM' observation sequences for each of 8 towers.)

Sensitivity and Robustness of Results to Inflow

Inflow of CO₂ from the boundaries has typically been a large concern of regional models (Gerbig et al., 2003; Peylin et al., 2005). In extremely limited domain problems, the variance of the CO₂ coming in from the boundary can easily dwarf the changes inside the domain due to local biotic uptake and release. Therefore it is of interest to gauge the sensitivity of the inversion to varying boundary inflows. The boundary conditions included in this model were constructed from a global simulation using SiB3 and PCTM (Parazoo et al., 2007). The CarbonTracker project has provided CO₂ mixing ratio data based upon globally optimized fluxes (Peters et al., 2007). SiB3 has no annual

source/sinks whereas CarbonTracker includes an annual source/sink estimated from observations of CO₂. A plot of the difference between the two inflows is shown in Fig. 5.6. The inflow annual mean and temporal pattern is very similar for PCTM and CarbonTracker with the main difference being a seasonally stronger cycle in the PCTM-SiB3 results, likely a result of the underlying biosphere model, SiB3, providing a stronger seasonal GPP/NEE signal than the corresponding CASA model used in CarbonTracker. In addition to running comparison inversions between these two CO₂ inflow estimates, we also run the inversion with a fixed inflow estimate of 378 ppm representing the annually averaged PCTM inflow over the period of the simulation in order to show the necessity of reasonable boundary inflow values in calculating reasonable source/sink estimates.

Fig 5.7 shows a comparison plot of maps of the annual mean NEE estimate based upon CarbonTracker (w/ CASA), PCTM (w/ SiB3), and the fixed inflow condition. The results are similar for the CarbonTracker and PCTM inflows but also surprising in their differences. The estimates have similar spatial and temporal characteristics and differ mainly in magnitude. However, the PCTM-based inversion results in a sink of 0.1 – 0.2 Pg/yr less than that of the CarbonTracker-based result, which is the opposite of what one might guess. Fig 5.6 shows inflow from CarbonTracker that is generally less than that of PCTM for the first 4 months of the year. During this period the inversion must add sinks to the model to account for a lower concentration of CO₂ coming in from the boundaries. During the summer, when the situation is reversed the opposite occurs, the inversion must add sources to the model to compensate for the fact that CT inflow is higher than PCTM inflow. However, the magnitude of this adjustment does not seem to be a simple

linear function of the concentration differences seen in Fig. 5.6, which would imply that larger sources are needed in the CT-inflow model during the summer time than in the winter. On the contrary, the relative carbon sources that are a result of CT inflow being higher during the summer months are actually less than the carbon sinks resulting from the CT inflow being less during the winter/spring months. This results in the CT-inflow based inversion having a larger annual sink estimate than the PCTM-inflow based inversion. The sink estimated with the PCTM inflow was 0.47 Pg/yr while the sink estimated with the CarbonTracker inflow was estimated at 0.58 Pg/yr. It does seem somewhat surprising that the results from the two inflows are so close, within approximately 20% of one another. This indicates that local observations may be affected significantly more by local fluxes than by larger scale fluxes in distant locations outside of the model boundary.

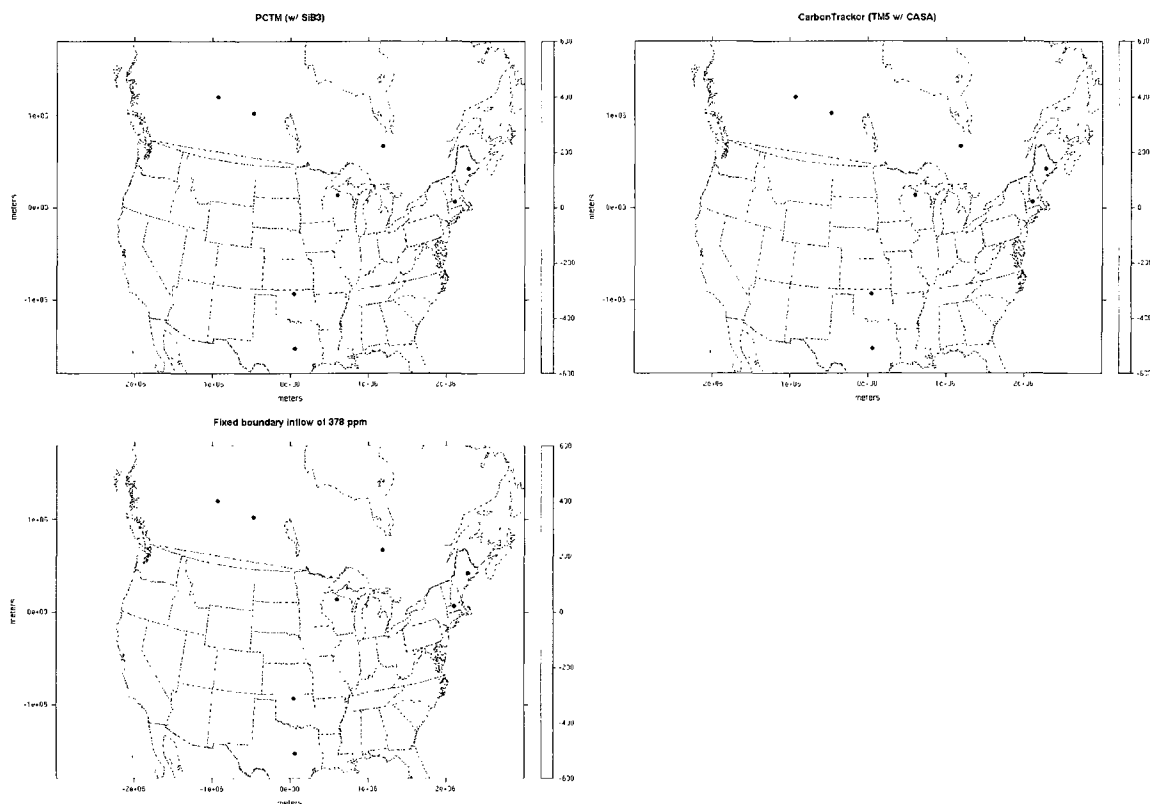


Figure 5.7: Inversion estimates for three different inflow scenarios, one without modeled annual source/sink (PCTM w/ SiB), one with modeled source/sink (CarbonTracker w/ CASA), and a uniform fixed 378 ppm inflow. Summed annual sinks are 0.47 PgC/yr, 0.59 PgC/yr, and 0.27 PgC/yr respectively.

Sensitivity of Results to Fossil Fuel Inventory

Until the release of the Vulcan fossil fuel inventory in 2008, most researchers were reliant upon the Andres et al. [1995] fossil fuel inventory, which was released at annual time scales and at a 1-degree resolution over the globe. For many large-scale inversion applications, this inventory is adequate. However, for higher resolution studies within the United States, the Vulcan fossil fuel inventory provides a dramatic improvement in both space and time accounting of fossil fuel fluxes. The main difference between these inventories is the redistribution of some fossil fuel sources from population centers to more distant locations representing mobile sources and power plants. The Vulcan fossil fuel flux estimates are at a much higher resolution in both time

and space. Previous inversions had to grapple with the fact that some observing stations are located within enormous fossil fuel flux regions. For example, a semi-rural location like Harvard Forest would very likely be located in the same grid cell as the large metropolitan city of Boston. Given no sub-annual temporal resolution to the fossil fuel fluxes, an observing tower located at Harvard Forest was often seeing a 24 hour continuous stream of fossil fuel fluxes arising from a city over 100 km away. However, the 10 km horizontal resolution of the Vulcan inventory allows these to be separated and additionally provides a diurnal and seasonal estimate of these fluxes, which is important for inversions based upon hourly observations.

In order to gauge the impact of incorporating the Vulcan data, we first contrasted the contributions to each of the 8 towers from each of the inventories. For many of the stations, the afternoon differences between the two were very small. Differences at the ARM site in Oklahoma, the WLEF site in Wisconsin, the Canadian sites, and the Argyle, Maine site were on the order of a few ppm. Differences at the Moody, Texas tower were in the range of -5 ppm to 5 ppm. While the differences across most towers were relatively small, the differences at Harvard Forest were between -25 ppm and 30 ppm!

The difference in the annual NEE estimate is shown in Fig. 5.8. The effect on the inversion is far from trivial with differences of up to 300 g/m² per year recorded along the northeast coast of the United States. These differences are a result of coarse fossil fuel flux fields providing artificially high sources of CO₂ to the Harvard Forest tower which must be neutralized via a large local sink.

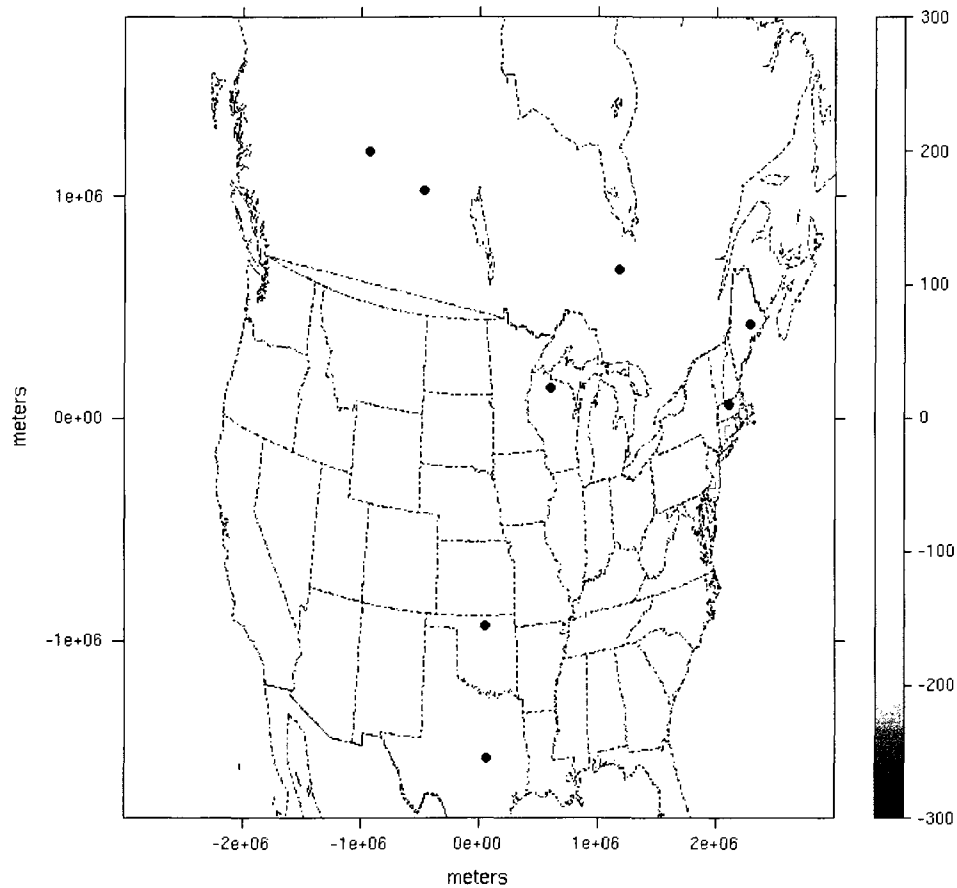


Figure 5.8: Difference in annual sink inferred by inversions based upon the Vulcan fossil fuel inventory and the Andres et al. [1995] fossil fuel inventory. Spatially-summed annual difference between Vulcan-based NEE estimate for 2004 and Andres[1995] based NEE estimate for 2004 is -0.05 PgC.

Sensitivity and Robustness of Results to Prior Variance Structure

A test of the sensitivity and effect of the prior upon results is important because of the use of an informative Bayesian prior, that is, a prior flux estimate in which the inversion will likely be sensitive. With reference to Eq. 5 and Eq. 7, the w , σ_0^2 , and h_0 parameters are varied and results are shown in Fig. 5.9. These figures show that results are sensitive to nearly all of these parameters, providing different degrees of RMSE and sink strength depending upon the particular combination. In particular, sink estimates range between 0 and 1 Pg/yr. The ensemble of estimates, over the various a priori

variance parameters, have a standard deviation of approximately 0.2 Pg/yr. This likely contributes another 0.1 Pg/yr to 0.15 Pg/yr (depending upon the existence of correlation between the variance shown here and earlier variance estimates due to jackknife resampling and the Kalman filter posterior variances) to the initial standard deviation estimate of 0.15 Pg/yr given earlier. This would give a corrected estimate of 0.5 Pg/yr +/- (0.25 Pg/yr - 0.3 Pg/yr) to the posterior annual NEE estimate shown in Fig. 5.4.

An RMSE-weighted average of the sink estimates show a sink of 0.57 PgC/yr, 20% higher than our single case scenario that we have followed throughout these results. Values very near the lower left of the plot are somewhat unrealistic since low spatial correlation (h_0) and a low variance on the prior (σ_0^2) will not provide a reasonable enough range around the prior to provide a realistic posterior sink estimate which generally is thought to range between 0 and 1.5 Pg/yr (Schimel et al., 2000; Gurney et al., 2002) inter-annually. Increasing either the variance multiplier (along x-axis) or the spatial decorrelation length scale (along y-axis), or both jointly, increases the error variance around the a priori mean allowing more realistic domain-wide summed posterior flux estimates. Therefore if one “de-weights” these sink estimates occurring in the lower left hand portions of the panels in Fig. 5.8, the RMSE-weighted sink will likely increase to more than 0.57 PgC/yr.

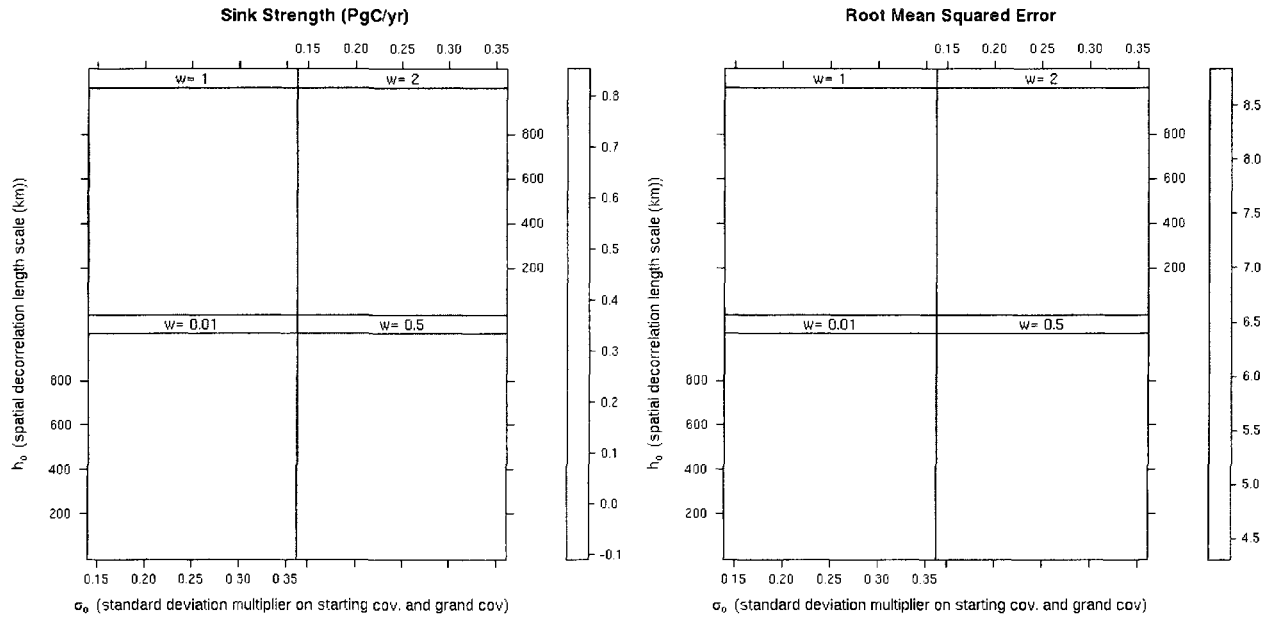


Figure 5.9: Sensitivity of (a) sink estimate and (b) root mean squared error to varying covariance parameters in inversion.

The weight of the grand prior (w) has two effects. First, it constrains solutions back towards the prior, essentially anchoring the Kalman filter so that, over time, it does not drift too far from the prior. Given the fact that this grand prior is fixed in time, it also provides a degree of variance inflation (over the regular KF) by providing a lower bound on the prior variance for each filtering step. It is interesting to note that, for cases in which the global prior is weaker (bottom two panels), the maximum sink estimate occurs on the inside of the plot bounds and not at the boundary. The Kalman filter becomes more entrenched without the grand prior since there is no lower limit on the prior variability at each inversion filter step and there is no inflation. Therefore it is likely that the initial reduction in respiration and associated “sink” of carbon in the early months of the year becomes entrenched and leaves a strong sink signature on the rest of the year resulting in the largest sink estimates. We did not test any additional forms of variance

inflation on the model and acknowledge that additional efforts are needed to construct more robust filter techniques.

Comparison to 2000-2005 NTGS NPP anomaly estimates

From a practical standpoint, the inversion results are more “well behaved” for longer correlation length scales since “di-poling” and large small-scale deviations from the prior are less likely. Annual NEE results are shown in Fig. 5.10 for $\sigma_{\text{grand}} = 0.15$, $\sigma_0 = 0.15$, $\sigma_{\text{obs}}^2 = 5.5$ ppm, and $h_0 = 1000$ km (instead of 250 km). NPP anomaly estimates from the Numerical Terradynamic Simulation Group (<http://www.ntsg.umt.edu/>) are presented in Fig. 5.11 for 2000-2006. Although not directly comparable because of the inclusion of respiration components in NEE, it seems feasible that there might be correlations in annual NPP anomalies and annual NEE estimates. Exceptionally productive years in growing forests for instance would likely leave a signature on annual NEE because of the carbon that is pulled into the wood portions of the vegetation. The inversions in this paper universally place a large sink to the east of the WKWT and ARM towers, centered over northern Louisiana and southern Arkansas. In general, the magnitude of the sink appears too high from an intuitive standpoint, considering it rivals the sink that would be induced by the growth and export of a crop like corn (Prince S. 2000) (and some speculation on reasons for this are provided in the conclusions). Fig. 5.11 shows a very large NPP anomaly centered a few hundred kilometers to the north over Missouri and Arkansas. Both figures show a significant carbon sink over the marine forests of the Northwest. The southeast experienced a very dry spring, following a dry conditions in late 2003, which could be responsible for reduced springtime NEE and the

source of carbon seen in Fig. 5.11. Our inversions show a source as well but positioned much further to the north. There is little constraint in this area of the inversions so it would seem reasonable that the sink may be placed incorrectly. Both figures show anomalous carbon sources in the northeastern reaches of Canada but the NTGS estimates place a large broad source over the northern boreal region of Canada while our inversion results generally show a slight sink there. Furthermore, NTGS estimates show sinks to the south of the boreal zone while our inversion results show little source or sink in lower British Columbia and Alberta. Finally, the NTGS estimates show strong sinks over the Rocky Mountains of the United States which are not evident in our inversions, possibly due to limited data constraints in the region. It is interesting to note that relative to the mean NPP field that NTGS provides, these estimates over the Rocky Mountains constitute sinks of nearly 50% over their estimated mean NPP levels.

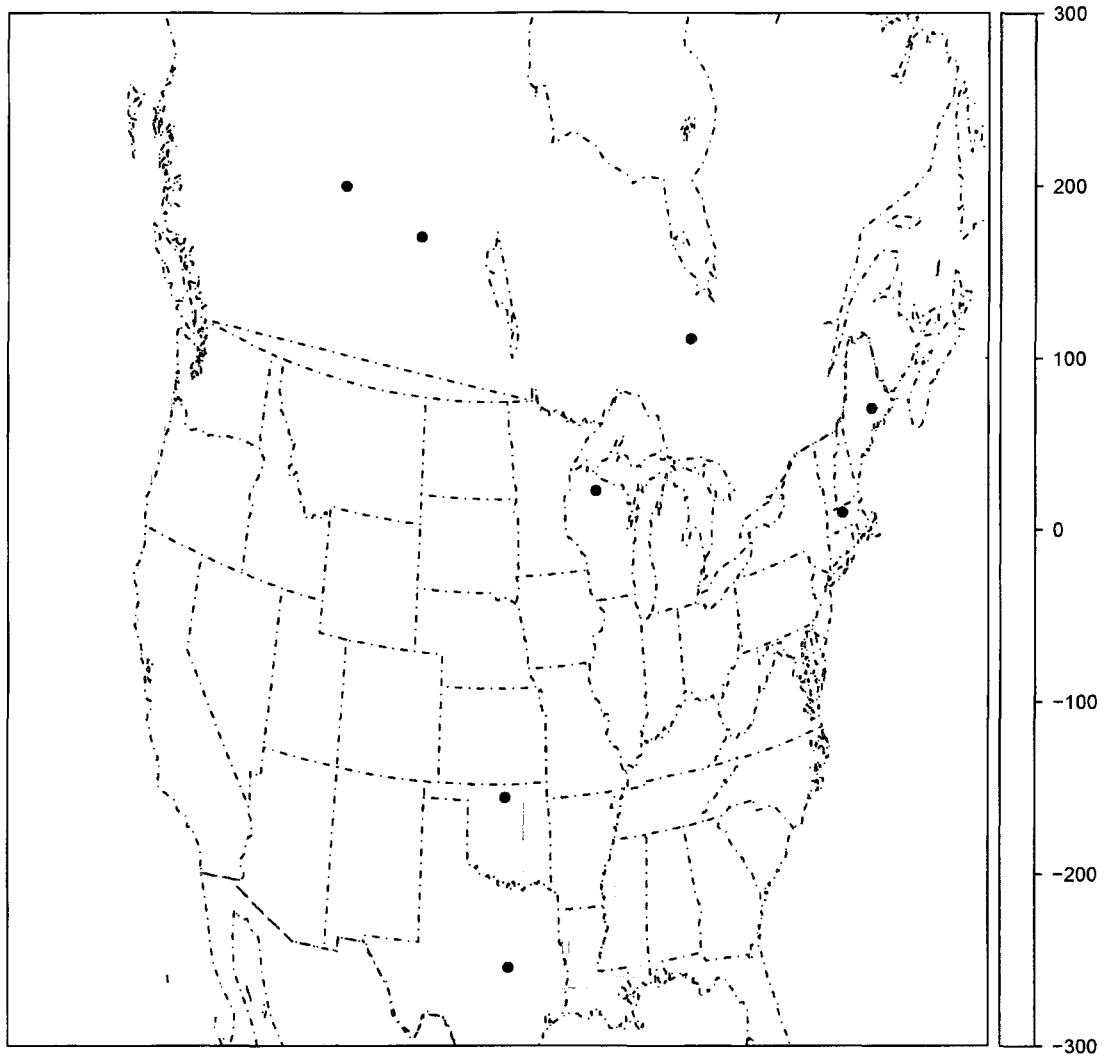


Figure 5.10: Inversion results for annual NEE (g/m^2) obtained by increasing decorrelation length scale from 250 km to 1000 km.

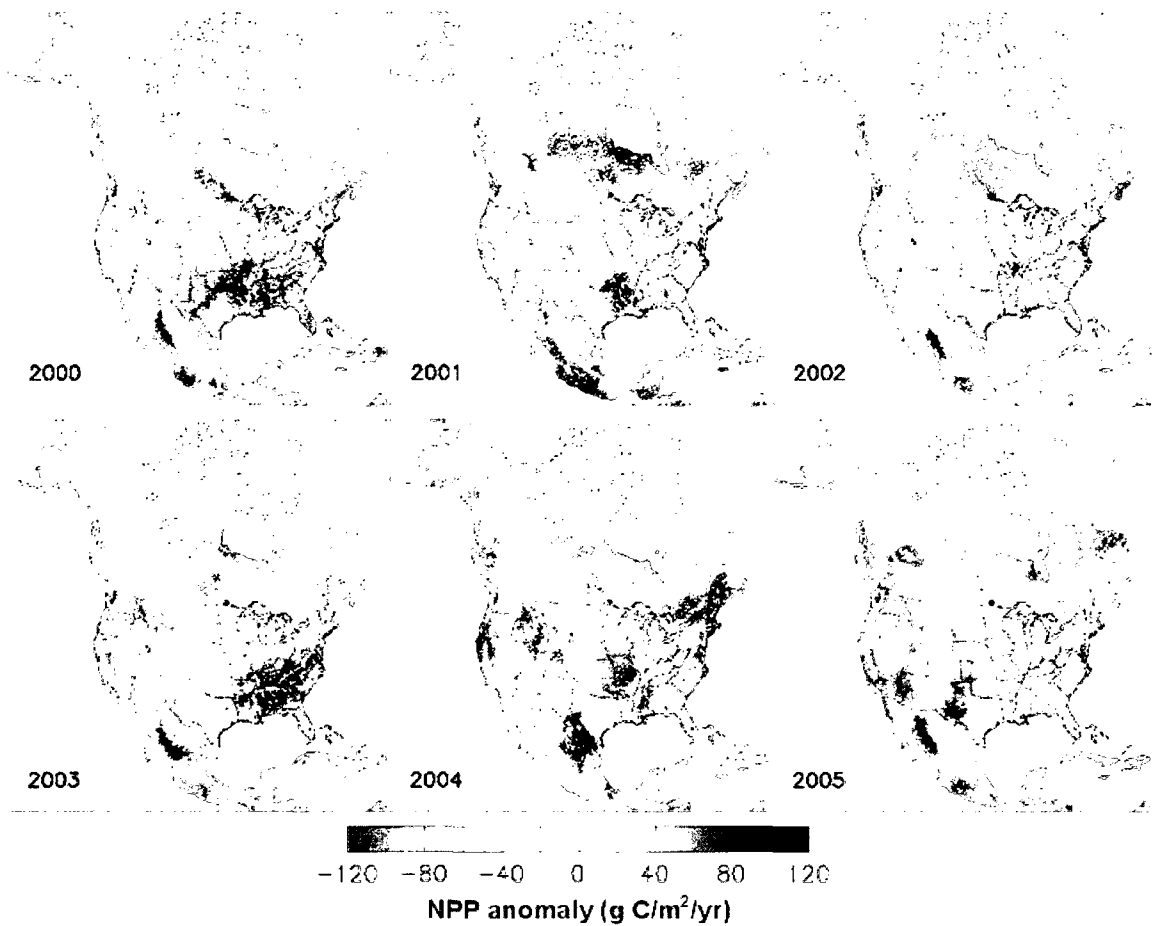


Figure 5.11: MODIS 17 NPP anomalies for 2000 - 2005

Comparison to CarbonTracker flux estimates

Given the fact that the majority of the underlying observations supporting the inversion were also used in the CarbonTracker project, one would expect posterior flux estimates to be somewhat similar. One of the most important differences between these inversions and CarbonTracker is the optimization of encompassing global fluxes, which affect CO₂ concentrations within our domain. However, this can be mitigated somewhat by the use of optimized CO₂ concentrations from CarbonTracker in the inversion. Under this scenario, one would expect the inversion results to be similar to CarbonTracker but there are still many differences. As can be seen in Fig. 5.12 , Fig. 5.13, Fig. 5.14, and

Fig. 5.15, the carbon fluxes in the priors, CASA and SiB3, play an important role in the posterior estimates. The posterior estimates of both inversion models display the signature of the a priori fluxes prominently. These results would lead one to believe that either the data does not provide sufficient constraint or the covariance structure is specified too tightly around the prior.

Comparison to filled Level 4 Ameriflux data

Posterior respiration and GPP estimates from the model can also be compared to Ameriflux level 4 data. As indicated earlier, there is a spatial representation mismatch in doing so due to the fact that the model estimate is an average over approximately 1600 km² and the associated flux tower estimate is over a much smaller footprint, likely less than 1 km². Nevertheless, some useful comparisons and observations can be made.

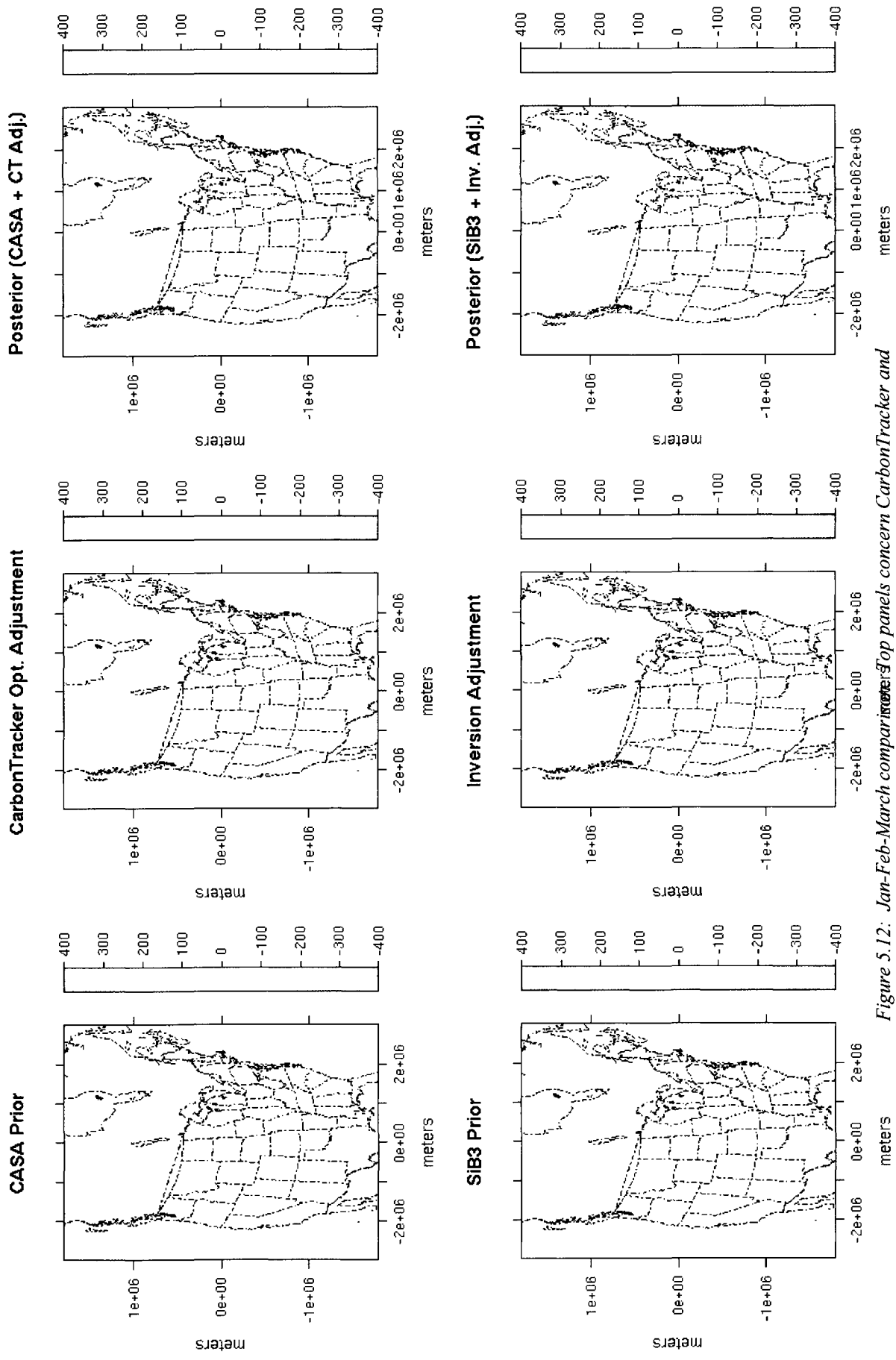


Figure 5.12: Jan-Feb-March comparison. Top panels concern CarbonTracker and lower panels concern our inversion. Left panels show a priori NEE, middle panels show inversion adjustment, and right panels show a posteriori NEE.

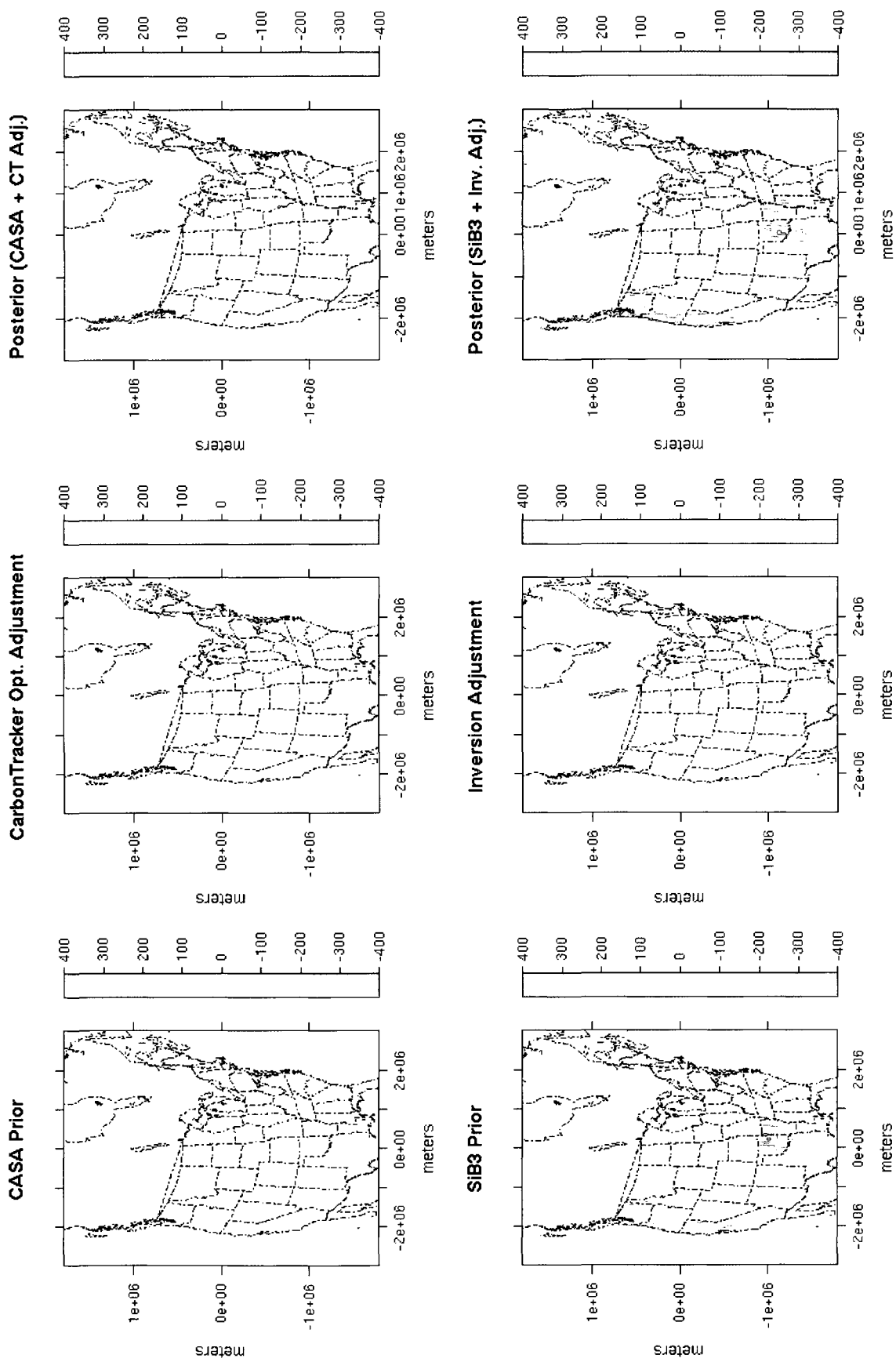


Figure 5.13 Apr-May-June comparison. Top panels concern CarbonTracker and lower panels concern our inversion. Left panels show a priori NEE, middle panels show inversion adjustment, and right panels show a posteriori NEE.

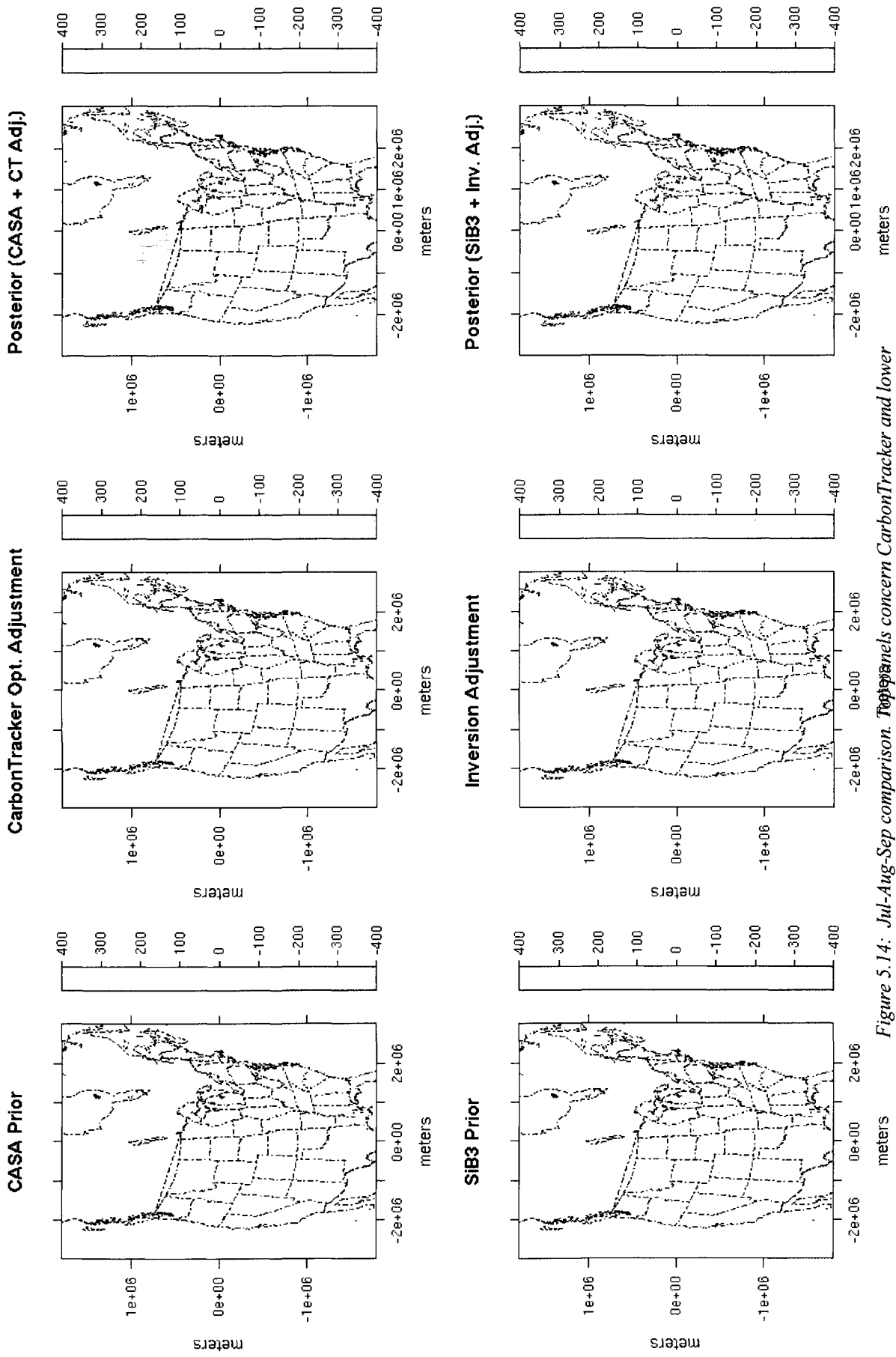


Figure 5.14: Jul-Aug-Sep comparison. Top panels concern CarbonTracker and lower panels concern our inversion. Left panels show a priori NEE, middle panels show inversion adjustment, and right panels show a posteriori NEE.

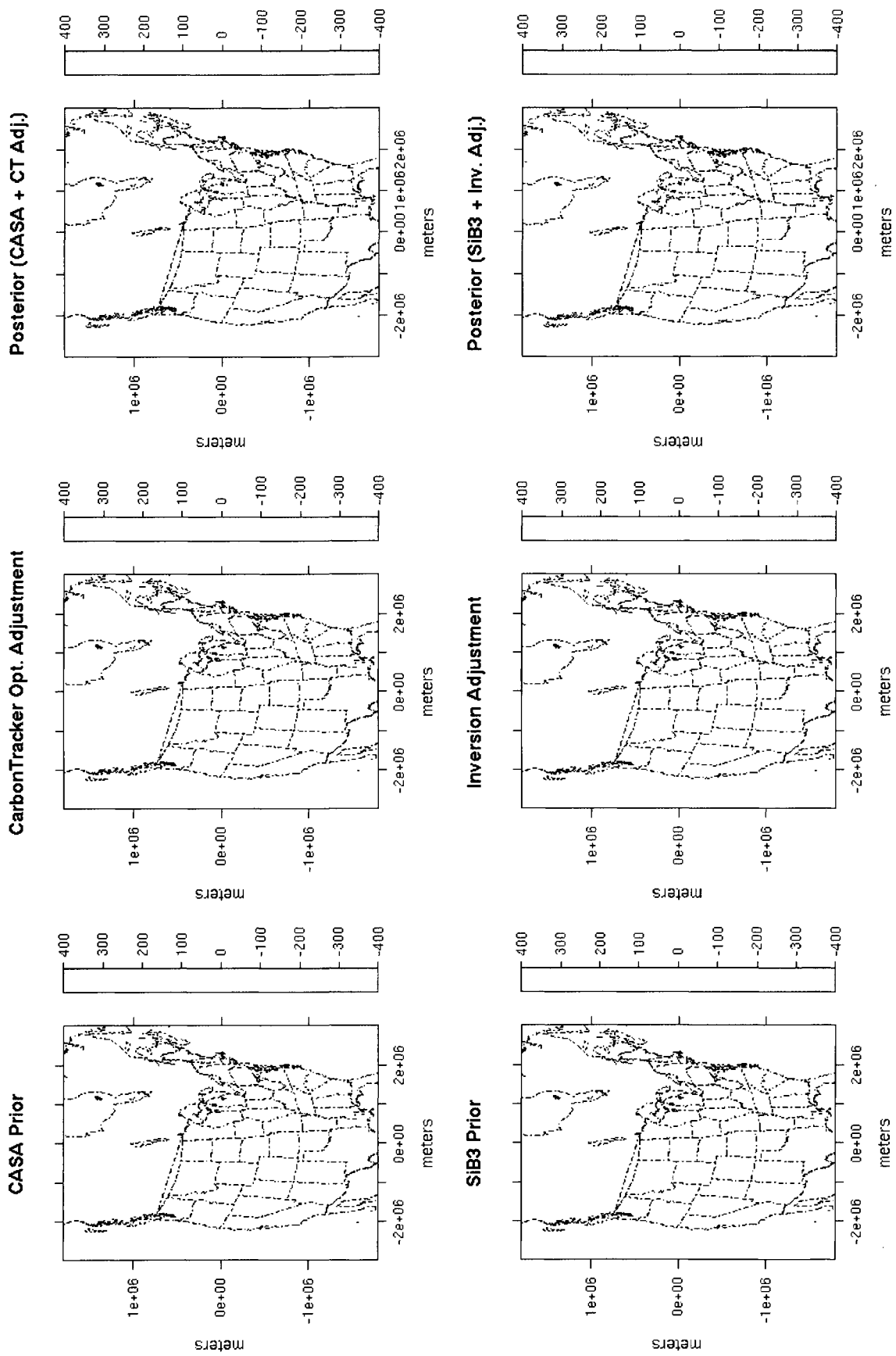


Figure 5.15: Oct-Nov-Dec comparisons Top panels concern CarbonTracker and lower panels concern our inversion. Left panels show a priori NEE, middle panels show inversion adjustment, and right panels show a posteriori NEE.

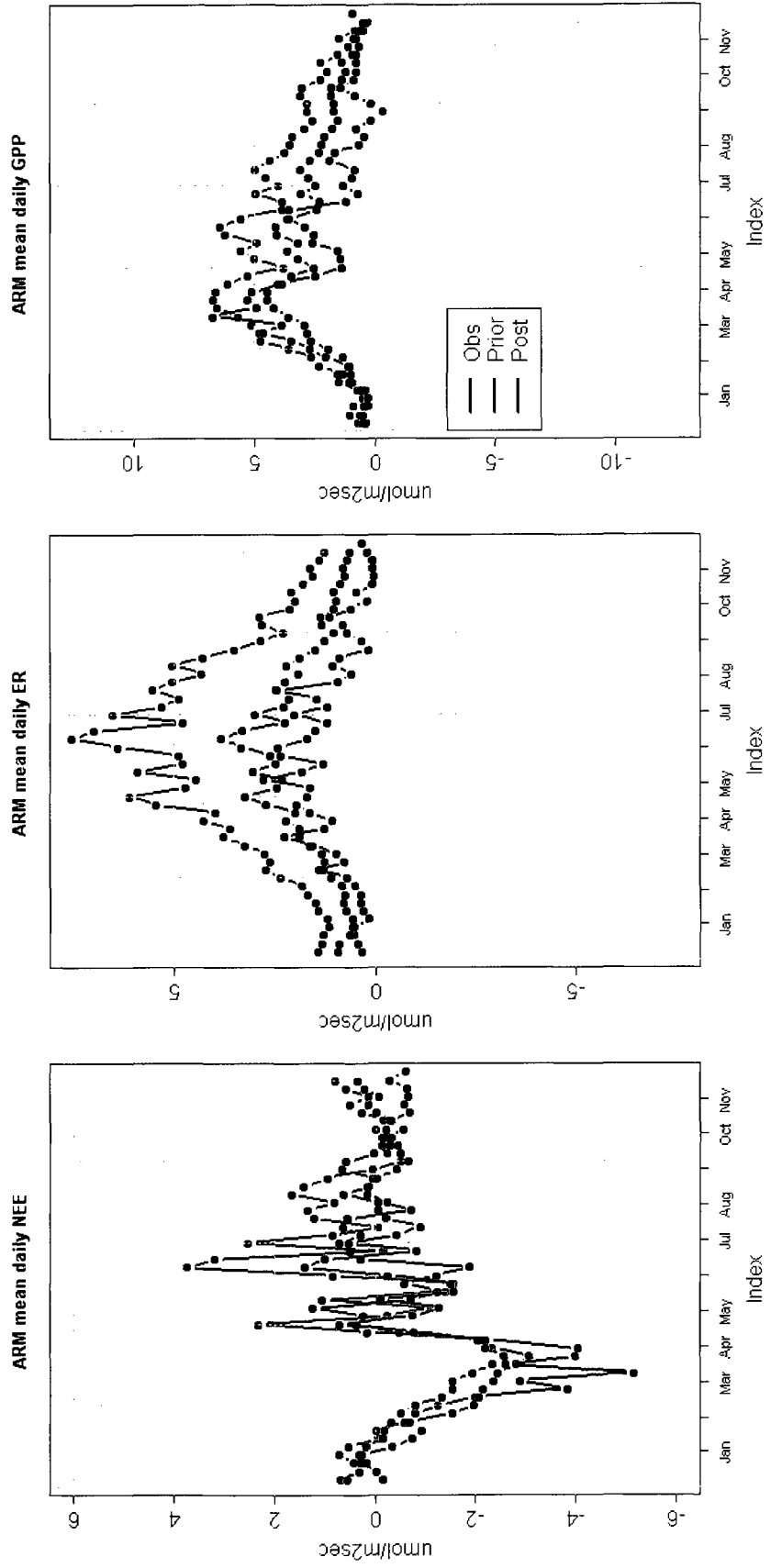


Figure 5.16: Comparison of posterior fluxes of GPP, ER, and NEE with Ameriflux Level 4 flux tower data for ARM Site in OK. Pay particular attention to the fact that the y-axes are different scales.

Fig. 5.16 shows comparisons of the model to the observations for weekly ER and GPP at three Ameriflux sites, which appear in the more observation constrained portion of the model domain. The ARM site is one of the more constrained sites in the domain and lies in a relatively homogenous landscape making it an excellent candidate for analysis. The prior site NEE estimate appears to be improved on average by the posterior flux estimates. In particular, the prior model is corrected significantly in the summer when it predicts significant respiration occurring. Clearly one can see an early spring winter wheat signal in the observations, forming a significant amount of carbon drawdown over an 8-10 week period. SiB3 necessarily balances GPP and ER annually and is thus forced to redistribute this carbon into respiration in other portions of the year. This is the likely reason for displacement of the prior estimate in the summer. The posterior corrects for a large portion of this but the large distance between the prior and observed fluxes make a complete correction difficult. Just as important, but perhaps more subtle, is the fact that the inversion is able to provide significant corrections to ER and GPP separately. SiB3 appears to significantly overestimate GPP. However, due to the annual NEE balance constraint, SiB3 will overestimate ER as well, providing an NEE signal that appears very reasonable. If the forward model is only compared to NEE estimates at various sites then this fact can be easily overlooked but is likely very important to biosphere dynamics on certain time scales.

Evaluation of annual NEE source/sinks against ancillary data and hypotheses

Using two sets of boundary conditions, we arrived at a final sink estimate of approximately 0.5 PgC per year +/- 0.25 PgC per year. This is significantly less than

CarbonTracker's sink estimate of 1.08 PgC per year and other estimates currently emerging from an ongoing top-down synthesis project. It is clearly possible that other globally based inversions provide more constraint on certain areas of North America, such as the Pacific Northwest forest regions of North America or the Southeastern United States. Both of these areas have large annual GPP signals and are thus capable of being a strong source/sink of CO₂. However, our inversion results show a generous sink in the coastal N.W. forests while CarbonTracker shows little sink there. Furthermore, CarbonTracker's sink is largely located in the agricultural Midwest of the United States (and a portion of Canada), an area reasonably constrained by the observation network we've used.

On the other hand, perhaps the globally based sink estimates are too high. The recently completed State of the Carbon Cycle Report (SOCCR 2007) provides an inventory-based sink estimate for North America of approximately 0.66 PgC per year (land sink) using a variety of data sources collected over the last ten to fifteen years. Uncertainty is presented as a 95% confidence interval, 0 PgC to 1.32 PgC. This is similar to what we've recovered in these inversions. However, this is a mean sink estimate over many years and 2004 is believed to be a year in which the sink in North America was very strong, likely putting the SOCCR estimate closer to 0.8 – 0.9 PgC/yr, the upper range of their annual estimates. Stephens et al. 2007 called into question the magnitude of the Northern Hemispheric (and North American) global annual NEE sink which has been a cornerstone of inversion results for the last 10 years (Fan et al. 1998, Gurney et al. 2002, Peters et al. 2007) indicating that it may be much smaller than previously assumed. In any case, the rapid expansion of the calibrated CO₂ tower network (currently over 30

towers in North America) should soon provide significant additional data constraints to researchers performing atmospheric CO₂ based inversions.

The spatial character of the annual NEE estimate has several distinctive features. The most definitive feature of the annual NEE estimate shown in Fig. 5.6 is the large sink estimated between the ARM and WKWT sites in south central portion of the domain. At first glance this may appear to be an artifact of incorrect transport, poor boundary conditions, or incorrect fossil fuel emissions specifications. However, summing the ARM NEE observations for the year provides a sink estimate of approximately 275 g/m², similar to that seen in Fig. 5.6. A likely hypothesis for this sink is the lateral export of crops, primarily winter wheat that draws most of its carbon from the atmosphere in the spring and then is harvested and exported in early summer. Nevertheless, the strength of the source, primarily in its center that is located a significant distance from both the ARM and WKWT towers, would appear to be too strong. Sinks of 500 g/m² rival the harvest and complete export of very high GPP crops such as maize/corn (generally not planted in this area) and thus the magnitude of this sink appears unrealistic. The WKWT tower concentrations have proven to be somewhat difficult to model given its late diurnal venting of nocturnally built up carbon dioxide, its close proximity to both the model boundary and the ocean, and its proximity to fossil fuel sources of major metropolitan areas and oil refining facilities. Given the negative correlation in annual NEE from the north of WKWT to the south of WKWT, it is likely that incorrectly estimated sources to the south are in part responsible for the strength of the sink to the north.

The second strongest sink area is located to the east and northeast of the ARM tower, largely along the Mississippi river. This is an area of significant crop production,

with corn and soybeans being grown extensively in the northern portions while soybeans, rice, and other crops are grown to the south in the Arkansas/Mississippi region. Similar to the sink seen between ARM and WKWT, this sink appears somewhat too strong and “spread out”. Crop growing regions are fairly tightly bound to the Mississippi river and the spread of the sink around the river is likely an artifact of spatial correlation, both a priori and induced by the data. Future work may focus on introducing some coarse landcover factors into the model in order to strengthen gradients in areas with rapid transitions in landcover. Again, the magnitude is likely overestimated due to uncertainties in the inversion process. It is also easy to see the negative correlations developing in the NEE estimate (upper left of Fig 5.6) between the lower Mississippi valley and the Appalachian Mountains region. These regions would likely be more constrained as a sum, resulting in a smaller magnitude NEE estimate for the combined area.

It is interesting to note that the most intensely cultivated portion of the Midwestern United States, centered on the state of Iowa, shows little to no sink. This is an area typically planted extensively with corn, which has been shown to be an extremely effective consumer of atmospheric CO₂. The a priori estimate of NEE based upon SiB3 included a very strong summer time sink of carbon over the Iowa region using a C4 photosynthesis scheme from Collatz et al. 1992. Whether the CO₂ flux is reasonably close to the truth is difficult to determine although the increased amplitude of the seasonal cycle due to the increased summer time GPP of the corn seems to have put a slight signature upon the inversion results (top left panel of Fig 5.6).

One other hypothesis for this disparity in sink strength concerns the lateral transport of crop harvest. Significant annual sinks can only occur if carbon is added or removed from the system. In the case of croplands, the mechanism for this is usually the export of harvested crops, which should provide the appearance of a carbon sink in the area. Annual NEE estimates from the corn-planted Bondville, IL Ameriflux site indicate a sink on the order of 500-600 g/m². Soybeans can be expected to provide sinks of about half of this. Assuming steady state conditions over several years, these types of sinks can be attributed directly to the harvest. Approximately 20% of the corn harvest and 35% of the soy harvest is exported overseas, mostly for animal feed, while approximately 60% of the corn harvest and 50% of the soy harvest is used to feed livestock domestically (Wise, 2005, National Corn Growers Association website: <http://www.ncga.com/03world/main/consumption.htm>, Soy Stats, <http://www.soystats.com>). Most of the carbon in this livestock feed is then returned to the atmosphere as CO₂ and CH₄ at locations where it is consumed by livestock. Almost 70% of the feedlots in the United States are located in just 3 states: Texas, Kansas, and Nebraska (<http://www.cattlenetwork.com>). This may provide a partial explanation for the lack of an agriculturally-induced sink over Nebraska and Kansas, states with very high crop production and intense livestock operations, and the existence of sinks over portions of Arkansas, Mississippi, Missouri and Illinois, states with relatively high crop production but with significantly less livestock operations.

Forested regions in the northwestern United States and boreal forests of Canada show slight sinks. However, variability estimates surrounding these sink estimates are typically much smaller than the variability estimates of similar sink magnitudes in the

Midwest or southeastern United States showing relatively more confidence in the sink despite the lack of proximity to the observing towers. The sink estimate in the northwestern United States is not surprising since the northwestern coastal mountains of California, Oregon and Washington have been intensely managed over the last 50 years and are expected to provide a sink of carbon for many decades into the future (Alig et al. 2006). The estimate for the boreal forest regions appears much harder to objectively evaluate. Most studies have indicated that Canadian sources should currently be a weak sink, although the projection of this weak sink into the future is highly uncertain. The inversion results show a fairly carbon neutral Canada on average, but shows the boreal forests of central Canada and the boreal and coastal forests of western Canada as slight sinks while the agricultural plains of Canada and the forests of eastern Canada provide slight sources. It is interesting to note that areas to the south of the two Canadian towers show an annual source of carbon in an area just to the east of large expansive forest ecosystems of British Columbia that have recently experienced unprecedented bark beetle invasions and tree mortality. It is important to note that forest fires were not included in the SiB3 domain run for the regional inversion. Average carbon emissions from Canadian forest fires were estimated at 27 +/- 6 Tg/yr (Amiro et al., 2001), a non-trivial amount that could increase the strength of the boreal forest sink predicted by the inversion.

Evaluation against 2004 INTEX aircraft data

High resolution CO₂ data collected during the Intercontinental Chemical Experiment-North America (INTEX-NA) provided a unique opportunity to evaluate both

a priori and a posteriori CO₂ concentrations produced from the SiB3-RAMS model and associated inversion framework. A DC-8 was outfitted with sensors to measure a number of different of chemicals including CO₂. Eighteen flights were made between July 1, 2004 and August 15, 2004. The majority of the ground covered was in the United States, primarily in areas east of the Mississippi River. The aircraft descended into the boundary layer several times over the course of each flight allowing one to assess the effect of the biosphere on the mixed layer of the lower troposphere. Given the wide range of measured chemicals, the authors were able to differentiate various convective and stratospheric-tropospheric exchange process as well as provide evidence of contributions to measured CO₂ from boreal wildfires, long range transport from Eastern Asia, and surface fluxes induced by the biosphere. A thorough summary of the mission in the context of CO₂ is available in [Choi et al., 2008]

Prior and optimized CO₂ fluxes were input as tracers into RAMS and resulting CO₂ concentrations were compared to INTEX observations in order the gauge the success of the inversion. The model was run from July 1, 2004 to July 31, 2004. While the optimized CO₂ concentrations provided improvement in certain spots where the INTEX mission flew, most observations were outside of the main area of constraint of the tower data and thus optimized concentrations were unlikely to provide much improvement over a priori concentrations. However, the flight data did provide important information to assess the quality of the a priori model used for CO₂ concentrations (SiB3-RAMS-LPDM). In certain flights, such as Flight 009, which flew from the Northeast United States into the Midwest and north into Canada, the model was able to capture a number of boundary layer CO₂ averages very well (Fig. 5.18).

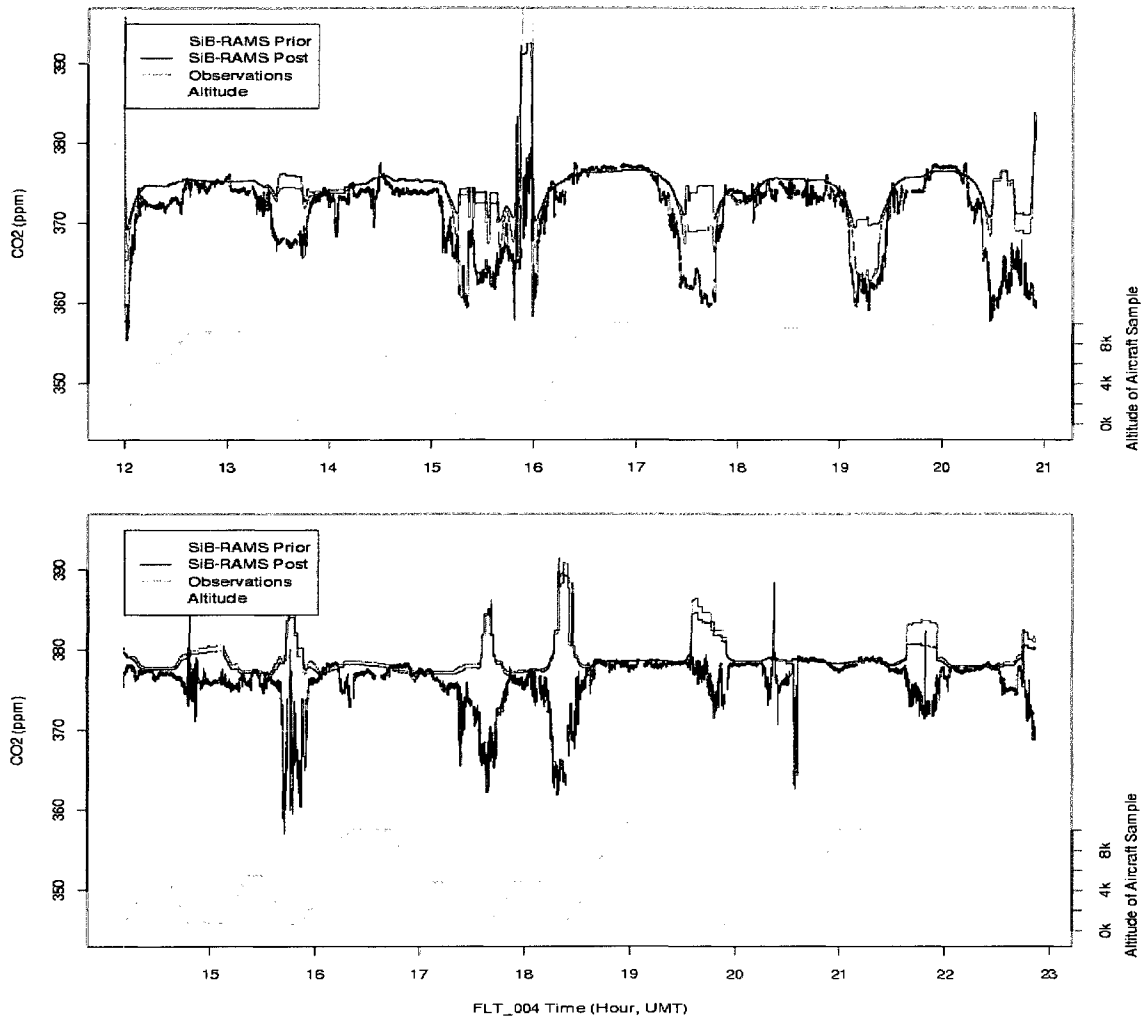


Fig 5.17 SiB3-RAMS CO2 compared to INTEX CO2 observations for Flight 009 (left) and Flight 004 (right)

However, there were also several flights like Flight 004 (Fig. 5.18), where the model clearly showed more CO₂ in the boundary layer than the aircraft as well as showing more CO₂ in the boundary layer than in the free troposphere above. It is important to note the sub grid-scale variability of CO₂ concentrations in the aircraft data that is theoretically provided as an average in the model. For example, in the second boundary layer descent of Flight 009 (or Flight 004), the data show a range of over 20 ppm in CO₂ over a very

short time interval. In the case of Flight 009, SiB3-RAMS captures the very sharp changes in CO₂ gradient while it does not in Flight 004. Nevertheless, the mean recorded concentrations in the boundary layer in these aircraft descents are generally less than the mean concentration above the boundary layer, as would be expected during summer conditions in North America, and this is often not shown in the model.

Given reasonable agreement of CO₂ concentrations at upper altitudes, differences such as these might be explained by incorrect vertical distributions of CO₂ induced by faulty mixing, badly specified prior carbon fluxes at the surface, or CO₂ increases due to low level advection of CO₂ anomalies from neighboring land. Specifically, CO₂ in the model was frequently higher in the boundary layer than in the free troposphere above, in many areas on the east coast of the United States, particularly the Piedmont regions of Virginia, North Carolina, South Carolina, and Georgia and also into Alabama and Mississippi which seems unrealistic for non-stressed mid-summer conditions. Investigations into the development of the mixed layer in the RAMS model did not illuminate any significant deficiencies although we do note that the mixed layer appeared slow to develop in the morning hours, forcing photosynthesis to consume nocturnally-derived respiration-caused CO₂ rather than start building a strong CO₂ deficit at the surface. Similarly, the boundary layer appeared slow to be separated from the ground in the early evening allowing the daytime minimum concentrations in the model to arrive at sunset in the lowest level of the model. WLEF tower has recorded calibrated CO₂ at levels of 11 meters, 30 meters, 76 meters, 122 meters, 244 meters, and 396 meters, which allows one to compare the effectiveness of the modeled mixing, at least in the lower portions of the boundary layer. While not ideally situated in the areas of interest, it at

least allows a cursory examination of general morning mixing behavior. Diurnal average vertical profiles for the month of July are presented for the WLEF site in Fig. 5.18. Although the effect is not strong, potentially because of the well-studied and presumably well-modeled location, one can see the late onset of morning mixing as well as the late development of the nocturnal boundary layer. Similar results were found by [Denning et al., 2003] as well as [Case et al. 2002].

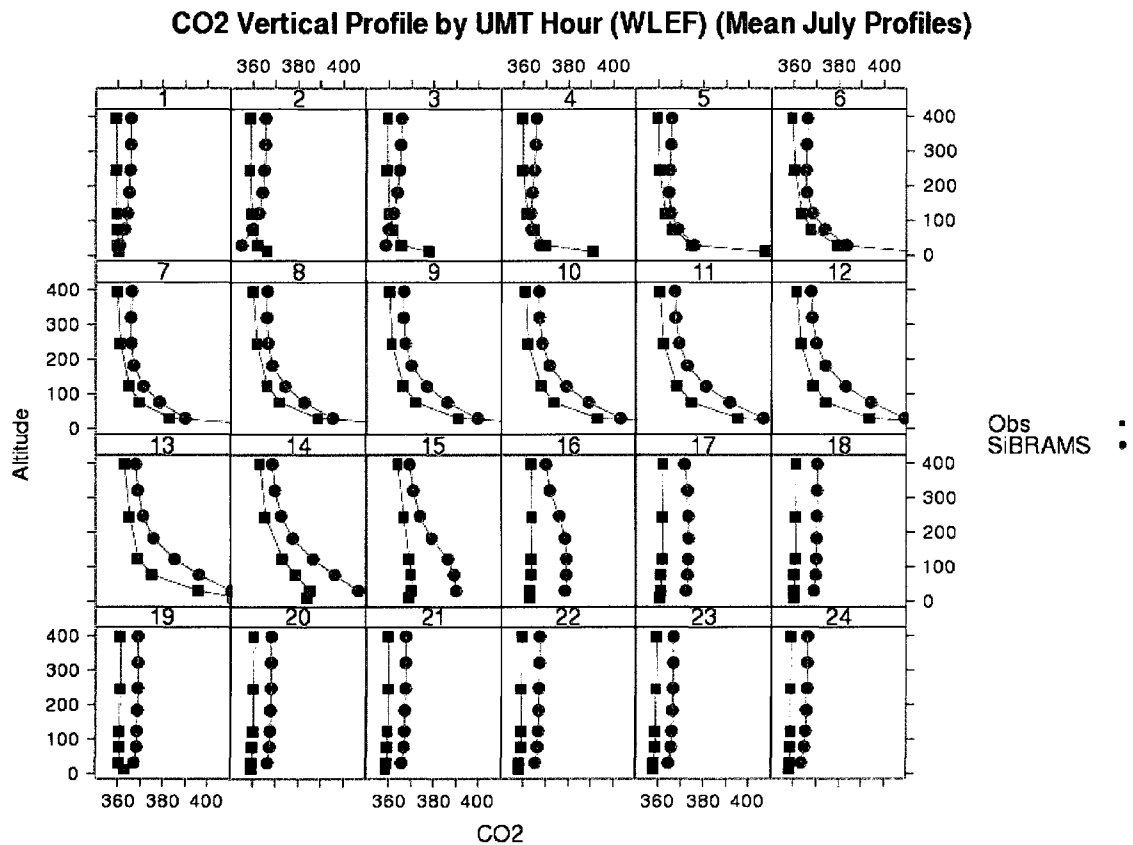


Fig. 5.18 Comparisons of CO₂ at surface to 400 meters for the forward SiB3-RAMS model.

Diurnal development of vertical profiles for locations in the southeast United States show similar traits to WLEF except for a large positive bias in boundary layer CO₂. Advection of CO₂ has been shown to be an important component to CO₂ tower measurements (Parazoo, 2004) but generally doesn't provide a consistent enough source of CO₂ to

explain the numerous positive CO₂ anomalies seen in the model. A more likely culprit is the relatively low NEE predicted by the a priori SiB3 model over many of these areas. Ecosystem respiration (ER) rates for some areas on the leeward side of the Appalachians in North Carolina had nocturnal ecosystem respiration rates of 10 $\mu\text{mol}/\text{m}^2/\text{sec}$, some of the highest rates during the month of July in the domain. However, these areas had peak daytime NEE rates only a few micromoles higher and often had average daily NEE rates of about $-1 \mu\text{mol}/\text{m}^2/\text{sec}$, indicating that the system was almost at balance with respect to carbon gains and losses over the course of a day. This effect appeared wide spread over the southeastern United States (Fig. 5.19) and

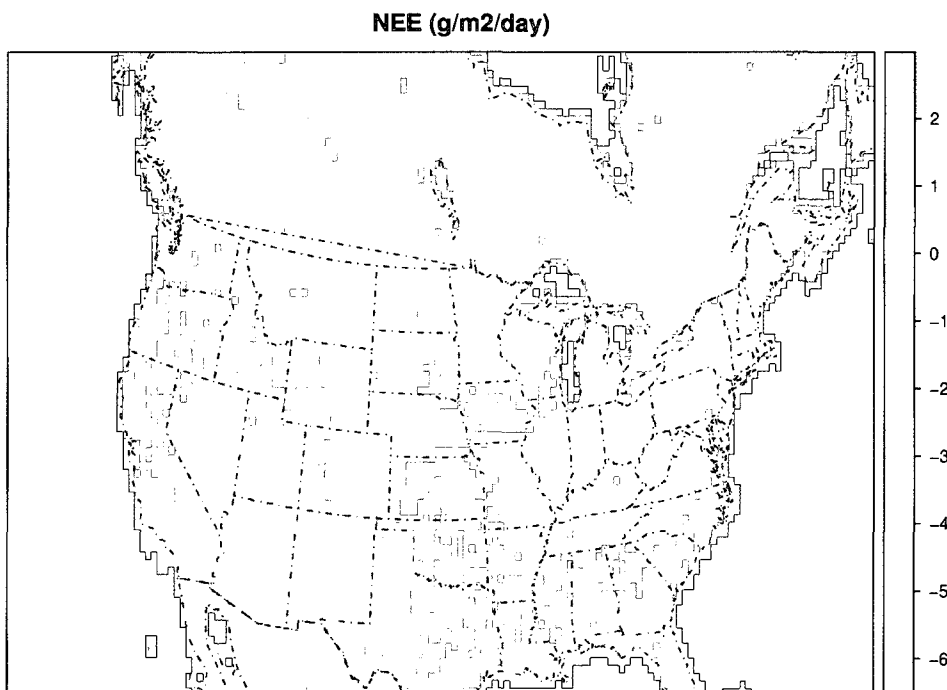


Fig. 5.19 Rates of Net Ecosystem Exchange (NEE) averaged for July 1, 2004 through July 31, 2004 from SiB3.

into the western portions of the United States. The western portions of the country were in the midst of a severe drought and thus the low NEE would appear reasonable there

although there is little INTEX data in that region to make comparisons to. Anomalous morning build ups of CO₂ are shown in Fig. 5.20. Although fossil fuel sources can contribute up to about 25% of this buildup for locations near the Appalachians, biological activity is generally the source of most of the build up of CO₂ seen in Fig. 5.20.

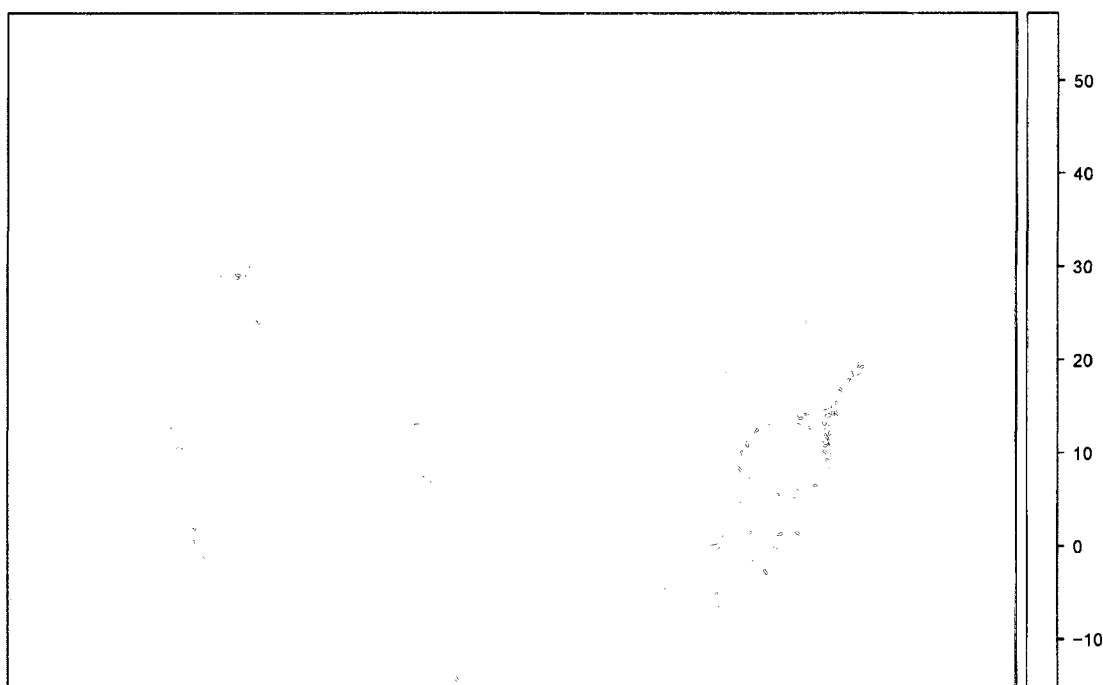


Fig. 5.20 CO₂ tracer(ppm) from biological sources and fossil fuel sources, averaged for July 1, 2004 through July 31, 2004 and shown for 12 UMT (6 A.M. MDT, 8 A.M. EDT).

Review of vegetation stress in the SiB3 model show that that anomalous patterns were largely due to long term soil moisture deficits originating from 2003 and continuing through the spring of 2004. The east and southeast had a relatively wet summer which lessened the stress but did not improve modeled soil moisture levels to the point at which average summertime NEE could be realized. Low NEE combined with relatively high

rates of nocturnal respiration and weak boundary layer mixing contribute larger errors in the early morning and sunset hours. Fig. 5.21 shows a measure of late morning / early afternoon surface winds and one can see that weak winds typically exist in several key areas seen as anomalous in Fig. 5.20.

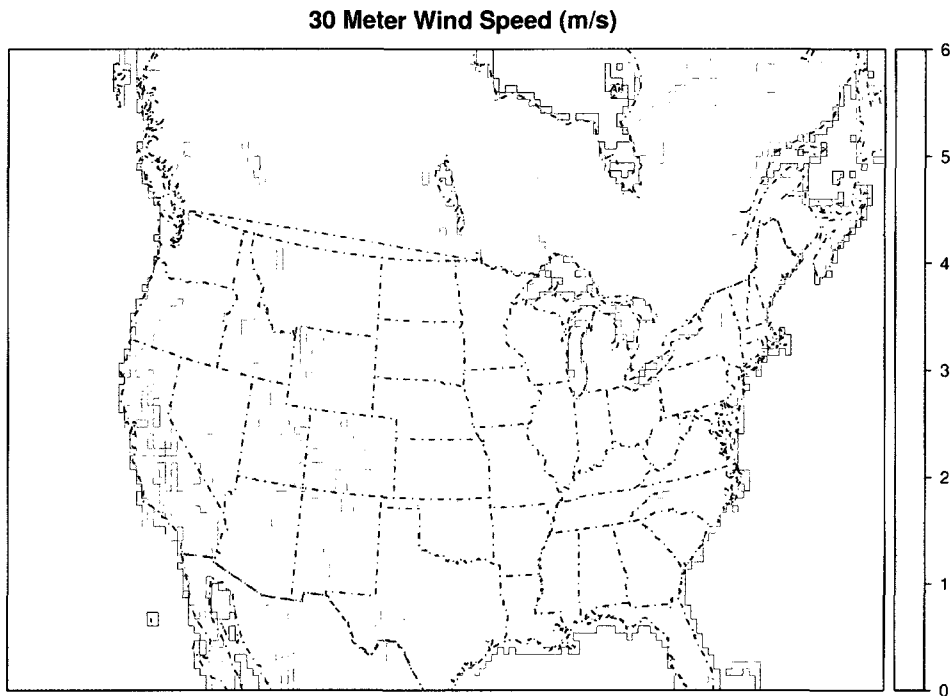


Fig. 5.21 Thirty meter winds from RAMS, averaged for July 1, 2004 through July 31, 2004 and shown for 18 UMT (12 P.M. MDT, 2 P.M. EDT).

In particular, two areas of morning CO₂ buildup on the Front Range of Colorado are correlated well to two areas with weak average winds in the late morning. Low NEE due to vegetation stress explains the source of CO₂ to the anomalous regions in Fig. 5.20 but weak winds and weak atmospheric mixing appear to amplify the effect in many spots, especially in the vicinity of topography like the Northern San Joaquin Valley, the Front Range of Colorado, and the Piedmont region of the east coast. Although it was not explored in detail, many mountainous areas appeared to have less nocturnal buildup of

CO₂ and thus cold air pooling cannot be ruled out as an additional contributor to the morning time anomalies of CO₂ in many locations.

It is then believed that plant stress in the model is artificially high due to incorrect soil moisture recovery from an extended dry period including the end of 2003 and the start of 2004. The effect is then a negative bias in GPP over the southeast during the spring and into the summer. It is important to realize that although these effects appear to be localized to certain portions of the domain, advection of these surface anomalies might heavily impact concentrations downwind and therefore inversion results. For example, Fig. 5.22 shows vertical profiles over a location in

Variability of 3PM EDT Vertical Profiles over WV, focusing on INTEX July 25

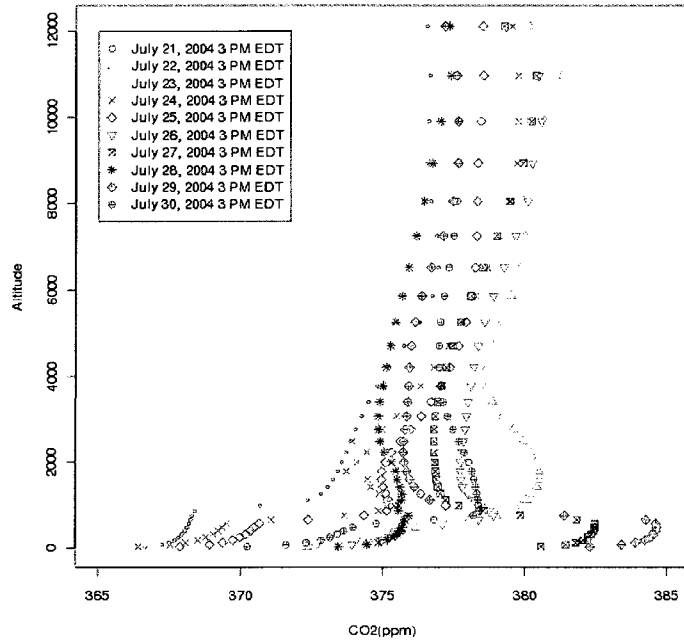


Fig. 5.22 Vertical profiles over West Virginia showing effects of upwind CO₂ buildup in model

Hourly CO₂(PPM) Influence to 1PM - 5PM (EDT)
West Virginia SiBRAMS concs. from biosphere 7/28/04

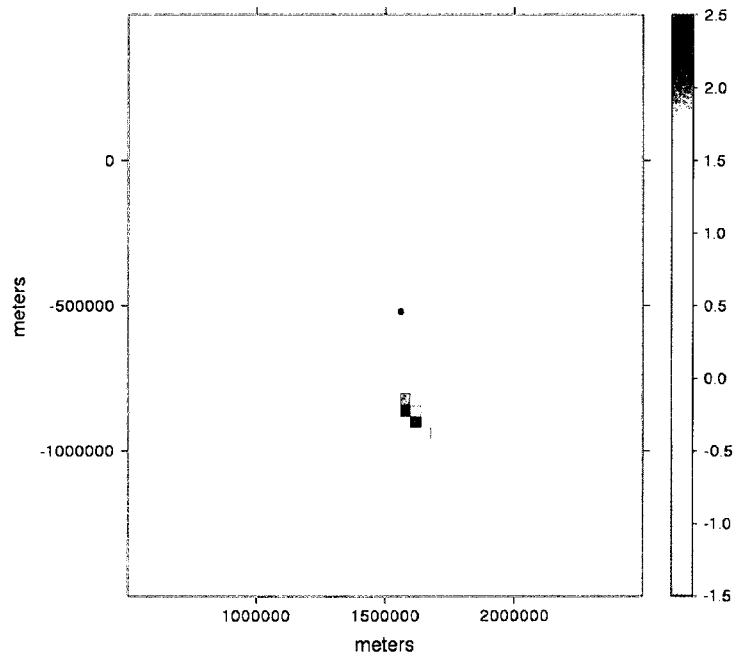


Fig. 5.23 Influence function at 1000 meters above ground, showing contributing sources to anomalously high boundary layer CO₂ in model for July 29th

West Virginia where the INTEX campaign aircraft flew. The multi-modal shape of the boundary layer CO₂ concentrations clearly indicates whether wind is coming from areas in the south with weak NEE. Influence functions were averaged for 1 P.M. to 5 P.M. EDT on the 29th of July for this location and produced a near perfect correlation to nocturnal buildup from the night before (Fig. 5.23).

Conclusions

GPP, ER, and NEE flux corrections implied by this inversion provide posterior annual NEE estimates similar to those provided by a number of independently derived models including CASA (via CarbonTracker optimized) and the MODIS 17 GPP product. NEE estimates for the entire domain appear on the low side of estimates derived from global models, which is understandable given the lack of constraint on some key regions of high annual GPP, and hence potentially high annual NEE. This was corroborated by the comparison to INTEX aircraft data which shows the existence of a deficit in GPP over the southeast which would, when all other things are considered equal, inflate the domain-wide sink closer to levels estimated from global models such as CarbonTracker. Results are relatively sensitive to a number of parameters in the inversion setup, which is also to be expected with an inversion constrained by such a sparse observing network. Using a temporally uniform boundary condition seems to produce a very unrealistic annual sink on the order of 0.27 Pg per year, supporting the notion that regional inversions require realistic boundary inflow of CO₂. However, much to our surprise, we find that two completely independent boundary inflow estimates provide very similar results with the main difference being an approximately 20%

difference in magnitude. This leads us to believe that, while probably not preferable to optimized global CO₂ fields, the inclusion of annual NEE balanced models in global models used to provide boundary inflow estimation does not significantly damage inversions based upon it.

In the course of trying to improve NEE estimates, we were able to find that the inversion was able to provide some degree of correction to the individual summands of NEE, ER and GPP, which are generally highly correlated at many different scales in time and space. Considering that SiB3 currently calculates ER as a relatively simple function of soil moisture and temperature such that annual ER equals annual GPP, the significant adjustment inferred upon GPP may prove to be valuable estimation of other quantities of interest in the biosphere. For example, while photosynthesizing, plants must generally release water to compensate, meaning that artificially high GPP may infer artificially high water exchange with the atmosphere and possibly associated latent heat fluxes.

The agricultural Midwestern United States appears to play a large role in the inversion results, providing a large sink. However, the sink does not correlate exactly with crop productivity, when compared to crop production maps from the United States Department of Agriculture, and several states with significant crop production such as Nebraska, Kansas, and Iowa, appear to be in approximate annual carbon balance. While the magnitude of this difference between carbon neutral states with crops and carbon sink states with crops is likely influenced by the lack of data in the inversion and the general unconstrained nature of the solution at fine scales, the discrimination between them seems likely to stay. One hypothesis proposed is the lateral movement of crops which has been shown to be a major portion of the carbon budget globally (Ciais et al., 2007).

The main crops of interest in the domain are wheat, soy and corn. Soy and corn are grown across large expanses of the north-central Midwest and are primarily used to feed livestock. These livestock are typically fed in feedlots in the states of Iowa, Colorado, Nebraska, Kansas, and Texas, generally located to the west and south of the areas of growth and harvest. The end result would be that eastern states within the Midwest would be a sink because of the near complete export of crops grown there. However, states in the western portion of the Midwest would receive the majority of these crops where they would be fed to cattle and other animals, returned to the atmosphere as CO₂ and CH₄ and largely balance any local sinks due to crop production.

Technical considerations concerning the inversion could also affect these results. In particular, a large amount of missing data for the WKWT (Moody, TX) tower leaves the southern boundary inflow unconstrained beyond the normal PCTM inflow. This could result in the inflation of an Oklahoma/Texas sink to account for a positive bias in the inflow at the southern boundary, particularly after July 1, 2004 when the Midwest receives its heaviest influence from the Gulf of Mexico. The WLEF tower was also missing most of its observations for June, a time of intense drawdown for croplands to the south of the site.

In 2004, the southern states of Texas, Oklahoma, Kansas, Louisiana, Arkansas, and Mississippi had the wettest summer ever potentially mitigating some degree of drought and providing an increase in GPP for the region which includes managed forests, a large percentage of the United States' exported wheat crop, and soybeans and other crops along the lower Mississippi river valley. Additional research is needed to determine if any of these could represent a plausible hypothesis that would result in the

net carbon neutrality of large crop growing states in the western portions of the Great Plains and the expansive southern and Mississippi river valley sink predicted by the inversion.

Literature Cited

Alig, Ralph J.; Krankina, Olga; Yost, Andrew; Kuzminykh, Julia, 79, Forest Carbon Dynamics in the Pacific Northwest (USA) and the St. Petersburg Region of Russia: Comparisons and Policy Implications, *Climatic Change*, pg 335-360, 2006

Amiro B.D.; Todd J.B.; Wotton B.M.; Logan K.A.; Flannigan M.D.; Stocks B.J.; Mason J.A.; Martell D.L.; Hirsch K.G., Direct carbon emissions from Canadian forest fires, 1959-1999, *Canadian Journal of Forest Research*, 31:3, pg 512-525, 2001

Andres, R. J.; Marland, G.; Fung, I. & Matthews, E. (1996), 'A 10x10 Distribution of Carbon Dioxide Emissions from Fossil Fuel Consumption and Cement Manufacture, 1950-1990', *Global Biogeochemical Cycles* 10, 419-429.

Baker, I.; Denning, A. S.; Hanan, N.; Prihodko, L.; Uliasz, M.; Vidale, P.; Davis, K. & Bakwin, P. (2003), 'Simulated and observed fluxes of sensible and latent heat and CO₂ at the WLEF-TW tower using Sib 2.5', *Global Change Biology* 9, 1262-1277.

Baker, I.; Denning, A.; Prihodko, L.; Schaefer, K.; Berry, J.; Collatz, G.; Suits, N.; Stockli, R.; Philpott, A. & Leonard, O. (2007), 'Global Net Ecosystem Exchange (NEE) of CO₂', Available on-line [<http://www.daac.ornl.gov>] from Oak Ridge National Laboratory Distributed Active Archive Center, Oak Ridge, Tennessee, U.S.A..

Baker, I. T.; Prihodko, L.; Denning, A. S.; Goulden, M.; Miller, S. & da Rocha, H. R. (2008), 'Seasonal drought stress in the Amazon: Reconciling 3 models and observations', *Journal of Geophysical Research* 113.

Case, J. L.; Manobianco, J.; Dianic, A.V.; Wheeler, M.M. (2002), 'Verification of High-Resolution RAMS Forecasts over East-Central Florida during the 1999 and 2000 Summer Months', *Weather and Forecasting* Vol 17, Issue 6, pp 1133-1151

Choi, Y.; Vay, S; Vadrevu, K.; Soja, A.; Woo, J.; Nolf, S.; Sachse, G.; Diskin, G.; Blake, D.; Blake, N.; Singh, H.; Avery, M.; Fried, A.; Pfister, L.; Fuelberg, H., 'Characteristics of the atmospheric CO₂ signal as observed over the conterminous United States during INTEX-NA', *Journal of Geophysical Research*, Vol 113, D07301, doi:10.10129/2007JD008899, 2008

Ciais P.; Bousquet P., Freibauer A., and Naegler, T., 'Horizontal displacement of carbon associated with agriculture and its impacts on atmospheric CO₂', *Global Biogeochemical Cycles*, Vol. 21, GB2014, doi:10.1029/2006GB002741, 2007

Collatz, G. J.; Ribas-Carbo, M. & Berry, J. A. (1992), 'Coupled photosynthesis-stomatal conductance model for leaves of C₄ plants', *Aust. J. Plant Physiol.* 19, 519-538.

Denning, A. S.; Collatz, J. G.; Zhang, C.; Randall, D. A.; Berry, J. A.; Sellers, P. J.; Colello, G. D. & Dazlich, D. A. (1996), 'Simulations of terrestrial carbon metabolism and

atmospheric CO₂ in a general circulation model. Part 1: Surface carbon fluxes', *Tellus* 48B, 521-542.

Denning, A. S.; Nicholls, M.; Prihodko, L.; Baker, I.; Vidale, P.; Davis, K. & Bakwin, P. (2003), 'Simulated variations in atmospheric CO₂ over a Wisconsin forest using a couple ecosystem-atmosphere model', *Global Change Biology* 9, 1241-1250.

Denning, A.S., N. Zhang, C. Yi, M. Branson, K. Davis, J. Kleist, and P. Bakwin (2008), 'Evaluation of modeled atmospheric boundary layer depth at the WLEF Tower', *Agricultural and Forest Meteorology*, 148, 206-215.

Engelen, R. J.; Denning, A. S. & Gurney, K. R. (2002), 'On error estimation in atmospheric CO₂ inversions', *Journal of Geophysical Research* 107, (10) 1-13.

Fan, S.; Gloor, M.; Mahlman, J.; Pacala, S.; Sarmiento, J.; Takahashi, T. & Tans, P. (1998), 'A large terrestrial carbon sink in North America implied by atmospheric and oceanic carbon dioxide data and models', *Science* 282, 442-446.

Freitas, S. R.; Longo, K.; Silva Dias, M.; Silva Dias, P.; Chatfield, R.; Fazenda, Á.; Rodrigues, L. F. (2006), 'The coupled aerosol and tracer transport model to the Brazilian developments on the Regional Atmospheric Modeling System: validation using direct and remote sensing observations.' *International Conference on Southern Hemisphere Meteorology and Oceanography (ICSHMO)*'.

Fuelberg, H. E. et al. Meteorological conditions and anomalies during INTEX-NA, *J. Geophysical Research*, doi: 10.1029/2006/JD007734, 2007, in press

Gerbig, C.; Lin, J. C.; Wofsy, S. C.; Daube, B. C.; Andrews, A. E.; Stephens, B. B.; Bakwin, P. S. & Grainger, C. A. (2003), 'Toward constraining regional-scale fluxes of CO₂ with atmospheric observations over a continent: 1. Observed spatial variability from airborne platforms', *Journal of Geophysical Research* 108.

Gurney, K. R.; Law, R. M.; Denning, A. S.; Rayner, P. J.; Baker, D.; Bousquet, P.; Bruhwiler, L.; Chen, Y.; Clals, P.; Fan, S.; Fung, I. Y.; Gloor, M.; Helmann, M.; Higuchi, K.; John, J.; Maki, T.; Maksyutov, S.; Masarie, K.; Peylin, P.; Prather, M.; Pak, B. C.; Randerson, J.; Sarmiento, J.; Tagucki, S.; Takahashi, T. & Yuen, C. (2002), 'Towards robust regional estimates of CO₂ sources and sinks using atmospheric transport models', *Nature* 415, 626-630.

Gurney, K. R.; Seib, B.; Ansley, W.; Mendoza, D.; Fischer, M.; Miller, C. & Murtishaw, S. (2008), 'The Vulcan Inventory, version 1.0', Purdue University, <http://www.purdue.edu/eas/carbon/vulcan/research.html>.

Hanan, N. P.; Berry, J. A.; Verma, S. B.; Walter-Shea, E. A.; Suyker, A. E.; Burba, G. G. & Denning, A. S. (2004), 'Model analyses of biosphere-atmosphere exchanges of CO₂, water and energy in Great Plains tallgrass prairie and wheat ecosystems', *Agricultural and*

Forest Meteorology.

Kalman, R. E. (1960), 'A New Approach to Linear Filtering and Prediction Problems', *Transactions of the ASME--Journal of Basic Engineering* 82, 35-45.

Kaminiski, T.; Rayner, P. J.; Heimann, M. & Enting, I. G. (2001), 'On aggregation errors in atmospheric transport inversions', *Journal of Geophysical Research* 106, 4703-4715.

Kawa, S. R.; III, D. J. E.; Pawson, S. & Zhu, Z. (2004), 'Global CO₂ transport simulations using meteorological data from the NASA data assimilation system', *Journal of Geophysical Research* 109, D18312.

Liang, Q., et al (2008), 'Summertime influence of Asian pollution in the free troposphere over North America', *J. Geophysical Research.*, 112, D12S11, doi:10.1029/2006JD007919.

McGrath-Spangler, E. L.; Denning, A. S.; Corbin, K. D.; and Baker, I. T. (2008): Implementation of a boundary layer heat flux parameterization into the Regional Atmospheric Modeling System (RAMS), *Atmos. Chem. Phys. Discuss.*, 8, 14311-14346.

Michalak, A. M.; Bruhwiler, L. & Tans, P. P. (2004), 'A geostatistical approach to surface flux estimation of atmospheric trace gases', *Journal of Geophysical Research* 109, 1-19.

Nicholls, M. E.; Denning, A. S.; Prihodko, L.; Vidale, P.; Davis, K. & Bakwin, P. (2004), 'A multiple-scale simulation of variations in atmospheric carbon dioxide using a coupled biosphere-atmospheric model', *Journal of Geophysical Research* 109.

Olson, J. S.; Watts, J. A. & Allison, L. J. (2001), 'Major World Ecosystem Complexes Ranked by Carbon in Live Vegetation: A Database', ORNL/CDIAC-134, NDP-017. Carbon Dioxide Information Analysis Center, U.S. Department of Energy, Oak Ridge National Laboratory, Oak Ridge, Tennessee, U.S.A..

Oren, R.; Ellsworth, D. S.; Johnsen, K. H.; Phillips, N.; Ewers, B. E.; Maler, C.; Schafer, K. V.; McCarthy, H.; Hendrey, G.; McNulty, S. G. & Katul, G. G. (2001), 'Soil fertility limits carbon sequestration by forest ecosystems in a CO₂-enriched atmosphere', *Nature* 411, 469-471.

Parazoo, N. (2007), 'Investigating synoptic variations in atmospheric CO₂ using continuous observations and a global transport model', Master's thesis, Colorado State University.

Peters, W.; Jacobson, A. R.; Sweeney, C.; Andrews, A. E.; Conway, T. J.; Masarie, K.; Miller, J. B.; Bruhwiler, L. M. P.; Pétron, G.; Hirsch, A. I.; Worthy, D. E. J.; van der Werf, G. R.; Randerson, J. T.; Wennberg, P. O.; Krol††, M. C. & Tans, P. P. (2007), 'An atmospheric perspective on North American carbon dioxide exchange: CarbonTracker',

Proceedings of the National Academy of Sciences of the United States of America 104, 18925-18930.

Prince S. (2000), 'NPP Cropland: Gridded Estimates for the Central U.S.A. 1982-1996', <http://knb.ecoinformatics.org/knb/metacat?action=read&qformat=nceas&sessionid=&docid=nceas.184>

Peterson, G. A.; Halvorson, A. D.; Havlin, J. L.; Jones, O. R.; Lyon, D. J. & Tanaka, D. L. (1998), 'Reduced tillage and increasing cropping intensity in the Great Plains conserves soil C', *Soil & Tillage Research* 47, 207-218.

Peylin, P.; Rayner, P. J.; Bousquet, P.; Carouge, C.; Hourdin, F.; Heinrich, P.; Ciais, P. & contributors, A. (2005), 'Daily CO₂ flux estimates over Europe from continuous atmospheric measurements: 1, inverse methodology', *Atmospheric Chemistry and Physics* 5, 3173-3186.

Pielke, R. A.; Cotton, W.; Walko, R.; Tremback, C.; Lyons, W.; Grasso, L.; Nicholls, M.; Moran, M.; Wesley, D.; Lee, T. & Copeland, J. (1992), 'A comprehensive meteorological modeling system -- RAMS', *Meteorology and Atmospheric Physics* 46, 69-91.

Raich, J.; Rastetter, E.; Melillo, J.; Kicklighter, D.; Steudler, P.; Peterson, B.; Grace, A.; III, B. M. & Ro" smarty, C. V. (1991), 'Potential net primary productivity in South America: Application of a global model.', *Ecological Applications* 1, 399-429.

Robertson, G. P.; Paul, E. A. & Harwood, R. R. (2000), 'Greenhouse Gases in Intensive Agriculture: Contributions of Individual Gases to the Radiative Forcing of the Atmosphere', *Science* 289, 1922-1925.

Rodenbeck, C.; Houweling, S.; Gloor, M. & Heimann, M. (2003), 'CO₂ flux history 1982-2001 inferred from atmospheric data using a global inversion of atmospheric transport', *Atmospheric Chemistry and Physics* 3, 1919-1964.

Schimel, D. S.; House, J. I.; Hibbard, K. A.; Bousquet, P.; Ciais, P.; Peylin, P.; Braswell, B. H.; Apps, M. J.; Baker, D.; Bondeau, A.; Canadell, J.; Churkina, G.; Cramer, W.; Denning, A. S.; Field, C. B.; Friedlingstein, P.; Goodale, C.; Heimann, M.; Houghton, R. A.; Melillo, J. M.; B. Moore III, D. M.; Noble, I.; Pacala, S. W.; Prentice, I. C.; Raupach, M. R.; Rayner, P. J.; Scholes, R. J.; Steffen, W. L. & Wirth, C. (2001), 'Recent patterns and mechanisms of carbon exchange by terrestrial ecosystems', *Nature* 414, 169-172.

Sellers, P. J.; Mintz, Y.; Y. C. Sud & Dalcher, A. (1986), 'A simple biosphere model (SiB) for use within general circulation models', *Journal of Atmospheric Sciences* 43, 505-531.

Sellers, P. J.; Randall, D. A.; Collatz, G. J.; Berry, J. A.; Field, C. B.; Dazlich, D. A.; Zhang, C.; Collelo, G. D. & Bounoua, L. (1996), 'A Revised Land Surface Parameterization (SiB2) for Atmospheric GCMs. Part I: Model Formulation', *Journal of*

Climate 9, 676-705.

Stephens, B. B.; Gurney, K. R.; Tans, P. P.; Sweeney, C.; Peters, W.; Bruhwiler, L.; Ciais, P.; Ramonet, M.; Bousquet, P.; Nakazawa, T.; Aoki, S.; Machida, T.; Inoue, G.; Vinnichenko, N.; Lloyd, J.; Jordan, A.; Heimann, M.; Shibistova, O.; Langenfelds, R. L.; Steele, L. P.; Francey, R. J. & Denning, A. S. (2007), 'Weak Northern and Strong Tropical Land Carbon Uptake from Vertical Profiles of Atmospheric CO₂', *Science* 316, 1732-1735.

Tilman, D.; Reich, P.; Phillips, H.; Menton, M.; Patel, A.; Vos, E.; Peterson, D. & Knops, J. (2000), 'Fire Suppression and Ecosystem Carbon Storage', *Ecology* 81(10), 2680-2685.

Tripoli, G. J. & Cotton, W. R. (1982), 'The Colorado State University three-dimensional cloud/mesoscale model—Part I General theoretical framework and sensitivity experiments.', *Journal de Recherches Atmospheriques* 16, 185–219.

Ulliasz, M. & Pielke, R. A. (1991), 'Application of the receptor oriented approach in mesoscale dispersion modeling', in H. Van Dop & D. G. Steyn, ed., 'Air Pollution Modeling and its Applications VIII', Plenum Press, New York, 399-408.

Wang, J. W.; Denning, A. S.; Lu, L.; Baker, I. T. & Corbin, K. D. (2006), 'Observations and simulations of synoptic, regional, and local variations in atmospheric CO₂', *Journal of Geophysical Research* 112.

Wise, T. A., 'Identifying the Real Winners from U.S. Agricultural Policies', Global Development and Environmental Institute, Working Paper No. 05-07, 2005

Zupanski, Dusanka; Denning, A. Scott; Marek Ulliasz; Zupanski, Milija; Schuh, Andrew E.; Rayner, Peter J.; Peters, Wouter & Corbin, Katherine D. (2007), 'Carbon flux bias estimation employing Maximum Likelihood Ensemble Filter (MLEF)', *Journal of Geophysical Research* 112.

(2007), 'The first state of the carbon cycle report (SOCCR)', Technical report, U.S. Climate Change Science Program and the Subcommittee on Global Change Research.

VI. Summary

There is little dispute about the first order effects of CO₂ as an insulating greenhouse gas in the earth's atmosphere. The amount of CO₂ in the atmosphere has steadily risen as a result of increased combustion from fossil fuels over the last century. However, the increase in CO₂ in the atmosphere only represents about half of the CO₂ resulting from fossil fuel burning. It has been concluded that a large terrestrial carbon sink must exist in order to balance this missing carbon. The specifics of this terrestrial sink are uncertain, in particular, the spatial and temporal dynamics of sources and sinks of carbon are not well understood. In order to understand these dynamics and predict into the future, carbon fluxes must be estimated at higher resolutions in time, space, and carbon source (ER/GPP).

Carbon flux estimation is generally based some combination of eddy-covariance tower measurements, biogeochemical inventory estimates, direct observations, and atmospheric inversions. Eddy-covariance flux towers provide a way to effectively estimate NEE. However, the sampling footprint of these towers is usually on the order of one square kilometer or less, meaning that it would be difficult to estimate large regional scale carbon fluxes with eddy-covariance towers. NEE estimates can also be constructed with observational data as they are in the State of the Carbon Cycle Report (SOCCR). While this provides the most comprehensive accounting of carbon, it is very expensive and time consuming and does not always provide full coverage over the area of interest. Biogeochemical models provide very complete estimates in time and space but generally do not directly use atmospheric carbon dioxide which is an obvious constraint on the carbon dynamics. Atmospheric carbon dioxide inversions provide an attractive

alternative to these other methods in situations where larger regional scale fluxes are sought.

It was shown in Chapter 4 that large-scale regional patterns in ecosystem respiration, gross primary productivity, and NEE can be estimated with atmospheric inversions effectively over North America with a relatively sparse network of carbon dioxide observing towers. Furthermore, this technique proved robust to variations in the correlation length scale of the pattern that was being estimated. When smooth regional carbon flux patterns are masked with small-scale spatial variability in the fluxes, the accuracy of the regional flux estimates is a natural concern. However, it was shown that large-scale spatial flux patterns are effectively estimated through significant levels of small-scale spatial variability modeled by Gaussian noise.

The inversion methods presented in Chapter 4 were applied to carbon dioxide data that was available from an eight-tower network in 2004. Results implied significant reductions to both ecosystem respiration and gross primary productivity. ER, GPP and NEE observations from the ARM site in Oklahoma provided corroborating evidence for this result. The a posteriori annual NEE for the entire domain ranged between 0.5 and 0.8 PgC per year. This is consistent with the estimates provided in the SOCCR report. The most distinct feature of the annual sink was a large regional sink positioned over the south-central United States, an area that often experiences drought and severe weather. This area had record summer rainfall in 2004, potentially providing beneficial summer time conditions for biomass growth. The eastern portion of this sink consists of croplands and young forests that are heavily managed for lumber production while the western portion of the sink contains vast expanses of winter wheat.

The results of this work are exciting but difficult to use confidently because of the lack of comparability to any 'ground truth'. For example, there are few inventory or observational results available on the scale of the results of this dissertation. Therefore, it is difficult to corroborate the large sink exhibited in the south central United States with any information other than with the results of a single flux tower in the northern portion of the sink. The future of this work involves extending the 2004 results to 2003-2008 and comparing to inventory-based methods, which is already underway. The longer time frame will provide valuable information on inter-annual variability while the synthesis work will provide information necessary to provide explanations for the fine scale source/sink structure that we are able to provide with these inversion techniques.